Synthesis and Stability Studies of Novel Tellurium(IV) Compounds

A thesis submitted to National University of Ireland in fulfillment of the requirements for the degree of

Masters of Science

By

Kenneth D'Arcy

Department of Chemistry

Maynooth University

Maynooth, County Kildare

Ireland

February 2020

Research Supervisor: Dr Diego Montagner

Table of Contents

Declaration of Authorship

I have read and understood the Departmental policy plagiarism.

I declare that this thesis is my own work and has not been submitted in any form for another degree or diploma at any university or other institute of tertiary education.

Information derived from the published or unpublished work of others has been acknowledged in the text and a list of reference is given.

Signed Kenneth D'Arcy Date: 20-02-2020

Dedication

I dedicate this thesis to my beloved wife and daughter Magda and Sophie.

Thank you for all your support over the last three years.

Acknowledgments

This thesis would not have been completed without the help and support of many people in Maynooth University. First and foremost, I would like to acknowledge the great support and guidance and his inspiration that my supervisor Dr. Diego Montagner has given me over the past 3 years. I am really grateful that I had this opportunity to work on his team and really enjoyed learning from such an experienced researcher. This was the first project on Tellurium for Diego and I hope that he will get the opportunity to continue more studies in the future. I would also like to acknowledge all the people who have also helped with this project such as Dr Kevin Kavanagh in biology in Maynooth for testing of some tellurium compounds, to Barbara Fresch in Padova University for her computational studies on our compounds and also Dr Pablo Sanz from the department of chemistry of Saragossa University (Spain) for his help in the crystal characterizations of our novel tellurium compounds. I also want to acknowledge all the staff and post graduates in Maynooth University who made my time in Maynooth enjoyable and also gave me training on all the analytical equipment required to complete my project. All the staff and postgraduates have made a huge impression on my life in the last few years and I have made many friendships on the way and I wish them all the best in their future careers and research.

I would also like to acknowledge Intel Ireland for the financial funding and support which allowed me to complete my Masters in research Chemistry. Finally, I would like to thank both my wife Magdalena and daughter Sophie who supported me over the last 3 years, for without the support of them this project would have been difficult to complete. To everyone I mentioned above I would like to say a massive Thank you.

List of Abbreviations

amu	Atomic mass unit	**GPx**	Glutathione peroxidase
a.q	Aqueous	**GSH**	Glutathione
AS101	Ammonium Trichloro (dioxoethylene-*O*, *O'*) tellurate	**IL-10**	Interleukin-10
ATP	ATPase	**IR**	Infra-red
ATR	Attenuated Total Reflectance	**kJ/mol**	Kilo Joules per mole
Bcl-2	B-cell lymphoma 2	**MeOH**	Methanol
C	Celsius	**MHz**	Mega Hertz
Conc	Concentration	**MRI**	Magnetic resonance imaging
CSIF	Cytokine synthesis inhibitory factor	**MRP**	Multi drug resistance protein
CTR	Copper transporter	**NMR**	Nuclear magnetic resonance
D_2O	Deuterated water	**NSAIDS**	Nonsteroidal anti-inflammatory drugs
DCM	Dichloromethane	**OCT1.**	Organic cation transporter 1
DFT	Density Functional Theory	**OCT2.**	Organic cation transporter 2
DMF	Dimethylformamide	**Ph**	Phenyl
DMSO	Dimethylsulfoxide	**ppm**	Parts per million
DMSO-d_6	Deuterated Dimethylsulfoxide	**r.t**	Room temperature
DNA	Deoxyribonucleic acid	**ROS**	Reactive oxygen species
E-coli	Escherichia coli	**SAS**	Octa-*O*-Bis-(*R,R*)-tartarate ditellurane
Elem Anal	Elemental Analysis	**SMD**	Solvation Model based on Density
Eq	Equivalent	**Stat3**	Signal transducer and activator of transcription 3
ESI	Electro Spray Ionization	**Te(IV)**	Tellurium(IV)
Et_2O	Diethyl ether	**THF**	Tetrahydrofuran
g/cm^3	Grams per cubic centimeter	**TrxR**	Thioredoxin reductase

Abstract

Metal-based compounds play a fundamental role in inorganic medicinal chemistry and the most important anticancer agents, approved worldwide as chemotherapeutic drugs, contain metals as *the* active component (i.e. platinum in cisplatin). Several examples of metal containing anticancer drugs are reported, including gold, ruthenium, silver, titanium, copper, cobalt. Surprisingly, Tellurium-based compounds never attracted the curiosity of the scientific community and tellurium chemistry with relevance to biological systems is poorly developed. Only recently, two Tellurium containing species have been investigated in clinical trials as anticancer agents, named AS101 (Ammonium trichloro(dioxoethylene-*O,O'*)tellurate) and Octa-*O*-Bis-(R,R)-tartarate ditellurane (SAS)). These species, whose target are the cysteine residues of proteins (they act as cysteine protease inhibitors), are not stable in physiological conditions and decompose forming oxo-chloro tellurium(IV) compounds that are retained to be the real active species. Inspired by the results obtained with the above mentioned Te species, we developed a series of analogues of Te(IV)-based compounds with the aim to enhance the physiological stability in order to clarify the biological mechanism of action of these species. The coordination sphere of tellurium has been modified with different ligands, tuning the steric electronic properties. The stability has been studied experimentally *via* multinuclear NMR spectroscopy (^{1}H, ^{13}C, ^{125}Te NMR) in solution with accurate experiments in the presence of different equivalents of water. The experimental data have been combined with theoretical calculations that confirmed the stability trend. More than twenty new compounds have been synthesized and characterized with many spectroscopic techniques (multinuclear NMR (^{1}H, ^{13}C, ^{19}F and ^{125}Te-NMR), IR, Elem. Anal., Mass spectroscopy) including X-ray structures. Reaction mechanisms for the formation of the new species have been proposed based on critical analyses of experimental and theoretical results. These species showed very high antibacterial potency, in particular against Gram negative *E. Coli* bacteria, with the activity produced by the hydrolysed product $[TeOCl_3]^-$.

Chapter 1

1.1 Introduction

1.1.1. The Biological role of metal ions

Metal ions have a crucial role in living organisms and it has been estimated that there are 11 common trace metal elements that make up 0.02 percent or around 8.6 g of the human body, including Iron, Copper, Zinc, Cobalt, Molybdenum and Vanadium. These elements have a tremendous influence on all biological functions in the body.[1] Most of the trace metals are involved in vital biochemical reactions in organisms, both acting as catalysts for many enzymatic reactions and acting as centres for building stabilized structures such as proteins and enzymes.[2] It is known that a build-up or deficiency of these metals can lead to many human diseases.[2] Trace metals are essential components of living cells and can be located in protein or enzyme catalytic sites and are involved in multiple biological processes ranging from catalytic site, electron exchanges to the biomolecules structural function.[3] They are generally utilised in biological reactions.[3] The elements iron, zinc and selenium for example are vital components in enzymes. Iron for example is involved in the binding, transporting and release of oxygen in humans.[4] In humans proteins such as haemoglobin contain an iron atom that bind and carry oxygen in the bloodstream. The active site of this protein contain a heme group where Fe(II) is bound (Figure 1.1).[4]

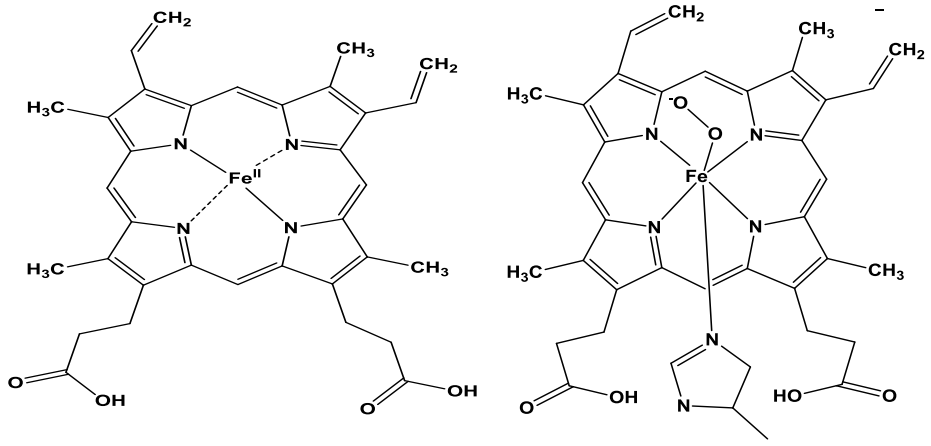

Figure 1.1. Structure of a heme group with central Fe(II) atom and the structure of a heme group with oxygen bound to the Fe atom.

As mentioned, trace metals are essential components of cells and are frequently found in enzyme catalytic sites aiding cellular activities. They are involved in multiple biological processes ranging from exchange of electrons to catalysis and also have a structural role in the protein or enzyme.[3] Transition metals such as cobalt, zinc, manganese, silver, copper and vanadium are essential in the human body in small concentrations in order for catalytic biological reactions to occur.[5] An example of a metal ion used in structural support of a protein is zinc, in a protein motif known as a zinc finger. Zinc fingers (Figure 1.2) are small protein motifs that contain multiple finger like protrusions, in which zinc ions are coordinated with a combination of histidine and cysteines residues. These zinc proteins are essential in DNA transcription processes.[6]

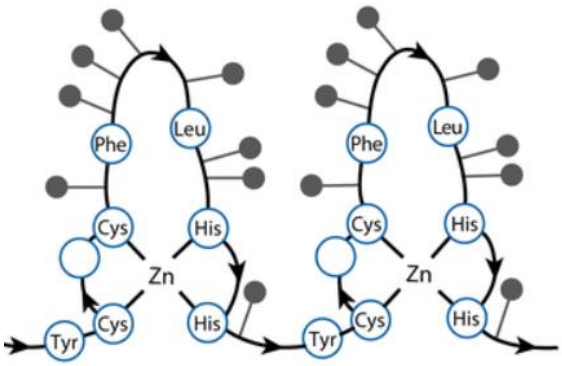

Figure 1.2. Structure of the repeating protein motif of a zinc finger, each zinc ion is coordinated to two cysteine and two histidine. The purpose of each zinc ion is support and formation of the protruding finger like structure. The grey dots are amino acids.[6]

Trace metals are important in the human body, but there must be a fine balance between the cellular need and the concentration available in the human body, because excess metals can be toxic to the human body and can lead to many human diseases. Some metals such as chromium, nickel, arsenic and cadmium, when present in excess, can lead to carcinogenesis and are therefore less advantageous for the body.[5] Trace metals can also induce human diseases if there is a notable deficiency in the cells. An example would be the cobalt found in the vitamin B_{12}. Vitamin B_{12} was first isolated by Folkers and Smith in 1948 and is also known as cobalamin (Figure 1.3). The structure of vitamin B_{12} is a highly functionalized tetrapyrrolic compound that contains three acetamides and four propionamides attached at the edges of the macrocycle corrin ring. The cobalt ion is coordinated to four nitrogen atoms of the corrin ring and two ligands situated

on both sides of the corrin ring.[7] It is a known cofactor for enzymes that can catalyse a varied amount of biological reactions including methyltransfers, isomeration and dehalogenation.[8]

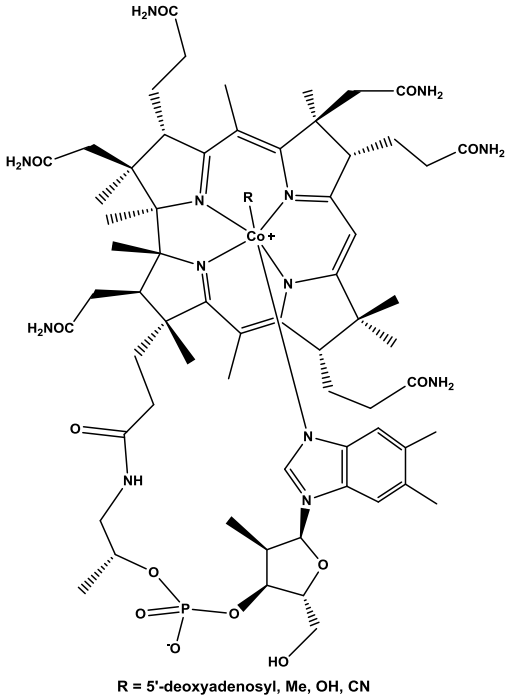

Figure 1.3. Structure of Vitamin B_{12} or cobalamin, involved in the catalysis of biological processes including methyltransfers, isomerisation and dehalogenation.

Vitamin B_{12} or cobalamin, a vitamin that is water soluble that is said to have an important role in the metabolism process of all cells in the human body. It is also a required component in DNA synthesis, and is involved in the metabolism of large biomolecules such as fatty acids and amino acids.[8] Vitamin B_{12} has an intrinsic role in the production and synthesis of myelin, therefore has a major influence in the normal functioning of the human nervous system. Deficiency in this vitamin can induce severe and irreversible damage to the brain and nervous system.[8, 9] Many of these metals that are seen in trace amounts in the body have over the years been utilised as medicinal compounds to aid or cure human diseases. Knowledge into the roles of metals in biological processes in the human body, are only being realised in the last 100 years but the therapeutic properties of metals are known throughout human history.

1.1.2. History of metals in medicine

Throughout history, humans have understood the therapeutic properties of metals and have been using metals in medicines as far back as the earliest times of recordable human history. Early civilizations have been known or documented in utilizing metal-based compounds as therapeutic agents. As far back as 2500BC, Chinese realized the medical benefits of using gold. The ancient Egyptians used copper and zinc, copper as a way to sterilize their water and zinc being used in ointments to treat wounds.[10] The famous Egyptian medical paper papyrus known as the *Papyrus Ebers,* dates from 1500BC and is said to be the first known written account of the use of metals in medicine, describing the use of copper to treat inflammation while iron was used to treat anaemia. While in 400 BC the Greek physician Hippocrates used mercury.[11] In the 16th century, the Swiss doctor and alchemist Paracelsus first pioneered the use of metals in compounds by using antimony, arsenic and mercury based salts for the prevention of certain human based diseases in medicine.[12] During the early 17th century, the herbalist Nicholas Culpepper used a gold elixir called *aurum potabile* to treat diseases in the vital spirits which included melancholy, fainting, fevers and falling sickness.[10] At the start of the 20th century, metals began to have an influence in modern day medicines. Paul Ehrlich (1854–1915) discovered the arsenic organometallic drug Arsphenamine, named Salvarsan, which proved to be affective against syphilis.[13] Arsphenamine was the 606th preparation to be tested in the laboratory of Ehrlich, hence when it first appeared it was known as number 606. It was then marketed in 1910 under its trade name Salvarsan. The structure of which had been debated for many years but in 2005 with mass spectrometry, it was seen to be a mixture of two small arsenic three and five membered rings (Figure 1.4).[14]

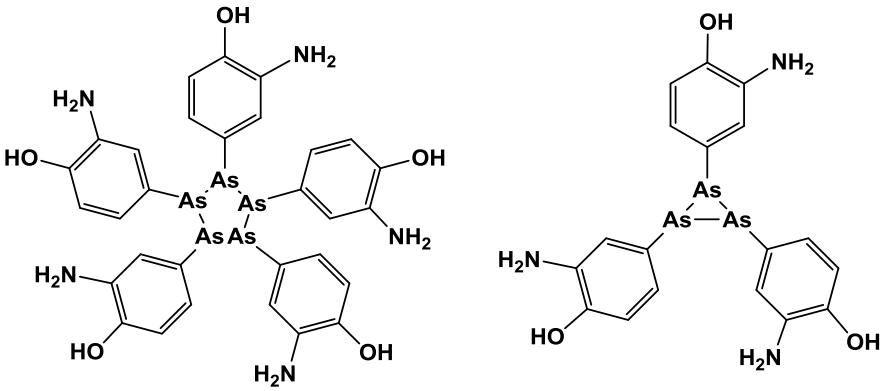

Figure 1.4. Structure of Salvarsan shows the two small arsenic molecules one a three membered ring structure and the other a five membered ring structure, the structure of Salvarsan was determined by mass spectrometry studies in 2005[14]

It was Ehrlich himself who first coined the words chemotherapy and magic bullet.[13] Based on work from Robert Koch, gold compounds were used in the treatment of tuberculosis. Koch found that compounds such as gold cyanide were extremely effective on cultures of *Mycobacterium tuberculosis*. Even though after a number of investigations into gold salt compounds had shown to have no effects on experimental tuberculosis in guinea pigs, the proposition of utilizing gold compounds in chemotherapy was further indorsed by the work of Paul Ehrlich with arsenicals.[15] In the 1920s Danish physicians who were desperate to find a remedy for tuberculosis, started implementing the treatment of gold sodium thiosulfate (Sanocrysin) (Figure 1.5).[16]

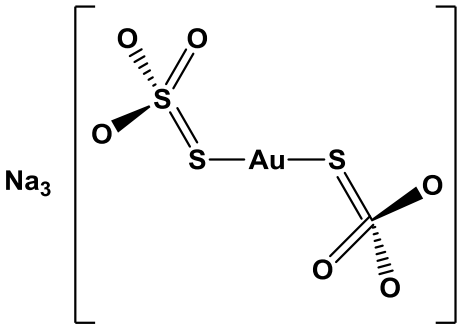

Figure 1.5. Structure of Sanocrysin or gold sodium thiosulfate used in the mid 1920's for the treatment of tuberculosis.[16]

In 1912, antimony based compounds were introduced for the treatment of leishmaniosis (Figure 1.6).[17]

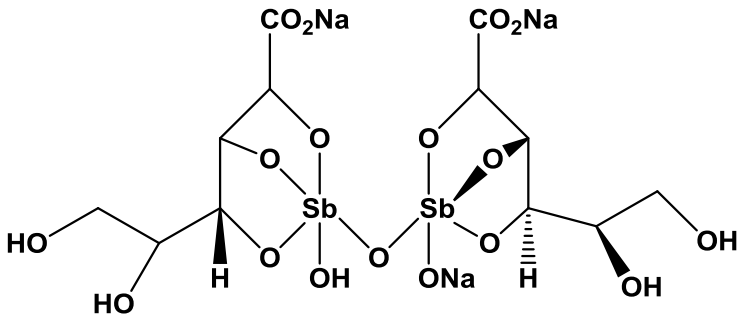

Figure 1.6. Structure of sodium stibogluconate used in the treatment of leishmaniosis.

Over the years, trace transition metals have been mainly used as the therapeutic agents because they have a unique physical-chemical properties.[18]

1.1.3 Transition metals in medicines

The development of metal-based therapeutics have played an immense role in anti-tumor medicines. These metal ions, when administered into the body, can be used either for therapeutic or diagnostic purposes.[19] The use of metal binding molecules (termed ligands derived from the Latin word "ligare") can also remove metal ions from the body and are used for treatments in metal poisoning.[19] These metal-based compounds can offer a greater versatility that is not often displayed by their rival organic or biological counterparts. For metal based compounds, ligand exchange reactions are possible within the cell or within the biological system, thus increasing the drugs potency and duration of its therapeutic effect.[20] The various oxidation numbers displayed by the metal centre can encourage the generation of ROS (Reactive Oxygen Species) inside the cell enhancing the drugs therapeutic effect.[21] Other properties that influence the activity of metal complexes are their coordination numbers, the electric charge it has and its hydrophilicity and lipophilicity.[19, 21] The variables that account for the activity of metal-based drugs are great, therefore both *in vitro* and *in vivo* studies are indeed necessary to gain knowledge of their mode of action on pharmacological targets.[22] Over the years, transition metal based drugs have shown to possess many benefits over the more popular organic based

products. This is due to the fact that they tend to offer a wide variety of coordinating numbers and geometries, usable redox states, tune-ability of ligand substitution thermodynamics and kinetics along with a vast range of structural diversity.[23] Research in medicinal inorganic chemistry has flourished over the last number of years since the discovery of the platinum based metallopharmaceutical complex cisplatin over 50 years ago.[24] There are currently several metal complexes in use for treatment of certain diseases. Gold complexes have been utilised since 1935 in the treatment of rheumatoid arthritis, starting in polymeric form and later on in the form of monomers such as auranofin (Figure 1.7). At present auranofin is currently in use in both phase I and phase II clinical trials either alone or in combination therapy for the treatment of ovarian cancer.[24] In addition to this, silver complexes such as silver sulfadiazine (Figure 1.6) and antimony (N-methylglucamine antimony) are being used as anti-infective agents.

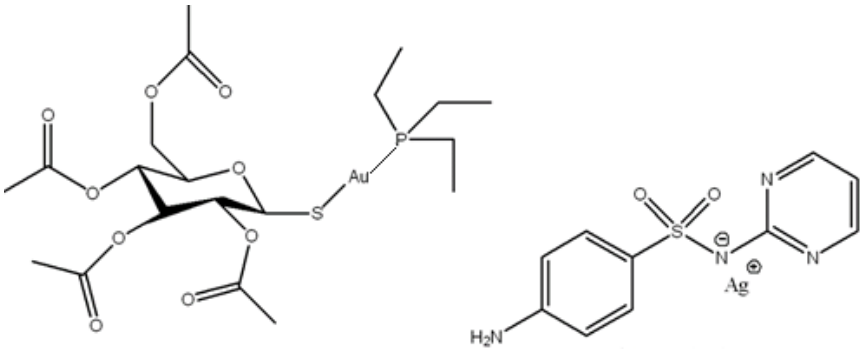

Figure 1.7. Structures of gold compound Auranofin (left) and silver sulfadiazine (right).

In addition to their therapeutic uses, metal based compounds also play a major role in radiological diagnostics and radiopharmaceuticals. Barium X-ray examinations are used in radiology in the study of the gastrointestinal tract.[25] In MRI (magnetic resonance imaging), the contrast agent Gadolinium exploits the paramagnetic characteristic of its +3 cation with seven unpaired electrons, which causes the rapid relaxation of water around the contrast agent, improving the accuracy of the MRI scan. It is mainly used for detailed images of the cardiovascular system, organs and the brain.[26]

In summary, metals show great versatility across a wide range of techniques in the medicinal chemistry field and over the years, numerous metal-based compounds have been designed which have shown therapeutic properties and toxicity.

1.1.4. Anti-cancer metal compounds

Several metal-based drugs have been explored, in particular containing platinum, ruthenium, copper, cobalt, vanadium, titanium, gold and rhodium. In this section only some ruthenium and platinum anticancer drugs will be described.

1.1.4.1. Platinum based anti-cancer complexes

Currently, the most common classes of anti-cancer drugs being utilised in chemotherapy treatments are platinum-based compounds. It is known that 50 percent of all cancer patients undergoing chemotherapy are treated with the drugs cisplatin, oxaliplatin or carboplatin (Figure 1.08). Cisplatin is effective against testicular cancer with cure rates exceeding 95 %.[27] Platinum drugs are also used on other cancers such as ovarian, bladder, non-small cell and small cell lung cancer, melanoma, lymphomas, myelomas, head and neck cancer and colon cancer.[28] Cisplatin, oxaliplatin and carboplatin are square planar Pt(II) complexes that contain two inert 'non leaving group' ligands and two labile 'leaving group' ligands. However, even though these drugs show great success, they have issues with cell resistance and toxicity, which has prompted new and improved therapies to be developed.[28]

The mechanism of action of all three platinum complexes combines the cellular uptake, the aquation/activation step, DNA platination and cellular processing that eventually leads to apoptosis. [29]

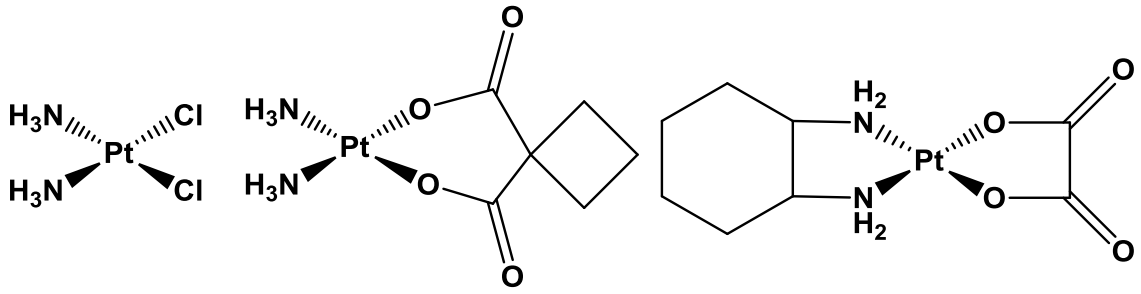

Figure 1.08. Platinum based anticancer compounds approved by FDA: cisplatin (left), carboplatin (centre) and oxaliplatin (right).[28]

Cisplatin was first synthesised in 1844 by M. Peyrone, while its chemical structure was only determined in 1893 by Alfred Werner. It did not gain any scientific relevance until 1965 when

Barnett Rosenberg a physicist at Michigan State University discovered that platinum electrodes after electrolysis formed compounds had the ability to inhibit cell division in *Escherichia coli*.[30] This platinum-based compound was identified as *cis*-dichlorodiammineplatinum(II) or cisplatin. Since its discovery of its chemotherapy properties, has given rise to a greater interest into the use of other coordination complexes of platinum, palladium and other noble metals in the treatment of cancer.[29, 31] The study of the effect of cisplatin on tumor cells was further carried out on two murine models of tumors, sarcoma 180 and leukaemia L1210. *In vivo* studies showed that among all proposed platinum complexes the most efficient and least toxic was that of cisplatin.[29, 31] The FDA approved cisplatin in 1978 for clinical use as an antineoplastic agent and since then it has become one of the most used drugs in chemotherapy. Cisplatin is recognised as one of the most effective anticancer drugs available on the market today and is included on the list of essential medicines by the World Health Organisations. Cisplatin is active and clinically proven in the fight against various types of cancers including sarcomas, cancers of soft tissue, muscles, bones and blood vessels.[29] During clinical trials problems with cisplatin arose regarding the toxicity of the compound as well as cell resistance against the compound.[28] To compensate this cisplatin and other cancer drugs such as 5-fluorouracil, methotrexate and paclitaxel has been trialled with success as part of a combination therapy to try and reduce cell resistance.[32]

Cisplatin is a square planar Pt(II) complex, consisting of two chlorides and two ammonia in cis position with respect to the central platinum +2.[28] Although it is still not fully known how cisplatin's uptake and efflux to and from the cell occurs, studies have shown that there are three possible routes of drug entry into the cell. The first is said to be passive diffusion through the transmembrane channels. The second type of transport is by protein carriers such as OTCs (organic cation transporters which are involved in the transport of endogenous cations, these are OCT1 and OCT2).[33] The third involves the use of protein carriers such as CTR1 (copper transporter 1, Figure 1.09). Studies have shown that mutation of this protein CTR1 increases cisplatin resistance and reduction of platinum levels in the cell. The efflux from the cell is mediated by two ATPases, ATP7A and ATP7B and by MRP (multidrug resistance Protein)[27, 34] The MRP family of proteins contains at least six members, MRP1 and five of its homologues, these are membrane proteins which in turn belong to the ABC superfamily (ATP binding cassette).[35]

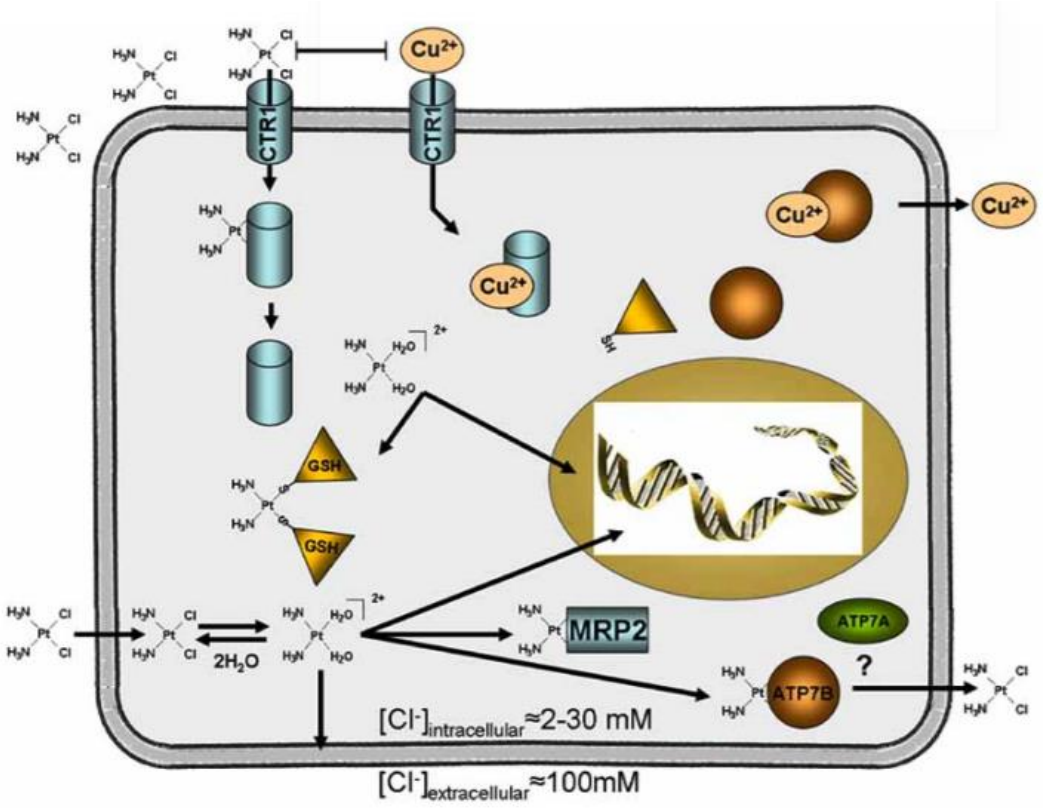

Figure 1.09. Schematic depiction of cisplatin uptake through passive diffusion, CTR1 transporter proteins, the aquation of the molecule in the cell cytoplasm to the entry of the cell nucleus and binding to DNA and efflux via ATPase ATP7B[27].

Cisplatin undergoes hydrolysis after it crosses the cell membrane, due to a drop of chloride concentration, leading to the formation of the monoaquo-species $[Pt(NH_3)_2Cl(OH_2)]^+$ and the diaquo-species $[Pt(NH_3)_2(OH_2)_2]^{2+}$ that act as acid forming a mixture of water soluble hydroxides, hydroxyl-complexes and even dimers (Figure 1.10)[36].

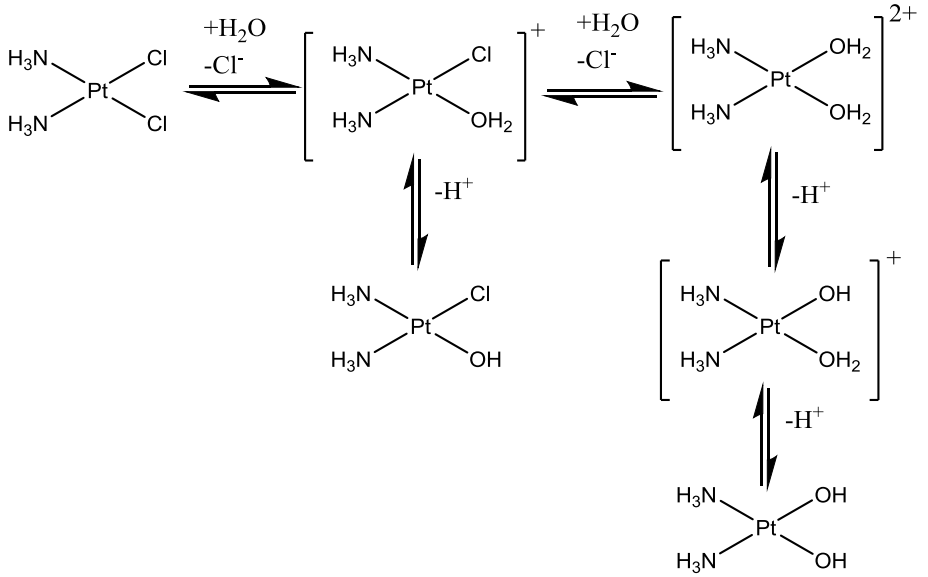

Figure 1.10. Schematic showing the equilibrium of cisplatin hydrolysis and the formation of hydrated complexes in aqueous solution.[37]

The aqueous species that is formed from this process are considered to be the reactive forms of cisplatin, being very electrophilic in nature and possessing excellent leaving groups react readily with nucleophilic species. The main target of cisplatin is DNA, with the target groups usually the secondary or tertiary nitrogen bases especially the purine ones (adenine and guanine) due to the nucleophilicity of the imidazole portion. The guanine bases that are situated in the major groove of DNA are sterically exposed and therefore are accessible to cisplatin and a covalent bond is therefore formed at position N7 (Figure 1.11).[27]

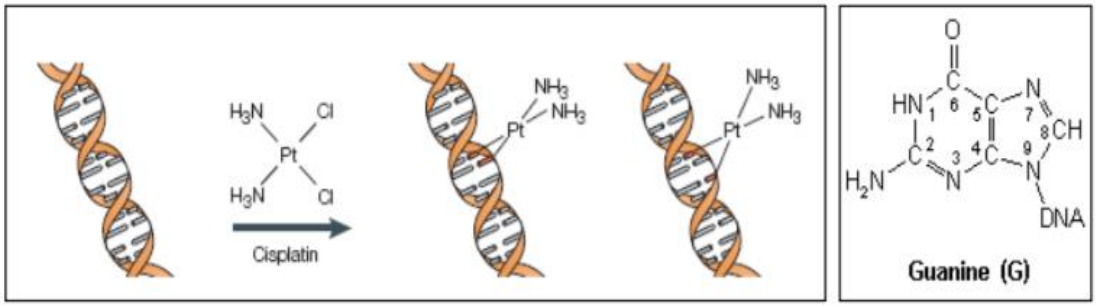

Figure 1.11. Cisplatin – DNA interaction, Figure shows the cisplatin binding to DNA forming both 1,2 intrastrand and 1,3 intrastrands. Also shows a guanine residue with N7 binding site for the Pt(II) complex.

Cisplatin forms 1,3 intrastrand and 1,2 interstrand crosslinks between both DNA strands inducing a variety of cellular responses such as transcription inhibition, replication arrest, cell cycle arrest which in turn leads to necrosis and apoptosis.[29] The main adducts formed between DNA and cisplatin are shown in Figure 1.12.[36]

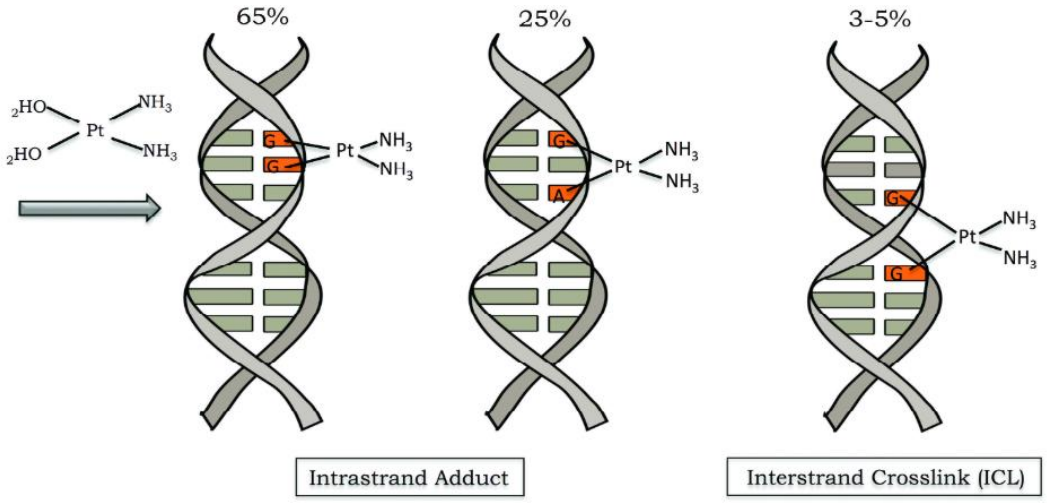

Figure 1.12. Covalent bonds formed with activated cisplatin molecule and DNA. The major DNA lesions are intrastrand DNA adducts and interstrand crosslinks.[36]

Cisplatin over the years has been used as the sole chemotherapy agent, but has also been seen that the complex is highly toxic on the patient with side effects that include fever, myelosuppression (condition where bone marrow activity is reduced), hyposthenia, nausea and vomiting, nephrotoxicity (kidney damage)[38] and neurotoxicity.[34] Although cisplatin treated cancer patients show high responsiveness towards the drug, some patients will relapse eventually with cisplatin resistance cancers. Cisplatin resistance mechanism is caused by changes in the cellular uptake of cisplatin and efflux of cisplatin from the cell, increased detoxification of the drug, inhibition of the apoptosis cycle and increased DNA repair see Figure 1.13.[39] Cisplatin resistance has prompted research into 2nd and third generation platinum drugs, Carboplatin being the second generation (used to treat in particular ovarian cancer) and oxaliplatin the third generation platinum drug (used to treat colorectal cancer, one of the most cisplatin resistant cancer).[27,30]

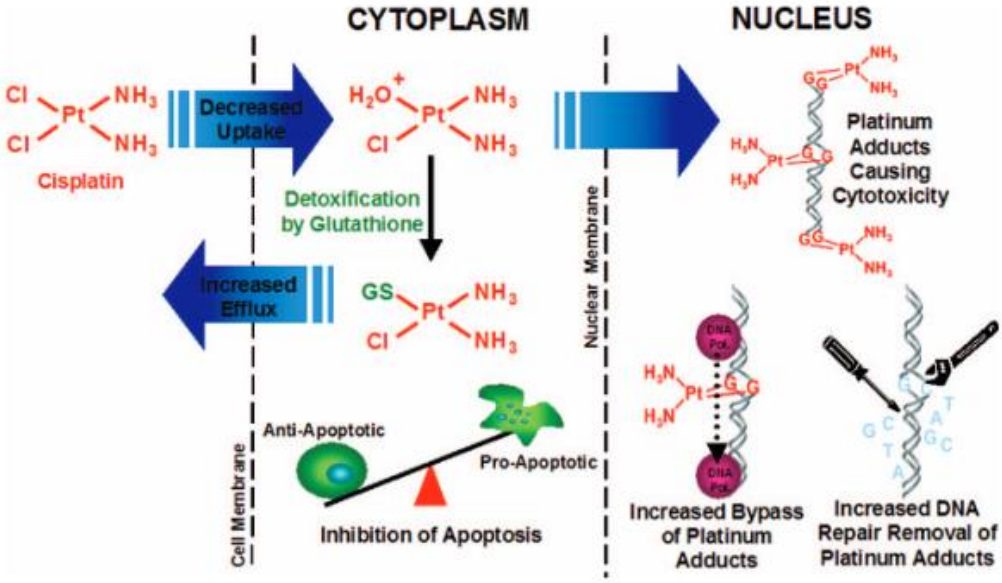

Figure 1.13. Shows the proposed mechanism of cellular resistance of the drug cisplatin. Increased efflux from the cell, decreased uptake of the drug into the cell and increased DNA repair, increased detoxification, inhibition of apoptosis and increases in platinum-DNA adduct bypassing all lead to cisplatin tumor resistance.[39]

1.1.4.2 Ruthenium-based Anticancer Agents

Ruthenium complexes are thought to be less harmful than platinum based agents and are thought to fragment DNA. Ruthenium(III) is considered to be a bio reductive metal which suits treatment of highly reductive tumor tissue over normal healthy tissue with ruthenium(III) becoming ruthenium (II). Ruthenium drugs are designed to mimic platinum based drugs for targeting DNA.[40] The toxicity of ruthenium drugs are less than those of platinum based drugs and the reactivity of Ru(II) complexes are greater than those of Ru(III) complexes. The non-toxic Ru (III) can be administered as a prodrug, at pH 7 the drug is inactive. The pH of cancer cells is lower than that of normal cells and when the Ru(III) enters the cell the complex is reduced to the active Ru(II) complex. It is thought that reduction occurs either inside the cell, by mitochondrial proteins or microsomal single electron transfer proteins or by trans-membrane electron transport systems which are situated outside the cell, which means that for the drug to be effective against cancer cells it does not require entry into the cell.[41] [42] One such ruthenium(III) drug is NAMI-A which has undergone clinical trials and has been found to have a different mode

of action relative to the platinum complex cisplatin. It is not cytotoxic but has anti-proliferative activity.[41]

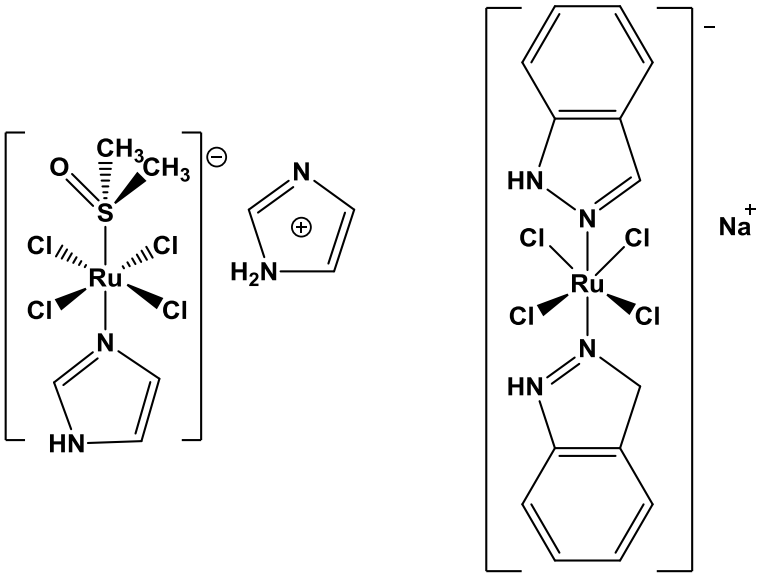

Figure 1.14. Structure of Ruthenium NAMI complex (left) and of NKP1339 (right).[43]

Another ruthenium based complex NKP1339, trans-[tetrachloridobis (1H-indazole) ruthenate(III) (Figure 1.14) has also had clinical trials and is found to active in solid tumors. The mechanism of action is thought to be via binding to serum proteins such as albumin which then accumulates in the endoplasmic reticulum of the cell. Since tumors have poor lymphatic drainage the accumulations of albumin in the tissue is detected and apoptosis is triggered. Under hypoxic conditions this Ru(III) complex is thought to generate ROS , which leads to protein damage and subsequent endoplasmic reticulum response that leads to cell death.[44]

1.1.4.3 Cobalt-based anticancer agents

Cobalt(III) complexes have been studied as potential carriers of drugs to the hypoxic environment of cells. Cobalt(III) can be reduced to cobalt(II) in a reductive tumor environment in some cases releasing the toxic active ligand to kill the cancer cells.[45]

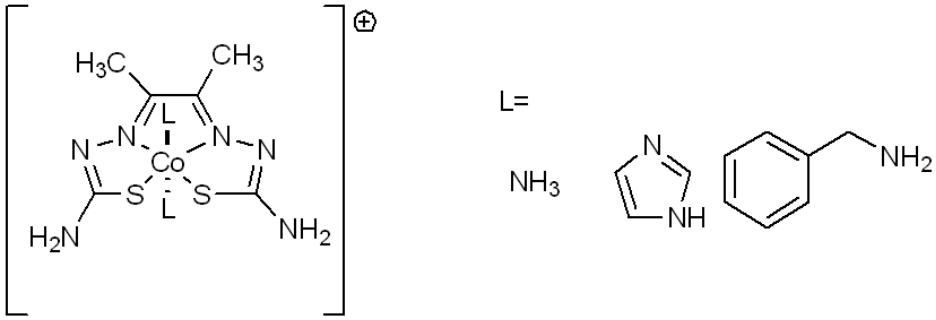

Figure 1.15. Structure of cobalt bis(thiosemicarbazone) complex.[46]

Cobalt bis (thiosemicarbazone) complex (Figure 1.15) is a cobalt(III) complex which becomes cobalt (II) in hypoxic environments leading to the loss of its ligands "L" which have been shown to be cytotoxic. The reduction to cobalt(II) produces a labile d^7 complex, which facilitates the removal of ligands within its coordination sphere. Therefore, these kind of complexes can perform as chaperones to selectively deliver cytotoxic ligands to hypoxic environments where metal reduction is favoured.[46]

1.1.4.4. Copper Anticancer based complexes

Copper is a common metal in the human body, serving as a cofactor for certain enzymatic reactions such as Cu/Zn-superoxide dismutase, cytochrome c oxidase, thyrosinase, ceruloplasmin and other proteins that are involved in respiration, iron transport, metabolism and cell growth.[47] Copper exists outside the body mainly as Cu(II) and when complexed it favours square planar, square pyramidal or distorted octahedral geometry due to its d^9 configuration and Jahn-Teller effect. Cu(II) prefers nitrogen and oxygen ligands and is capable of coordinating 4-6 ligands to the metal centre. Copper complexes are ideal alternatives to metal based complexes due to their range in oxidation states and coordination ability.[48]

The role of copper in cancer is not straightforward as copper is thought to aid in the generation of new blood vessels, through the activation of epidermal growth factor which promotes cancer cell survival. It is also increase the formation of ROS, has an involvement in necrotic cell death and is involved in the upregulation of Bax that can induce apoptosis.[49] The study of copper complexes has been undertaken since cisplatin was introduced as a chemotherapy drug. Various copper(II) complexes were found to be cytotoxic, with NSAIDs or Schiff bases being the most common ligands. These Cu(II) complexes display catalytic activity against ROS and may cause DNA strand breakages.[50] The copper complex of 1,10-phenanthroline (Figure 1.16) has been studied for its chemical nuclease activity. Over the years there has been many Cu-complexes synthesised and reported as cytotoxic agents which have shown anticancer activities in both vitro and in vivo tests. The dichloro(1,10-phenanthroline)copper(II) complex showed to oxidatively degrade DNA and RNA by attacking the sugar group.[51, 52] The clinical activities of complexes of 1,10-phenanthroline have shown great potential with antiturmoural, antimycobacterial, antifungal and antimicrobial activities.[53-55]

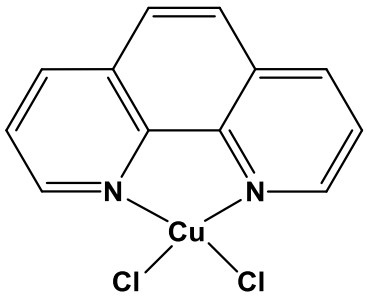

Figure 1.16. Structure of the anticancer complex dichloro(1,10-phenanthroline)copper(II)

1.1.5. Chalcogens

The elements found in group 16 of the periodic table are classed as chalogens.[56] The word chalcogens derived from the Greek word *khalkós*, which means copper, and the Latinized Greek work *genes*, meaning born or produced. This group of elements are also referred to be members of the oxygen family. They comprise of the elements oxygen (O), sulphur (S), selenium (Se), tellurium (Te) and the radioactive element polonium (Po).

Sulphur has been known since before the Middle Ages and in the 18th century oxygen was first discovered as an element. The elements selenium, tellurium and polonium were all discovered in the 19th century, while livermorium was discovered as late as 2000. All elements in the chalcogens family have six valence electrons and so are two electrons short of a full outer shell. They have oxidation states ranging from -2, +2, +4 and +6. They have relatively low atomic radii, especially the lighter ones.[56] Lighter chalcogens are typically non-toxic in their elemental form, and they are very often critical to life and are involved in most biological activities. However, the larger or heavier chalcogens are normally more toxic to an organism. Chalcogens are involved in many biological processes, either it being a nutrient or a toxin. The lighter ones such as oxygen and sulphur are rarely toxic and are usually helpful in their pure form and are the building blocks for many proteins and enzymes. Selenium is an important nutrient but can be toxic in high concentrations. Tellurium has unpleasant effects (micro-organisms however can utilize it) and polonium is extremely harmful due to its chemical toxicity and its radioactivity properties.

Tellurium lies in the diagonal that identify the metalloids, together with Boron (B), Silicon (Si), Germanium (Ge), Arsenic (As) and Antimony (Sb). These metalloid elements show properties of both metals and non-metals and are referred to as semi-metals. One of the properties metalloids have is they act like non-metals when reacting with a metal and act like metals when reacting with non-metals.[57] Some physical-chemical properties of chalcogens are listed in Table 1.1.

Table1.1. Selected properties of elements in group 16 of the periodic table.[58, 59]

Property	**Oxygen**	**Sulfur**	**Selenium**	**Tellurium**	**Polonium**
Atomic symbol	O	S	Se	Te	Po
Atomic Mass (amu)	16	32.07	78.96	127.6	209
Atomic number	8	16	34	52	84
Atomic radii (pm)	48	88	103	123	135
Density (g/cm^3) at 25^{o}C	1.31 (g/L)	2.07	4.81	6.24	9.2
Electron affinity (kJ/mol)	-141	-200	-195	-190	-180
Electronegativity	3.4	2.6	2.6	2.1	2
First ionization energy (kJ/mol)	1314	1000	941	869	812

Ionic radii (pm)	140 (-2)	184 (-2), 29 (+6)	198 (-2), 42 (+6)	221 (-2), 56 (+6)	230 (-2), 97 (+4)
Melting point/ boiling point (°C)	(- 219/-183)	115/445	221/685	450/988	254/962
Normal oxidation states	-2	(-2), (+4), (+6)	(-2), (+4), (+6)	(-2), (+4), (+6)	(-2), (+4)
Reaction with Oxygen		SO_2	SeO_2	TeO_2	PoO_2
Reaction with Hydrogen	H_2O	H_2S	H_2Se	None	None
Reaction with Nitrogen	NO, NO_2	None	None	None	None
Reaction with X_2 (where X_2 is halogen)	O_2F_2	SF_6, S_2Cl_2, S_2Br_2	SeF_6, SeX_4	TeF_6, TeX_4	PoF_4, $PoCl_2$, $PoBr_2$
Valence electron configuration	$2s^22p^4$	$3s^23p^4$	$4s^24p^4$	$5s^25p^4$	$6s^26p^4$

1.1.6. Tellurium

Tellurium was first discovered in 1782, by the chemist Franz-Joseph Mueller von Reichenstein (1742 – 1825) while studying gold containing ores. The name Tellurium is derived from the Latin word *tellus*, meaning Earth. It's abundance in the earth's crust is 0.027 ppm which is similar to that of silver, however since its discovery back in 1782, tellurium chemistry was mostly ignored in the biochemical field and it has only started in recent years.[60] Tellurium can be found naturally in two elemental forms, one of them a metallic silver in form whilst the other is brownish black in form. Tellurium exhibits some spectroscopic properties that are ideal for the characterization of tellurium compounds. Tellurium found in its natural form contains a mixture of several different isotopes, ^{120}Te (natural abundance 0.09%), ^{122}Te (2.55%), ^{123}Te (0.89%), ^{124}Te (4.74%), ^{125}Te (7.07%), ^{126}Te (18.84%), ^{128}Te (31.74%) and ^{130}Te (34.08%).[60]

Metalloid complexes have been noted to have particular biological effects on cells and tissues and their particular therapeutic potential have been studied for the last number of years.[61].

Since its discovery in 1782, tellurium has been considered to be of little significance in normal daily life. There are some exceptions, however, such as the ever-increasing presence of CdTe particles in photochemical devices present in solar panels and photovoltaic systems (Figure

1.17).[62] For years, tellurium has been considered toxic and therefore its various inorganic, complex and organic compounds have been ignored until recently in medicine, toxicity, and pharmacology and drug development. It is however surprising the disinterest in tellurium in life sciences is considering the variety of tellurium chemistry.

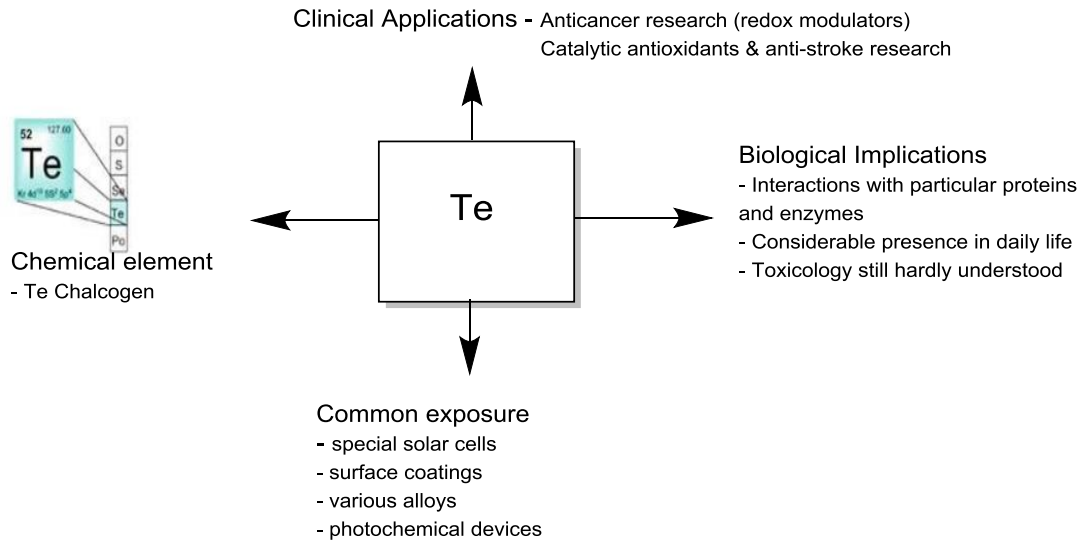

Figure 1.17. Presence of Tellurium in daily life.[63]

Tellurium chemistry gives rise to a rich array of inorganic and organic compounds, including inorganic salts (for example tellurides Te^{2-}, tellurites TeO_3^{2-}, and tellurates TeO_4^{2-}), inorganic complexes and a vast variety of organotellurium compounds (Figure 1.18). Many of these compounds have been found to be stable. Tellurium and its many compounds are reactive and interact freely with biomolecules, including cysteine- and selenocysteine- proteins and enzymes. The selective inhibition by tellurium compounds of certain main enzymes can be essential in future therapeutic interventions. Even though tellurium is a non-essential trace element, it does not mean that its applications are limited in terms of drug design but can be as effective as those complexes of gold and platinum.[63]

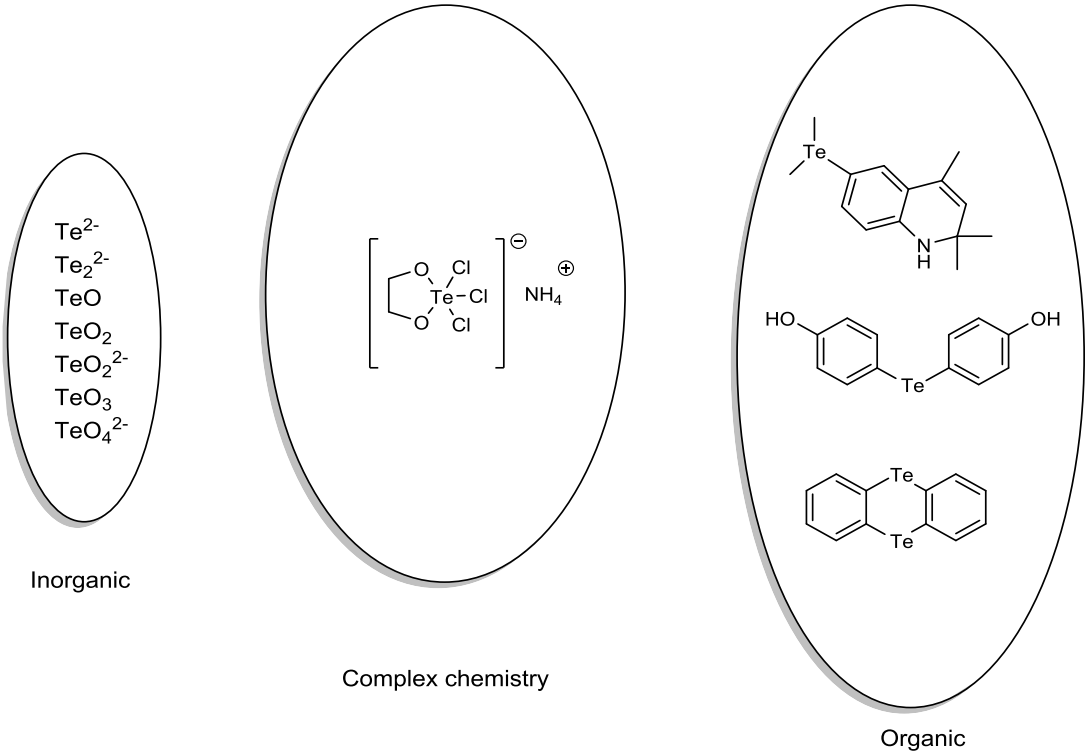

Figure 1.18. Range of tellurium chemistry from its in-organic compounds, complexes and organotellurium compounds. All three types of tellurium complexes have been of interest recently for their biological activities.[81,82]

In particular, some tellurium(IV) complexes have shown excellent anticancer properties and have been the subject of many research papers over the last years. It has been found that by inactivating cysteine proteases in the human body, specific Te(IV) complexes influence thiol redox biological activity. The mechanism of action of these Te(IV) complexes consists on the formation of Te(IV) – thiol chemical bond or a disulfide bond in a specific protein which in turn leads to a conformational change in the activity site of the protein which possibly results in the loss of that proteins biological activity.[61]

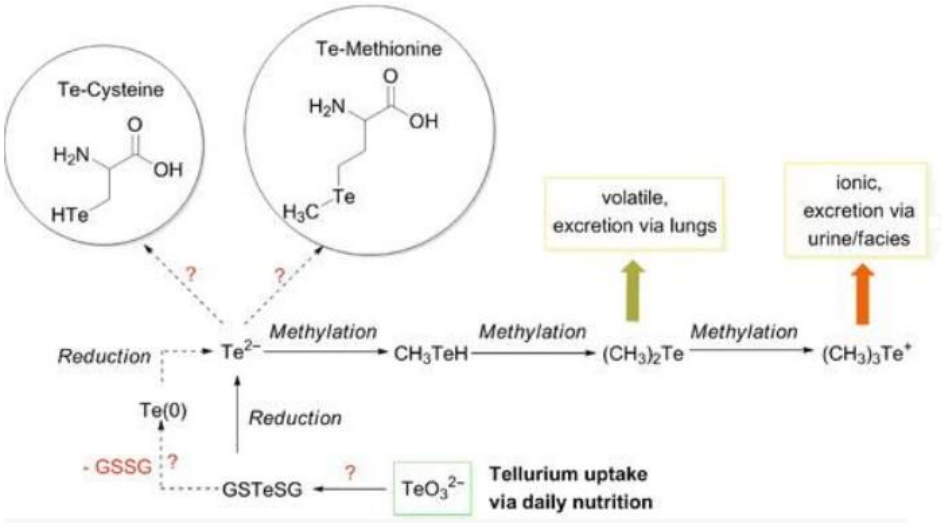

Figure 1.19. Tellurium is metabolism. Some micro-organisms can reduce tellurium salts to the non-toxic Te(0) or elemental form while humans after ingesting tellurium can excrete it through their lungs or urine following methylation.[63]

Tellurium is not required in living organisms and does not have any benefit to life and so is regarded as non-essential trace element in nature. Even though tellurium is not required for any organism's survival, many organisms are still able to utilise tellurium and have the ability to excrete many forms of tellurium in its methylated form (Figure 1.19).[63] The method of tellurium metabolism varies between different organisms, but it follows the same metabolic pathways which are used in the metabolism of selenium and sulfur.[63]

Studies have shown that microorganisms can exist in environments that contain tellurium salts and have developed high toxicity resistance against tellurium. Many of these organisms overtime have evolved to form a bio-reductive approach in coping with tellurium and also enhancing their ability to remove tellurium by generating elemental tellurium. Some of these microorganisms have the ability to survive in environments that are rich in tellurate and tellurite and have adapted in a way as to cause the reduction of these tellurium compounds to a less toxic form, in this case elemental tellurium Te.[64] Also in oxygen depleted environments, reduction of these anions to metallic Te allows some of these organisms to support anaerobic growth by enabling respiration by using these salts or anions as electron acceptors as a substitute for oxygen. These organisms that can utilise tellurate and tellurite are rare and three such bacteria have been identified as *Bacillus selenitireducens, Sufurospirillum barnesii and Bacillus beveridge*i.[64] These three bacteria have been isolated from deep ocean hydrothermal vent worms by Csotonyi and Baesman et al.[65, 66] When these bacteria were grown with tellurate or

tellurite as terminal electron acceptors they produced uniformly sized nanoparticles of elemental Te, such as nanorods of 10nm x 200nm in size for *Bacillus selenitireducens* and irregular spheres less than 50nm by *Sufurospirillum barnesii*.[65, 66]

In certain organisms reduction of tellurium salts continues further to H_2Te which is then converted through methylation to $(CH_3)_2Te$ or to ionic $(CH_3)_3Te^+$ and in these two states can be excreted by the organism. Certain fungi can produce $(CH_3)_2Te$ which can be toxic, but because of its volatility can be easy removed.[67] Biovolatization plays a key role in removal of tellurium from the fungi but also from the environment that the fungi resides in. The tellurium species H_2Te, $(CH_3)_2Te$ and $(CH_3)_3Te^+$ are not the only tellurium compounds that can created by living organisms. It has been known that in cases of low or no sulfur sources some fungi, if in the presence of Na_2TeO_3, can produce tellurium containing amino acids such as tellurocysteine, and telluromethionine.[67] It is not understood if these tellurium amino acids play any biochemical role in these fungi but fact that they are present tells that: (1) Tellurium may not be as foreign to biochemistry as once thought but is in fact metabolised by various microorganisms which possess the ability to utilize these tellurium compounds; (2) in harsh environments such as sulfur depletion, tellurium can breach the void and be exchanged for sulfur in some biomolecules. Therefore, tellurium can be considered as having an essential role in biochemistry, even if it is due to deprivation of sulfur for these organisms to exist.

Tellurium compounds in nature have high reactivity and selectivity towards sulfur and selenium biomolecules. These interactions often occur in the form of redox reactions. Tellurium based compounds such as tellurides (RTeR), telluroxides (RTe(O)R), tellurols (RTeH) and ditellurides (RTeTeR) are redox-active and the oxidation states range from -2 to +6.[68] Tellurium shows a high affinity to other chalcogens such as oxygen, sulfur and selenium.[68] The reactive oxygen species (ROS), such as H_2O_2 has the ability to oxidise telluroxides and tellurols to ditellurides with the peroxide acting as an electrophile. Thiols on the other hand readily behave as reducing agents for tellurium agents, and in doing so transform telluroxides to tellurides and ditellurides to tellurols and in this instance the nucleophile is the thiol.[68]

Most tellurium compounds display glutathione peroxidase (GPx)-like activity and when glutathione (GSH) is present can catalyse H_2O_2 reduction (Figure 1.20). Organotellurides were studied by Kumar et al and have shown to be chain breaking antioxidants whose biochemical activities resemble vitamin E. These vitamin E mimics can reduce peroxyl radicals with greater efficiency than α-tocopherol and in the presence of thiol reducing compounds are capable of decomposing hydroperoxides.[69]

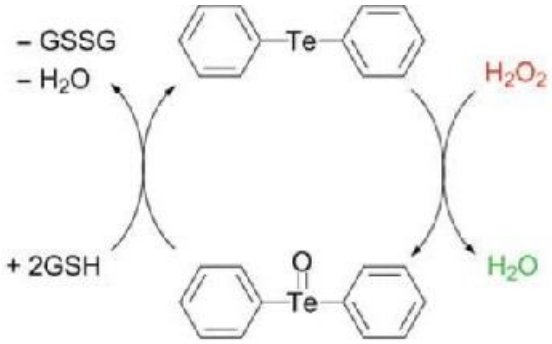

Figure 1.20. Reduction of H_2O_2 in the presence of glutathione with a tellurium catalyst.

Tellurium agents interact with proteins and enzymes that contain cysteine residues in a way that can be detrimental to the proteins and enzymes activity by interfering with the 'cellular thiolstat' eventually leading to cell death via apoptotic pathways.[70] *In vivo* studies with tellurite on rats and mice show that ingestion of TeO_3^{2-} cause inhibition of squalene epoxidase which results in transient demyelination of peripheral nerves caused by the binding of methyl-tellurium complexes to the thiol groups of vicinal cysteine residues that are situated in the active site.[71] Toxicity studies of organotellurium compounds were also studied by Nogueira on mice and rats and found that the toxic effects of these compounds coincide with interactions between the tellurium and the thiol groups of the cysteine.[72]

As mentioned earlier tellurium has a high affinity to sulfur compounds and therefore certain biological effects are associated with this tellurium-sulfur chemistry. However tellurium has also a high affinity to selenium, therefore some selenium containing targets may include enzymes such as selenoprotein P and also various GPx enzymes.[73] Tellurium compounds can also effect the activity of the human selenoenzyme thioredoxin reductase (TrxR) due to selenium-tellurium interactions. Tellurium interactions with antioxidant selenium type proteins and enzymes may indirectly bring about oxidative stress rather than acting as antioxidants. The effects of these

interactions with these proteins and enzymes can result in problems ranging from severe liver damage to impairment and quite possibly hippocampal and prefrontal cortex neuron damage.[74]

1.1.6.1. Oxidative stress on cancer cells *versus* non cancer cells

Reactive Oxygen Species (ROS) are all chemically reactive species which all contain oxygen. The ROS species include the free radicals such as superoxide anion (O_2•-) and the hydroxyl (OH•) radical. They are also made up of non-radical oxygen forms, which include hydrogen peroxide (H_2O_2) or nitroperoxide (ONOOH). These ROS species are constantly being produced by eukaryotic cells during aerobic cellular metabolism.[75] These ROS species play a key role in signaling pathways in response to intra- and extra-cellular changes. They are also removed from the cell by the anti-oxidant systems that are located inside the cell. The redox status of a cell is a function of the relative concentrations of both the oxidized and reduced forms of ROS, proteins, enzymes, RNS (reactive nitrogen species, thiol containing molecules and other cellular factors.[76] In a normal cell there is a balance between the generation and elimination of ROS species, and under normal physiological conditions there is an equilibrium between the these ROS species and the antioxidants. Oxidative stress occurs when this equilibrium is changed by an increase in ROS species which lead to damage of the cellular macromolecules.[77]

Cancer cells are cells that exhibit uncontrolled growth that potentially metastasize leading to lethal malignancy. For these cells to continue to undergo cell division and proliferation, these cells must adapt their metabolic processes to promote their survival.[78] Even though the mechanisms of cellular transformation during carcinogenesis in different cancer cells can occur in variety of cellular pathways, the metabolic requirements of all these cells are generally similar.[79] It is seen that cancer cells have increased metabolic rates and therefore have increased ROS formation which leads to an increased oxidized environment. Therefore, these cells must adapt their antioxidant scavenging pathways to evade ROS induced death. To achieve this cancer cells must up-regulate their antioxidant scavenging molecules such as glutathione peroxidase (GPx), glutathione-S-transferase (GST), glutaredoxin (Grx), thioredoxin (Trx), superoxide dismutase (SOD) and catalase (CAT).[78, 79] Several of these antioxidants rely on the reducing properties of NADPH, which is found to be induced in cancer cells and is seen as a key metabolite of the pentose phosphate pathway, to help maintain their activity to removed ROS

and repair any ROS induced damage. This therefore leaves cancer cells with little or no room to adapt future ROS induction and so if the ROS system is altered slightly it would result in oxidative stress dependent cell death.[78-80] In normal healthy cells, ROS occurs in steady levels and so are easily removed from the cell thus preventing cellular damage. If however, there does occur an elevated level of ROS in a healthy cell, these cells can counteract these increased ROS levels by induction of the antioxidant system.[78, 81]

The fact that cancer cells have such small room to adapt to any extra ROS induced damage it makes them more susceptible to oxidative stress than non-cancer cells. Therefore, the induction of oxidative stress can be achieved by using redox modulators such as Tellurium compounds. These redox modulating compounds can provide an interesting therapeutic window and has been seen as a promising avenue in anti-cancer therapy.[82] Tellurium compounds have shown higher selectivity and sensitivity in cancer cells and can induce oxidative stress on these cells which result in cell apoptosis. The pro-oxidant properties of these Te compounds, that are responsible for their cytotoxicity and anti-cancer activity are mainly down to ROS generation and oxidation of thiol containing proteins.

1.1.6.2. Antimicrobial properties of Tellurium compounds

Throughout human history bacteria has been the main causes of infectious diseases and in particular the Gram-negative pathogens *Escherichia coli (E.Coli)*,and *Enterobacter cloacae (E.Cloacae).* Most foods consumed daily can harbor the bacterial strain *E.Coli* which when consumed can lead to illness. These Gram-negative pathogens are treated with antibiotics, however over the years these pathogens have built up a resistance to these antibiotics which has in recent years become a concern to world health organisations.[83] This resistance to antibiotics has made the fight against disease causing bacteria much more difficult. It is therefore important to find new drug compounds that can combat these bacterial strains. *E.Cloacae* is a member of the Enterobacteriaceae bacteria family. These bacteria are responsible for infectious diseases and is treated with antibiotics such as gentamicin or tobramycin. However, these two antibiotics are seen to be very toxic, in particular to people who suffer renal failure.[84] Therefore, over the last few years there has been advances in research and

development into alternative drug compounds that are both non toxic and effective against antibiotic resistant bacteria.

One such drug is tellurium AS101, which has shown antibacterial properties against bacteria *K. pneumonia*, *E. Cloacae* and has been investigated for its antimicrobial effects against the bacteria *Aeromonas salmonicida.*[85] AS101 has been shown to be non-toxic in various cell cultures as well as *in vivo* models. It is presently undergoing phase II clinical trials for the treatment of psoriasis and atopic dermatitis.[86] It therefore appears that AS101 maybe a potential substitute or supplement to antibiotic treatments. The mechanism of action of AS101 against Gram-negative bacteria indicates that the molecule can penetrate the cells of the bacteria through the outer membrane. The purpose of this outer membrane on bacterial cell walls is to serve as a permeability barrier, preventing entry of toxic compounds while allowing the influx of nutrient molecules through porins.[87, 88] Porins are pore forming proteins found on the cells outer membrane. The porins on the outer membrane of Gram-negative bacteria are large enough to allow AS101 (MW 312Da) to penetrate the cell.[86] AS101 enters the bacteria via the bacterium porins which leads to swelling and eventually to cell death.

Another tellurium compound that has shown antimicrobial activity is tellurium SAS. This molecule has shown strong antimicrobial action against *E. Coli.*[85] Investigations into the compounds mechanism of action against this bacteria has determined that it is different from that of AS101. In AS101, the molecule penetrates through the outer membrane of the cell via the protein porins, SAS is too large to enter through the porins so it is assumed that the molecule penetrates through the lipid layer of the outer membrane.[89] When SAS enters the cell membrane it causes damage to the Na^+/K pumps that are located in the inner membrane. This damage causes a leakage of ions through the damaged membrane. The leakage of phosphorus ions indicates loss of phosphorus containing molecules such as ATP and other nucleotides from the cell. These cells cannot multiply under these conditions; therefore the bacteria growth is inhibited.

These two tellurium compounds have shown interesting activity against antibiotic resistant strains of bacteria and therefore these and other future tellurium compounds can be utilized in the fight against present and future bacterial induced diseases.

1.1.6.3. Anticancer properties of Tellurium compounds

Tellurium occurs in both inorganic and organometallic complexes. Some of these compounds have been studied and have shown to express specific biological activities.[90] Alkali metal tellurites and tellurates show activity in microbiology, organotellurides and diorganoditellurides have potent antioxidant activity, while inorganic and organic tellurium compounds are potent inhibitors of caspase and cathepsin proteases.[90] Caspases are a family of protease enzymes that have crucial importance in programmed cell death which include apoptosis, pyroptosis, necroptosis as well as inflammation.[91, 92] Caspases get their name due to their specific cysteine protease activity, in that a cysteine residue located in the active site which nucleophillically attacks and cleaves a target protein only after an aspartic acid residue.[91] It is estimated that up to 11 or 12 confirmed and named caspases in humans are involved in various cellular functions.[91] Cathepsins B, L and D are lysosomal cysteine and aspartic proteases which are found in almost all mammalian cells. The main function of cathepsins is protein recycling within the lysosome and are said to be involved in a variety of other physiological, as well as pathological processes, which include maturation of the MHC class II complex, bone remodelling, tumor progression and metastasis, rheumatoid arthritis and osteoarthritis. Overexpression and secretion of cathepsins induces invasion and metastasis of tumor cells (Figure 1.21).[93]

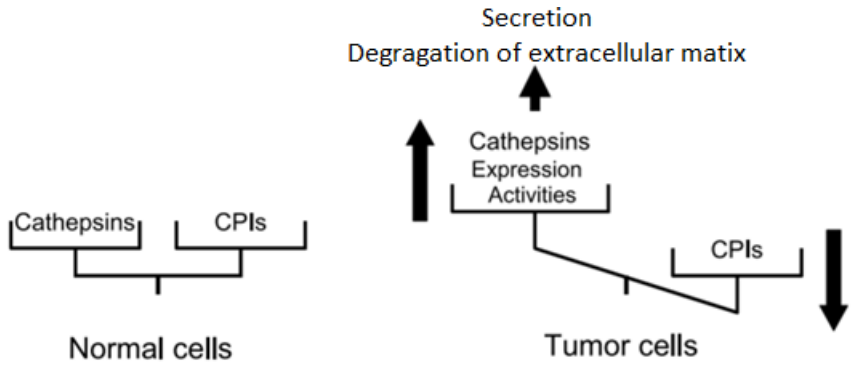

Figure 1.21. Imbalance between cathepsins and cysteine protease inhibitors (CPIs) in tumor cells. Overexpression and secretion of cathepsins induce the invasion and metastasis of tumor cells[99]

At present two inorganic tellurium(IV) compounds have been studied for their anti-cancer properties and their mechanism of action. These compounds are trichloro(dioxoethylene-*O,O'*)tellurate or AS101 and Octa-*O*-Bis-(*R,R*)-tartarate ditellurane (SAS) (Figure 1.22).

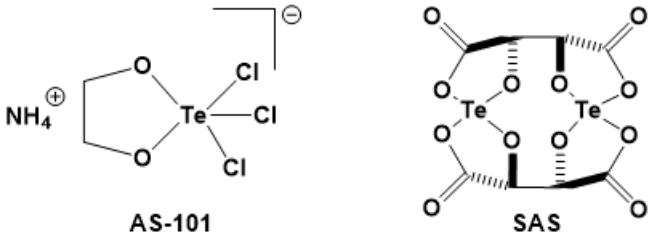

Figure 1.22. Structure of: left, tellurium(IV) compound AS101 (Ammonium trichloro(dioxoethylene-*O,O'*)tellurate) and, right, Octa-*O*-Bis-(*R,R*)-tartarate ditellurane (SAS).

Over the last few years, AS101 has been the most studied synthetic tellurium compound with respect to its biological activity. AS101 is a potent immunomodulatory agent both in *vitro* and *in vivo* and has shown a variety of potential therapeutic applications. It has been trialled in phase I and phase II clinical studies with cancer patients.[100] The biological activities primarily results from the specificity of Te(IV) redox-modulating activities which enable inactivation of certain cysteine proteases such as cathepsin B, inhibition of specific tumor survival proteins such as survivin, or the obstruction of tumor IL-10 production.[94] IL-10 or interleukin-10 is an anti-inflammatory cytokine and is also known as human cytokine synthesis inhibitory factor (CSIF).[95] Most or all of these properties have direct influence on anti-cancer activity or sensitization of tumors to chemotherapy. Along with these properties, inorganic Te(IV) compounds show excellent safety profiles which means that both tellurium complexes SAS and AS101 have a promising future in anti-cancer therapy.[94]

1.1.6.4. Ammonium trichloro(dioxoethylene-*O,O'*)tellurate (AS101)

Ammonium trichloro(dioxoethylene-*O,O'*)tellurate (AS101, Figure 1.22) is an inorganic ammonium tellurate with high affinity to thiols which gives it its therapeutic property against certain cysteine proteases. The mechanism of action of AS101 relates to its ability to react with thiols of cysteine residues and catalyzing their oxidation.[96] AS101 is a small tellurium(IV) compound that has already undergone phase II clinical trials in cancer patients,[97] is a potent immunomodulatory both in *vitro* and in *vivo* and shows a variety of potential therapeutic applications.[96, 98]

Over the years, all the gathered information suggests that the biological activity of AS101 is related directly to the specific tellurium-cysteine chemical interactions. The Te(IV)-thiol bond may lead to conformational changes or disulfide bond formation in specific proteins or enzymes which in turn lead to that protein or enzyme losing its biological activity.[99, 100] It has been reported that the AS101 molecule specifically cause the inactivation of cysteine proteases yet exhibit no effect on other families of serine, aspartic and metalloproteases based upon their unique Te(IV)-thiol chemistry. This inactivation of cysteine proteases can be reversed by reducing agents such as $NaBH_4$, which supports the claims that inactivation of these cysteine proteases involves the oxidation of the catalytic thiol to a disulfide (Figure 1.23).[101, 102]

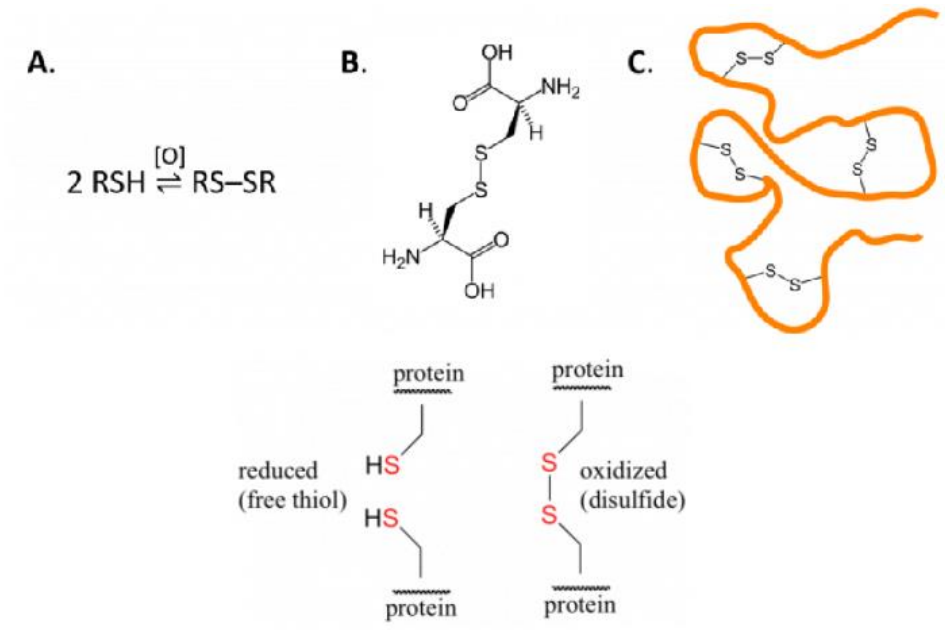

Figure 1.23. (A) Formation of disulfide from two thiol molecules; (B) Structure of cysteine amino acids containing S-S bridge; (C) Cysteine residues on a protein sequence with internal disulfide bridges. Disulfide bridges are important in proteins as they can maintain correct 3D structure its overall function within the biological system.

The thiol-Te interaction of AS101 inhibits activity of specific integrins by redox modulation. Integrins are transmembrane proteins receptors that facilitate cell extracellular matrix (ECM) adhesion. When chemically bound to a specific ligand, integrins can initiate signal transduction pathways that mediate cellular signals. Integrins are made up of two subunits, α and β and their combination has its own specific binding and signaling properties.[103] The development of cancer depends on the blood supply. Angiogenesis, the process of forming new blood vessels involves the migration, growth and differentiation of endothelial cells, is regulated through the activation of integrins including α1β1, α2β1, α6β1, αvβ3, and αvβ5 that are expressed on the surface of endothelial cells.[104, 105] The interactions between thiols and AS101 enables the inhibition of the integrin αvβ3 on endothelial cells. In solid tumors, the cancer cells express various growth factors that allows cells to escape from body's immune surveillance. IL-10 (Interleukin 10) which is an anti-inflammatory cytokine[95] is secreted spontaneously from a variety of human cancer cells which include ovarian carcinoma, melanoma, lymphoma, neuroblastoma, renal cell carcinoma, colon carcinoma, glioma and non-small cell lung cancer.[106-109] Patients found with various solid and hematopoietic tumors are seen to have elevated levels of IL-10.[110] In preclinical and clinical

studies of AS101, the activities of AS101 showed the molecules ability to cause the direct inhibition of the anti-inflammatory cytokine IL-10 and at the same time showed an increase in specific cytokine levels.[96, 111] These immunomodulatory properties were seen to be a crucial factor for clinical trials of AS101. Inhibition of the IL-10 by AS101 results in the de-phosphorylation of Stat3 (Signal transducer and activator of transcription 3) which is then followed by the reduced expression of Bcl-2 shown in Figure 1.24. These activities of AS101 are associated also to its ability to sensitize tumor cells to other chemotherapeutic drugs that results in increased apoptosis. AS101 was sensitizing the human aggression tumor GBM to paclitaxel (Taxol) in *vivo* and in *vitro* by IL-10 inhibition. Inhibition of IL-10 by AS101 due to Te(IV)-thiol interaction, result in the functional inhibition of integrin activity which give rise to a reduced expression of pAkt (which is a combination of proteins PI3K (phosphatidylinositol 3-kinase) and Akt (Protein Kinase B) that in turn leads to the decrease in pGSK3β (which is a multifunctional serine/threonine kinase found in all eukaryotes)[112] expression and in IL-10 production.[113]

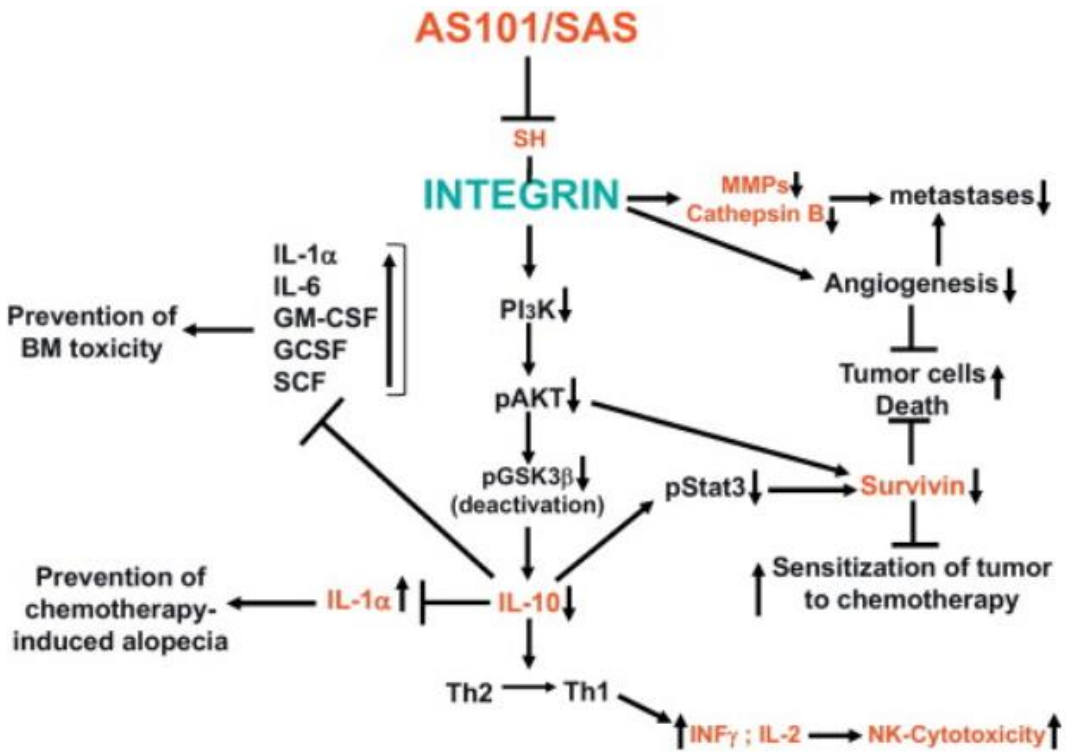

Figure 1.24. Protein expression pathway cascade when AS101 interact with integrin. The decrease in the IL-10 expression results in a decrease in pStat3 which in turn lowers expression of survivin increasing cell death, decreasing angiogenesis and metastases.[118]

Tellurium compounds have been ignored by research biologist in the past, because their instability in aqueous/physiological conditions. AS101 compound in an aqueous environment hydrolyses, forming $[TeOCl_3]^-$ which is understood to be the active part of the compound (Figure 1.25).[114]

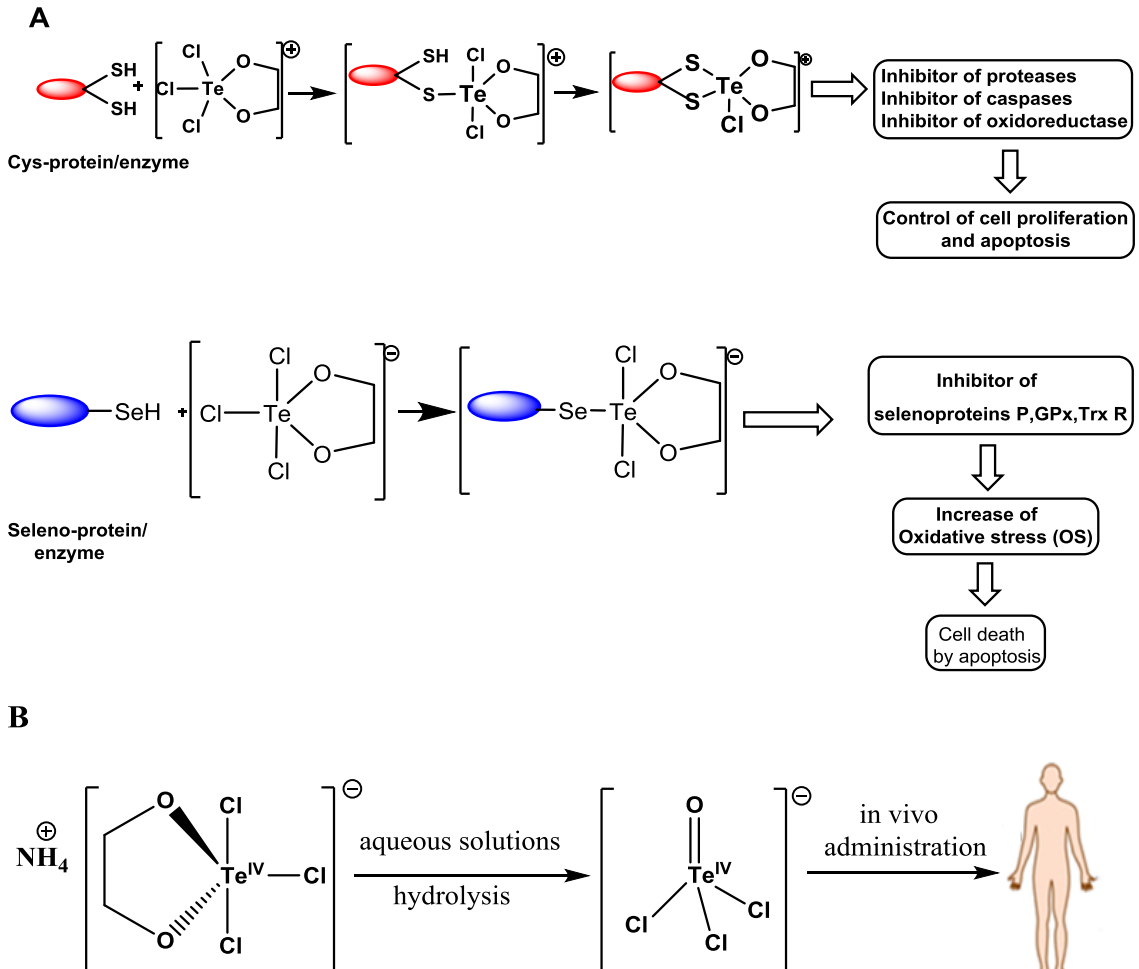

Figure 1.25. (A) Interaction between AS101 and cysteine and seleno-cysteine and related mechanism of action. (B) Hydrolytic cleavage of AS101 with the displacement of the diol ligand and formation of the real reactive component $[Te(IV)OCl_3]^-$.[115]

AS101 is an effective inhibitor of cysteine proteases and has shown several protective therapeutic applications *in vivo* preclinical and clinical studies.[96, 98, 116, 117] Tellurium(IV) compounds have the ability to inhibit integrin functions such as adhesion, migration and metalloproteinase secretion mediation in murine melanoma cells B16F10. AS101 in particular,

can stimulate the proliferation of normal lymphoid cells producing lymphokines that are said to regulate lymphopoiesis and myelopoiesis.[96] AS101 has also shown strong antibacterial activity against Gram-negative bacteria such as the *Enterobacter cloacae* and also *Klebsiella pneumoniae*, which is an opportunistic pathogen and is one of the more common Gram-negative pathogens that is said to cause pneumonia, urinary tract infections and also sepsis in patients that suffer with low immunity.[123,118, 119] AS101 enters the bacteria via the bacterium porins which leads to swelling and eventually to cell death.[120, 121] AS101 activity against Gram-negative pathogens shows great promise in the fight against infectious diseases due to the increase in antibiotic resistant pathogens worldwide.

1.1.6.5. Octa-*O*-bis-(*R,R*)-tartarate ditellurane (SAS)

Octa-*O*-bis-(*R,R*)-tartarate ditellurane (SAS, Figure 1.20) is a relatively new Te(IV) compound. It comprises of two Tellurium atoms bound to four oxygen atoms of two carboxylates and two alkoxide of two tartaric acids residues. Studies have shown that SAS is highly stable in aqueous solutions compared to many other Te(IV) compounds.[122] Te(IV) complexes such as TeX_4 and $Te(OR)_4$ interact with nucleophiles such as alcohols, carboxylates and thiols to form $Te(Nu)_4$ products and SAS interacts with thiols forming unstable $Te(SR)_4$ products.[122, 123] The mechanism of action of SAS is different from AS101 and the interactions cysteine thiols leads to the reduction of tellurium to Te(0) and the oxidation of the thiol functional group to a disulfide.[122,124] SAS is non-toxic to mice even after months of continuous treatment and the biological activity its activity is directly related to its specific chemical interactions with cysteine thiol residues. These interactions lead to conformational changes or disulfide bond formation in a specific protein or enzyme that will result in the inhibition of biological activity for that particular protein or enzyme.[125, 126] The molecule SAS has shown antibacterial activities against Gram-negative bacteria such as E coli. The transport of the molecule into the bacteria was studied and found to be different from that of AS101. In AS101, the transport of the molecule occurs *via* the pore forming proteins or porins that are located on the outer membrane of the bacteria, while the larger SAS molecule in internalized by passive diffusion (Figure 1.24).[85]

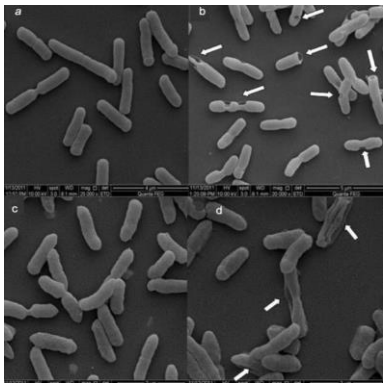

Figure 1.26. Scanning electron microscope image of the bacteria *E-Coli*. Screen shots (a) and (c) are of untreated cultures while (b) and (d) show SAS treated cultures, the arrows indicate holes in the bacteria's cell wall.[85]

1.2. Project Aim

The aim of this research project is to develop, starting from the already known Te(IV) compounds AS101 and SAS, new inorganic Te(IV) compounds with increased physiological stability and antibacterial/anticancer activity. AS101 is currently undergoing phase I and phase II clinical trials for cancer and treatment, and have shown less toxicity compared to other metal-based drugs. Chapter two regards the syntheses, characterization and antibacterial studies of a series of new analogues of AS101. One of two vicinal carbon of the diol ligands in AS101 was modified with different alkylic chain, tuning the steric and electronic properties. The new compounds were fully characterized (^{1}H, ^{13}C and ^{125}Te-NMR, IR, mass and Elemental Analyses) and the effect of the substituents in the aqueous stability of the new compounds was investigated. Theoretical calculations, in collaboration with Dr. Barbara Fresch (Chemistry Department, Padua University, Italy), allowed to identify the hydrolytic cleavage mechanism and confirmed the stability results obtain experimentally via NMR studies. Antimicrobial activity was investigated in collaboration with Dr. Kevin Kavanagh of the Department of Biology in Maynooth University. This work has been published in Journal of Inorganic Biochemistry: "Stability of antibacterial Te(IV) compounds: A combined experimental and computational study", Kenneth D'Arcy, Alan Doyle, Kevin Kavanagh, Barbara Fresch, Diego Montagner, *J. Inorg. Biochem*. **2019**.

Due to interesting results obtained in chapter 2, in chapter 3 the effect of the substitution of both vicinal carbon of the diol ligand was investigated. Several new diol ligand were reacted with $TeCl_4$ in a similar manner of chapter 2, but completely new and different species were obtained.

In particular, with the use of pinacol, 1,1,2,2 tetramethyl-1,2 ethanediol, completely new species were formed. Some of them have also been characterized by X-ray crystallography, multinuclear NMR and IR spectroscopies. These new species are salts where the cationic part is an oxazoline derivative formed by the activation of the nitrile solvent with pinacol and the anion is a $[TeCl_6]^{2-}$ moiety. $TeCl_4$ act as a catalyst and the effect of different nitriles (acetonitrile, benzonitrile, fluoroacetonitrile) in the formation of analogues species have been investigated. The stability of these species in aqueous environment was studied via NMR in a similar way as in chapter 2 and the role of the cation and of the $[TeCl_6]^{2-}$ was determined.

1.3. References:

1. E. Frieden, *Scientific American*, 1972, **227**, 52-64.
2. S. J. Stohs and D. Bagchi, *Free Radical Biology and Medicine*, 1995, **18**, 321-336.
3. P. C. A. Bruijnincx and P. J. Sadler, *Current opinion in chemical biology*, 2008, **12**, 197-206.
4. R. C. Hardison, *Proceedings of the National Academy of Sciences of the United States of America*, 1996, **93**, 5675-5679.
5. V. Mouriño, J. P. Cattalini and A. R. Boccaccini, *Journal of the Royal Society, Interface*, 2012, **9**, 401-419.
6. A. Klug, *Annual review of biochemistry*, 2010, **79**, 213-231.
7. K. o. óProinsias, M. Giedyk and D. Gryko, *Chemical Society reviews*, 2013, **42**, 6605.
8. M. Giedyk, K. Goliszewska and D. Gryko, *Chemical Society reviews*, 2015, **44**, 3391-3404.
9. J. Higdon and V. Drake, *An evidence-based approach to phytochemicals and other dietary factors*, Thieme, Stuttgart, 2nd edn., 2013.
10. S. P. Fricker, *Dalton Transactions*, 2007, 4903-4917.
11. G. J. Higby, *Gold Bulletin*, 1982, **15**, 130-140.
12. J. F. Borzelleca, *Toxicological sciences*, **53**, 2-4.
13. K. J. Williams, *Journal of the Royal Society of Medicine*, 2009, **102**, 343-348.
14. A. Sosnik, in *Biomedical Applications of Functionalized Nanomaterials*, eds. B. Sarmento and J. das Neves, Elsevier, 2018, pp. 1-32.
15. S. Norn, H. Permin, P. R. Kruse and E. Kruse, *Dansk medicinhistorisk arbog*, 2011, **39**, 59.
16. *American journal of public health (New York, N.Y. : 1912)*, 1925, **15**, 144-145.
17. M. Solomon, F. Pavlotzky, A. Barzilai and E. Schwartz, *Journal of the American Academy of Dermatology*, 2013, **68**, 284-289.
18. K. L. Haas and K. J. Franz, *Chemical Reviews*, 2009, **109**, 4921-4960.
19. T. Storr, K. H. Thompson and C. Orvig, *Chemical Society reviews*, 2006, **35**, 534-544.
20. S. Bharti and S. Singh, *Der Pharmacia Lett*, 2009, **1**.
21. K. H. Thompson and C. Orvig, *Dalton Transactions*, 2006, 761-764.
22. J. Rautio, N. A. Meanwell, L. Di and M. J. Hageman, *Nat Rev Drug Discov*, 2018, **17**, 559-587.
23. S. H. van Rijt and P. J. Sadler, *Drug discovery today*, 2009, **14**, 1089-1097.
24. D. Oommen, D. Yiannakis and A. N. Jha, *Mutat Res*, 2016, **784-785**, 8-15.
25. I. Mocikova, K. Polakova, R. Zboril, M. Mashlan and M. Heřman, *Biomedical papers of the Medical Faculty of the University Palacký, Olomouc, Czechoslovakia*, 2010, **154**, 123-132.
26. A. Traboulsee, J. Oh, L. Barlow, J. Chan, B. Cohen, K. Costello, J. Halper, C. Harris, D. Jones, E. Kanal, D. Li, K. Maravilla, F. Nelson, S. Newsome, D. Pelletier, K. Rammohan, D. Reich, A. Rovira, L. Stone and J. Wolinsky, *Journal of the Neurological Sciences*, 2017, **381**, 957-957.
27. V. Cepeda, M. A. Fuertes, J. Castilla, C. Alonso, C. Quevedo and J. M. Pérez, *Anti-cancer agents in medicinal chemistry*, 2007, **7**, 3.
28. S. M. Aris and N. P. Farrell, *European journal of inorganic chemistry*, 2009, **2009**, 1293-1293.
29. S. Dasari and P. B. Tchounwou, *European journal of pharmacology*, 2014, **740**, 364-378.
30. L. Kelland, *Nature Reviews Cancer*, 2007, **7**, 573.
31. G. Ferraro, L. Massai, L. Messori and A. Merlino, *Chem. Commun.*, 2015, **51**, 9436.

32. A. Popovtzer, H. Burnstein, S. Stemmer, D. Limon, O. Hili, G. Bachar, V. Sopov, R. Feinmesser, D. Groshar and J. Shvero, *Head & Neck*, 2017, **39**, 227-233.
33. L. S. J. Johnstone, C. Timothy , *Journal of Chemistry*, 2015, **373**, 295-299
34. D. Wang and S. J. Lippard, *Nature Reviews Drug Discovery*, 2005, **4**, 307-320.
35. D. Montagner, V. Gandin, C. Marzano and B. Longato, *Journal of Inorganic Biochemistry*, 2011, **105**, 919-926.
36. C. R. R. Rocha, M. M. Silva, A. Quinet, J. B. Cabral-Neto and C. F. M. Menck, *Clinics*, 2018, **73**.
37. S. Ahmad, *Polyhedron*, 2017, **138**, 109-124.
38. N. Pabla and Z. Dong, *Kidney International*, 2008, **73**, 994-1007.
39. B. Stordal and M. Davey, *IUBMB Life*, 2007, **59**, 696-699.
40. A. Bergamo and G. Sava, *Dalton Transactions*, 2011, **40**, 7817-7823.
41. A. Amin and M. A. Buratovich, *Mini reviews in medicinal chemistry Journal Article*, 2009, **9**, 1489.
42. Z. Adhireksan, G. E. Davey, P. Campomanes and M. Groessl, *Nature communications*, **5**.
43. G. Sava, A. Bergamo, S. Zorzet and B. Gava, *European journal of cancer (1990)*, 2002, **38**, 427-435.
44. J. Wang, Z. Zhao, S. Zhou, X. Zhang and H. Bo, *Inorganic Chemistry Communications*, 2017, **87**.
45. V. Thamilarasan, N. Sengottuvelan, A. Sudha, P. Srinivasan and G. Chakkaravarthi, *Journal of Photochemistry and Photobiology B: Biology*, 2016, **162**, 558-569.
46. A. P. King, H. A. Gellineau, J.-E. Ahn, S. N. MacMillan and J. J. Wilson, *Inorganic Chemistry*, 2017, **56**, 6609-6623.
47. S. Puig and D. J. Thiele, *Current opinion in chemical biology*, **6**, 171-180.
48. P. Szymański, T. Frączek, M. Markowicz and E. Mikiciuk-Olasik, *Biometals : an international journal on the role of metal ions in biology, biochemistry, and medicine*, 2012, **25**, 1089-1112.
49. F. Chen, J. Wang, J. Chen and L. Yan, *Oral diseases*, **25**, 80-86.
50. M. Barceló-Oliver, Á. García-Raso, Á. Terrón and E. Molins, *Journal of inorganic biochemistry*, 2007, **101**, 649-659.
51. D. S. Sigman, R. Landgraf, D. M. Perrin and L. Pearson, *Metal ions in biological systems*, 1996, **33**, 485.
52. C. Acilan, B. Cevatemre, Z. Adiguzel, D. Karakas, E. Ulukaya, N. Ribeiro, I. Correia and J. C. Pessoa, *Biochimica et Biophysica Acta (BBA) - General Subjects*, 2017, **1861**, 218-234.
53. J. H. Parish, *Biochemical Education*, 1990, **18**, 157-157.
54. J. D. Ranford, P. J. Sadler and D. A. Tocher, *Journal of the Chemical Society, Dalton Transactions*, 1993, 3393-3399.
55. D. K. Saha, U. Sandbhor, K. Shirisha and S. Padhye, *Bioorganic & medicinal chemistry letters*, 2004, **14**, 3027-3032.
56. T. Chivers, *A Guide to Chalcogen-Nitrogen Chemistry*, World Scientific Publishing Co Pte Ltd, Singapore, SINGAPORE, 2005.
57. B. S. Sekhon, *Research in pharmaceutical sciences*, 2013, **8**, 145-158.
58. T. Chivers, *A guide to chalcogen-nitrogen chemistry*, World Scientific, Hackensack, NJ, 2005.
59. P. Bhattacharyya, *Annual reports on the progress of chemistry. Section A. Inorganic chemistry*, 2005, **101**, 117-127.
60. M. D. Lalla Aicha Ba, Vincent Jamier and Claus Jacob, *Organic & Biomolecular Chemistry*, 2010, 4203 - 4216.
61. B. S. Sekhon, *Research in Pharmaceutical Sciences*, 2013, **8(3)**, 145-158.
62. G. Contreras-Puente, O. Vigil, M. Ortega-López and A. Morales-Acevedo, *Thin solid films*, **361-362**, 378-382.

63. T. Burkholz and C. Jacob, in *Encyclopedia of Metalloproteins*, eds. R. H. Kretsinger, V. N. Uversky and E. A. Permyakov, Springer New York, New York, NY, 2013, pp. 2163-2174.
64. S. M. Baesman, T. D. Bullen, J. Dewald, D. Zhang, S. Curran, F. S. Islam, T. J. Beveridge and R. S. Oremland, *Applied and environmental microbiology*, 2007, **73**, 2135-2143.
65. J. T. Csotonyi, E. Stackebrandt and V. Yurkov, *Applied and environmental microbiology*, 2006, **72**, 4950-4956.
66. S. M. Baesman, J. F. Stolz, T. R. Kulp and R. S. Oremland, *Extremophiles : life under extreme conditions*, **13**, 695-705.
67. T. G. Chasteen and R. Bentley, *Chemical Reviews*, 2003, **103**, 1-26.
68. L. A. Ba, M. Döring, V. Jamier and C. Jacob, *Organic & Biomolecular Chemistry*, 2010, **8**, 4203-4216.
69. S. Kumar, H. Johansson, T. Kanda, L. Engman, T. Müller, H. Bergenudd, M. Jonsson, G. F. Pedulli, R. Amorati and L. Valgimigli, *The Journal of Organic Chemistry*, 2010, **75**, 716-725.
70. C. Jacob, E. Battaglia, T. Burkholz, D. Peng, D. Bagrel and M. Montenarh, *Chem Res Toxicol*, 2012, **25**, 588-604.
71. I. Abe, T. Abe, W. Lou and T. Masuoka, *Biochemical and biophysical research communications*, 2007, **352**, 259-263.
72. C. W. Nogueira, L. N. Rotta, M. L. Perry and D. O. Souza, *Brain research*, 2001, **906**, 157-163.
73. P. Garberg, L. Engman, V. Tolmachev and H. Lundqvist, *The international journal of biochemistry & cell biology*, 1999, **31**, 291-301.
74. E. Widy-Tyszkiewicz, A. Piechal, B. Gajkowska and M. Śmiałek, *Toxicology letters*, 2002, **131**, 203-214.
75. C. Nicco, F. Batteux, N. Carole and B. Frédéric, *Molecules (Basel, Switzerland)*, 2017, **23**, 84.
76. D. Trachootham, W. Lu, M. A. Ogasawara, R.-D. V. Nilsa and P. Huang, *Antioxidants & redox signaling Journal Article*, 2008, **10**, 1343.
77. D. P. Jones, *American journal of physiology. Cell physiology*, 2008, **295**, C849.
78. V. Gandin, P. Khalkar, J. Braude and A. P. Fernandes, *Free Radical Biology and Medicine*, 2018, **127**, 80-97.
79. C. Gorrini, I. S. Harris and T. W. Mak, *Nature reviews. Drug discovery*, 2013, **12**, 931-947.
80. C. R. Justus, E. J. Sanderlin and L. V. Yang, *International journal of molecular sciences*, 2015, **16**, 11055-11086.
81. A. Holmgren and J. Lu, *Biochemical and Biophysical Research Communications*, 2010, **396**, 120-124.
82. L. Chaiswing, W. H. St Clair and D. K. St Clair, *Antioxidants & redox signaling Journal Article*, 2018, **29**, 1237.
83. M. U. Rasheed, N. Thajuddin, P. Ahamed, Z. Teklemariam and K. Jamil, *Revista do Instituto de Medicina Tropical de São Paulo*, 2014, **56**, 341-346.
84. A. P. Bath, R. M. Walsh, M. L. Bance and J. A. Rutka, *The Laryngoscope*, 1999, **109**, 1088-1093.
85. R. Yalew, D. Kenigsbuch-Sredni, B. Sredni and Y. Nitzan, *Archives of Microbiology*, 2014, **196**, 51-61.
86. M. Daniel-Hoffmann, B. Sredni and Y. Nitzan, *Journal of antimicrobial chemotherapy*, 2012, **67**, 2165-2172.
87. H. Nikaido and M. Vaara, *Microbiological reviews*, 1985, **49**, 1-32.
88. H. Nikaido, *Microbiology and Molecular Biology Reviews*, 2003, **67**, 593-656.
89. H. Nikaido, E. Y. Rosenberg and J. Foulds, *Journal of Bacteriology*, 1983, **153**, 232-240.
90. R. L. O. R. Cunha, I. E. Gouvea and L. Juliano, *Anais da Academia Brasileira de Ciencias*, 2009, **81**, 393-407.

91. D. S. Goodsell, *The Oncologist*, 2000, **5**, 435-436.
92. D. R. McIlwain, T. Berger and T. W. Mak, *Cold Spring Harbor Perspectives in Biology*, 2013, **5**, a008656-a008656.
93. T. Nomura and N. Katunuma, *The journal of medical investigation : JMI*, 2005, **52**, 1.
94. B. Sredni, *Seminars in Cancer Biology*, 2012, **22**, 60-69.
95. J. Eskdale, D. Kube, H. Tesch and G. Gallagher, *Immunogenetics*, 1997, **46**, 120-128.
96. B. Sredni, R. R. Caspi, A. Klein, Y. Kalechman, Y. Danziger, M. Benya'akov, T. Tamari, F. Shalit and M. Albeck, *Nature*, 1987, **330**, 173-176.
97. B. Sredni, T. Tichler, A. Shani, R. Catane, B. Kaufman, G. Strassmann, M. Albeck and Y. Kalechman, *JNCI: Journal of the National Cancer Institute*, 1996, **88**, 1276-1284.
98. B. Sredni, R.-H. Xu, M. Albeck, U. Gafter, R. Gal, A. Shani, T. Tichler, J. Shapira, I. Bruderman, R. Catane, B. Kaufman, J. K. Whisnant, K. L. Mettinger and Y. Kalechman, *International Journal of Cancer*, 1996, **65**, 97-103.
99. B. Sredni, R. Geffen-Aricha, W. Duan, M. Albeck, F. Shalit, H. M. Lander, N. Kinor, O. Sagi, A. Albeck, S. Yosef, M. Brodsky, D. Sredni-Kenigsbuch, T. Sonino, D. L. Longo, M. P. Mattson and G. Yadid, *Journal Article*, 2007, **21**, 1870.
100. M. Brodsky, G. Halpert, M. Albeck and B. Sredni, *Journal of Inflammation*, 2010, **7**, 3-3.
101. S. Yosef, M. Brodsky, B. Sredni, A. Albeck and M. Albeck, *ChemMedChem*, 2007, **2**, 1601-1606.
102. A. Albeck, H. Weitman, B. Sredni and M. Albeck, *Inorganic Chemistry*, 1998, **37**, 1704-1712.
103. F. G. Giancotti and E. Ruoslahti, *Science*, 1999, **285**, 1028-1032.
104. C. J. Avraamides, B. Garmy-Susini and J. A. Varner, *Nature Reviews Cancer*, 2008, **8**, 604-617.
105. J. Folkman, in *Encyclopedia of Genetics*, eds. S. Brenner and J. H. Miller, Academic Press, New York, 2001, pp. 66-73.
106. F. Y. Yue, R. Dummer, R. Geertsen, G. Hofbauer, E. Laine, S. Manolio and G. Burg, *International Journal of Cancer*, 1997, **71**, 630-637.
107. G. Galizia, M. Orditura, C. Romano, E. Lieto, P. Castellano, L. Pelosio, V. Imperatore, G. Catalano, C. Pignatelli and F. De Vita, *Clinical Immunology*, 2002, **102**, 169-178.
108. R. Domenis, D. Cesselli, B. Toffoletto, E. Bourkoula, F. Caponnetto, I. Manini, A. P. Beltrami, T. Ius, M. Skrap, C. Di Loreto and G. Gri, *PloS one*, 2017, **12**, e0169932.
109. S. Zhao, D. Wu, P. Wu, Z. Wang and J. Huang, *PloS one*, 2015, **10**, e0139598.
110. F. De Vita, M. Orditura, G. Galizia, C. Romano, A. Roscigno, E. Lieto and G. Catalano, *Chest*, 2000, **117**, 365.
111. G. Strassmann, T. Kambayashi, C. O. Jacob and D. Sredni, *Cellular Immunology*, 1997, **176**, 180-185.
112. J. Luo, *Cancer letters*, 2009, **273**, 194-200.
113. J. R. Woodgett and P. S. Ohashi, *Nature Immunology*, 2005, **6**, 751-752.
114. M. V. A. CLEVERSON R PRINCIVAL, ALCINDO A DOS SANTOS, MAURICIO P FRANCO, ATAUALPAAC BRAGA, ANDRE F RODRIQUES-OLIVERA, THIAGO C CORRERA, RODRIGO LOR CUNHA AND JOAO V COMASSETO, *AMERICAN CHEMICAL SOCIETY*, 2017, 4431-4439.
115. A. Silberman, M. Albeck, B. Sredni and A. Albeck, *Inorganic Chemistry*, 2016, **55**, 10847-10850.
116. H. Rosenblatt-Bin, Y. Kalechman, A. Vonsover, R. H. Xu, J. P. Da, F. Shalit, M. Huberman, A. Klein, G. Strassmann, M. Albeck and B. Sredni, *Cellular Immunology*, 1998, **184**, 12-25.
117. E. Okun, Y. Dikshtein, A. Carmely, H. Saida, G. Frei, B. A. Sela, L. Varshavsky, A. Ofir, E. Levy, M. Albeck and B. Sredni, *FEBS Journal*, 2007, **274**, 3159-3170.
118. R. C. M. D. P. Couto, E. A. A. M. D. M. Carvalho, T. M. G. M. D. M. Pedrosa, Ê. R. M. D. P. Pedroso, M. C. M. D. Neto and F. M. M. D. Biscione, *AJIC: American Journal of Infection Control*, 2007, **35**, 183-189.

119. I. Kappstein, G. Schulgen, T. Friedrich, P. Hellinger, A. Benzing, K. Geiger and F. D. Daschner, *Am J Med*, 1991, **91**, 125s-131s.
120. H. M. Wexler, C. Getty and G. Fisher, *Journal of Medical Microbiology*, 1992, **37**, 165-175.
121. M. Daniel-Hoffmann, M. Albeck, B. Sredni and Y. Nitzan, *Archives of microbiology*, 2009, **191**, 631-638.
122. M. B. Sigal Yose, Benjamin Sredni, Amnon Albeck and Michael Albeck, *ChemMedChem*, 2007, **2**, 1601-1606.
123. S. Yosef, M. Brodsky, B. Sredni, A. Albeck and M. Albeck, *ChemMedChem*, 2007, **2**, 1601-1606.
124. R. Dardik, T. Livnat, G. Halpert and S. Jawad, *Molecular vision*, 2016, **22**.
125. S. Yosef, M. Brodsky, B. Sredni and A. Albeck, *ChemMedChem*, **2**, 1601-1606.
126. A. Albeck, H. Weitman, B. Sredni and M. Albeck, *Inorganic Chemistry*, 1998, **37**, 1704-1712.

Chapter 2

AS-101, [ammonium trichloro (diol-O,O')tellurate] derivatives

2.1. Introduction

Tellurium is a metalloid element with several available oxidation states going from -2 to +6.[1] Tellurides of formula M_2Te are compounds formed by Te(-II) and noble elements such as Au or Ag that are highly unstable and in the presence of oxygen are oxidized to tellurite $[Te(IV)O_3]_2^-$. The biological properties of tellurium are poorly characterized, but it is known that some bacteria and fungi are able to uptake Te as amino acids, replacing the Sulfur atom and forming Tellurium-cysteine and Tellurium methionine.[2, 3] The oxidation state +4 is the most stable and interesting from biological application, with multiple complexes of organo-tellurium(IV), containing a direct Te-C bond , reported. These complexes are stable in aqueous solution and seem to have a promising and potential role in protease inhibition and integrin inactivation.[4-8] Besides these families of organo-tellurium complexes, Albeck and co-workers ultimately developed two "inorganic" tellurate Te(IV) compounds, named AS-101 and SAS whose structure is depicted in Figure 2.1. These complexes are effective inhibitors of cysteine protease and showed several protective therapeutic applications and in vivo, preclinical and clinical studies have been conducted.[3, 6, 9-16]

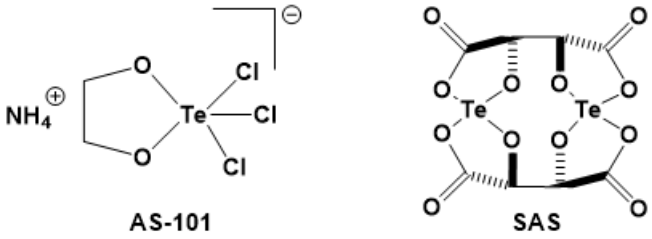

Figure 2.1. Structure of the "inorganic" Te(IV) compounds AS-101 and SAS

Te(IV) compounds can inhibit integrin functions such as adhesion, migration and metalloproteinase secretion mediation in B16F10 murine melanoma cells. AS-101 in particular, can stimulate the proliferation of normal lymphoid cells producing lymphokines that are regulators of lymphopoiesis and myelopoiesis.[9] AS-101 also showed strong antibacterial activity in particular on Gram-negative bacterium *Enterobacter cloacae*.[17] Recently, Albeck and Cunha, reported that AS-101 is not stable in physiological conditions and is subjected to hydrolysis

where the diol ligand is displaced with the formation of $[Te(IV)OCl_3]^-$, which is likely the bioactive species in biological investigation (Figure 2.2).[18, 19] Due to the promising activity of AS-101 in term of anticancer and immune-modulating properties, the aim of the study presented in this chapter was to design, synthesize and characterize a series of AS-101 analogues with different ligands, in order to investigate their stability properties in aqueous environment and ultimately found a tellurate Te(IV) complex stable enough to perform biological studies in physiological conditions.

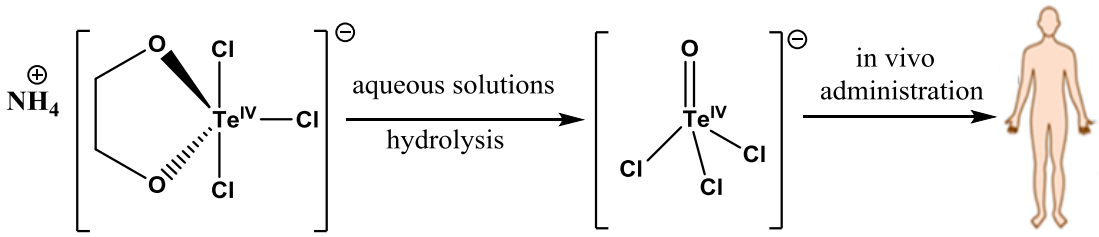

Figure 2.2. Hydrolysis of tellurium AS101 complex in aqueous solution forming the active species $[Te(IV)OCl_3]^-$, after diol ligand is displaced.

The ethylene glycol of AS-101 has been substituted with a series of diols with increasing alkyl chain length and electron withdrawing groups, producing eight novel Te(IV) complexes with formula $NH_4[(RC_2H_3O_2)Cl_3Te]$ (where R =H (**201**); CH_3 (**202**); CH_2CH_3 (**203**); $CH_2CH_2CH_3$ (**204**); $CH_2CH_2CH_2CH_3$ (**205**); $CH_2CH_2CH_2CH_2CH_2CH_3$ (**206**); CH_2Cl (**207**); Ph. (**208**)). The aqueous stability has been evaluated using ^{1}H, ^{13}C and ^{125}Te NMR and theoretical studies allowed an understanding of the molecular basis of the observed trend. The modelling of the reaction mechanism suggests that a longer alkyl chain substituent enhances the stability of the complex by interfering with the formation of water clusters necessary for mediating the proton transfer steps involved in the hydrolysis of the Te-O bonds. The antimicrobial activity was evaluated in vitro on *Escherichia coli* and other bacteria strains.

2.2. Results and discussion

2.2.1. Synthesis and characterisation

A series of eight complexes, which are the analogues of the AS101 compound, which has the formula $NH_4[(RC_2H_3O_2)Cl_3Te]$ (where R = H (**201**); CH_3 (**202**); CH_2CH_3 (**203**); $CH_2CH_2CH_3$ (**204**); $CH_2CH_2CH_2CH_3$ (**205**); $CH_2CH_2CH_2CH_2CH_2CH_3$ (**206**); CH_2Cl (**207**); Ph. (**208**)), have been synthesized in the laboratory as described in the synthesis and characterization section and in **scheme 2.1** below. In short, $TeCl_4$ and the correspondent diol were stirred in dry acetonitrile and mixtures refluxed at 80°C for intervals ranging from 4 to 120 hours. All solids formed were extracted by filtration after the CH_3CN solution was concentrated by rotary evaporation or by the addition of Et_2O.

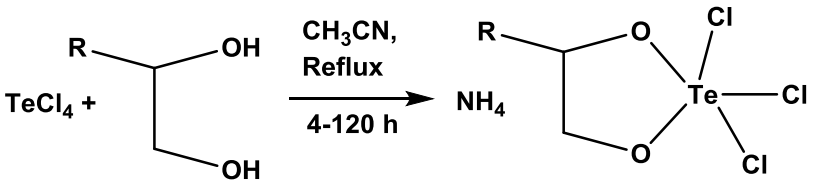

Scheme 2.1. Synthesis of the complexes, where R =H (**201**); CH_3 (**202**); CH_2CH_3 (**203**); $CH_2CH_2CH_3$ (**204**); $CH_2CH_2CH_2CH_3$ (**205**); $CH_2CH_2CH_2CH_2CH_2CH_3$ (**206**); CH_2Cl (**207**); Ph (**208**).

These complexes can also be synthesized using the microwave as previously observed for the AS101 compound, thus reducing reaction times on all compounds from several hours to 40mins.[20, 21] The reaction mechanism for all complexes involves four steps as described by Sredni et al and is shown below in scheme 2.2.[22]

$$TeCl_4 + 2HOCH_3CH_2OH \longrightarrow HOCH_2CH_2Cl + HOCH_2CH_2OTeCl_3 + H_2O$$

$$CH_3CN + HOCH_2CH_2Cl \longrightarrow CH_3CNHOCH_2CH_2Cl$$

$$CH_3CNHOCH_2CH_2Cl + HCl + H_2O \longrightarrow CH_3CO_2CH_2CH_2Cl + NH_4Cl$$

$$HOCH_2CH_2OTeCl_3 + NH_4Cl \longrightarrow OCH_2CH_2OTeCl_3^-NH_4^+ + HCl$$

Scheme 2.2. The mechanism of reaction of the AS101 compound involves four steps shown, all complexes formed of the AS101 analogue are assumed to be formed this way.

All the compounds synthesised were characterised by elemental analysis, IR spectroscopy, Mass spectrometry, ^1H, ^{13}C, and ^{125}Te NMR (all the spectra are reported at the end of this chapter in the supporting information Figures 2.14-2.20).

All the complexes show a unique ^{125}Te NMR peak in DMSO-d_6 around 1680 ppm, the typical region for these kind of species [23, 24] and in the IR spectra is clearly visible the stretching of the ammonium counter cation at 3200 cm^{-1} (all IR spectra are reported at end of this chapter Figures 2.22-2.27). A detailed IR study in the range 4000–200 cm^{-1} was performed for compounds **201** and **203**. Further insights into the coordination sphere of tellurium can be obtained by comparison with the IR spectra of the starting ethylene glycol, whose vibrations have been fully assigned previously[25]. For instance, in the mid-IR spectrum of compound **201** (Figure 2.3) the bands associated with the –COH moieties of the diol (ν(OH) = 3400, δ_{ip}(COH) = 1424, δ_{oop}(COH) = 644 cm^{-1}) have disappeared, consistent with the coordination of the deprotonated glycol to the Te(IV) center.

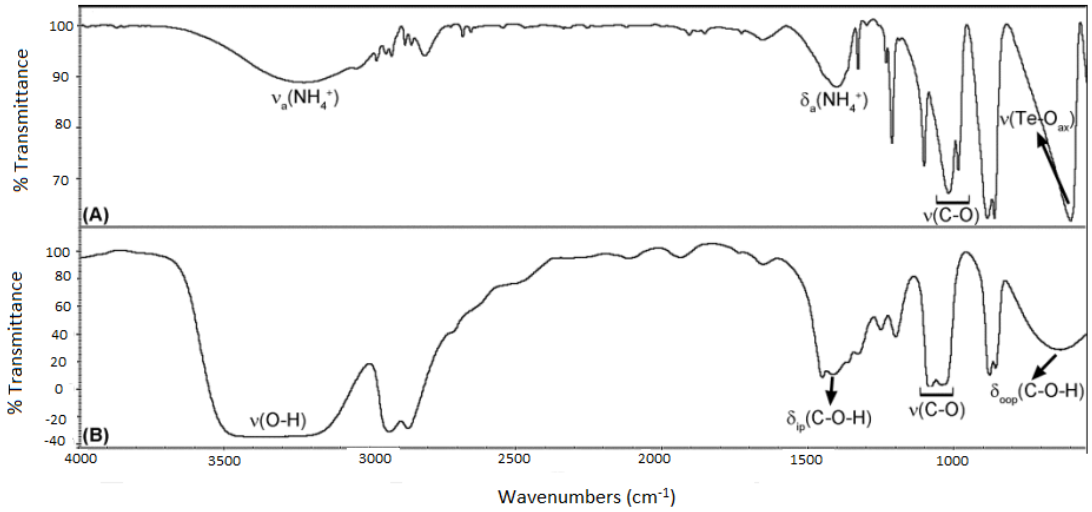

Figure 2.3. Mid IR spectra of (A) compound **201** and (B) free ethylene glycol.

The C-O stretching vibrations were detected at lower energy, in agreement with values reported for analogous derivatives[11]. New bands were recorded at 3234 ($\nu_a(NH_4^+)$) and 1408 ($\delta_a(NH_4^+)$) cm^{-1} accounting for the presence of the ammonium counterion[26]. In the far-IR region (Figure 2.4), the spectrum of compound **201** appears dramatically different from that of ethylene glycol, the latter showing only one weak broad band at 520 cm^{-1} assigned to the δ(CCO)[25]. In line with the results reported by Albeck et al.,[11] in the solid state the complex should present a distorted square-pyramidal geometry in which the two oxygen atoms of the deprotonated diol occupy the axial and one equatorial positions.

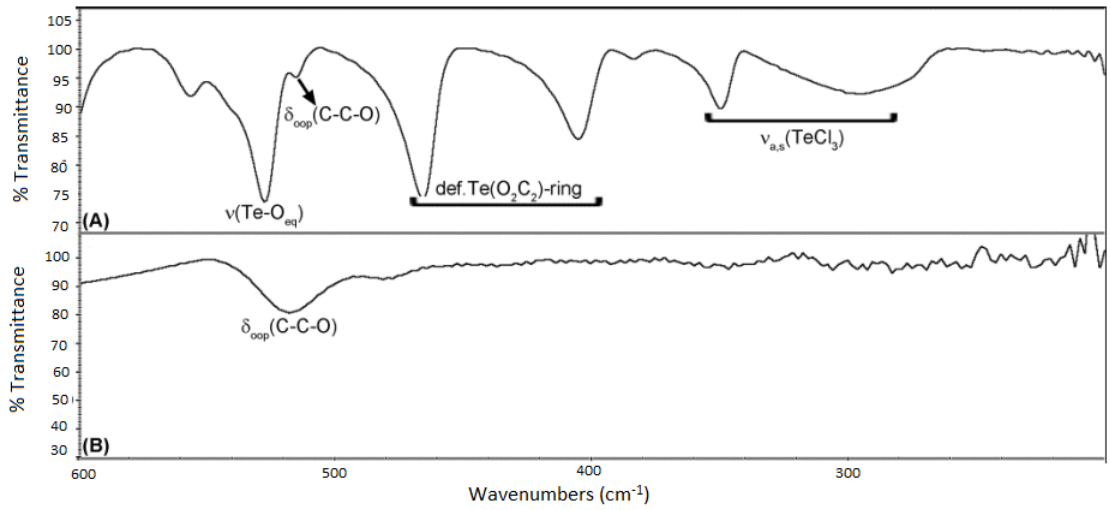

Figure 2.4. Far IR spectra of (A) compound **201** and (B) free ethylene glycol

Accordingly, two tellurium-oxygen stretching vibrations are foreseeable, *ν*(Te-O_{ax}) and ν(Te-O_{eq}), the former expected at higher frequency[26]. For **201**, Te-O vibrations were assigned to two new bands recorded at 607 and 528 cm^{-1}, respectively. Such assignments, together with the two intense bands observed at 467 and 406 cm^{-1} assigned to the overall deformation of the Te(O_2C_2)-ring, are fully consistent with those reported for analogous derivatives[27]. According to the very few relevant papers published to date, tellurium-chloride derivatives exhibit Te-Cl stretching vibrations in the range 400–200 cm^{-1}, such as 378/312 ($TeCl_4$)[28], 220–250 ($[TeCl_6]^{2-}$)[29, 30], 286/263 (Ph_2TeCl_2)[31] and 271/221 ([Te(dioxoethylene-*O*,*O*')Cl_3], Raman) cm^{-1} [32]. In the present study, two new intense bands were recorded at 351 and 298 cm^{-1}, which can be reasonably assigned to the antisymmetric and symmetric stretching involving the -$TeCl_3$ moiety. The IR spectra of derivative **202** resemble closely those of **201**. The same pattern of bands was observed in the far-IR region, whereas in the 4000–600 cm^{-1} range the only minor differences would be attributed to the new vibrations involving the CH_3CH_2CH- pendant, such as those recorded at 3048 (*ν*(CH)), 2967/2872 ($\nu_{as}(CH_3)$), 1354 ($\delta_s(CH_3)$) and 776 ($\rho(CH_3)$) cm^{-1} [32]. The complexes are very stable in pure CH_3CN or DMSO solution, but they decompose upon addition of H_2O, as previously described by Albeck and co-workers[16]. The hydrolysis reaction releases the free diol with the formation of trichloro-tellurium(IV) oxide $[TeOCl_3]^-$, as shown in Figure 2.5.

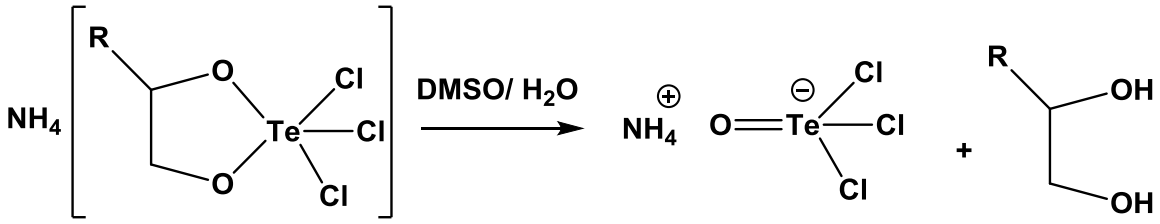

Figure 2.5. Hydrolysis reaction of Te(IV) complexes

The displacement of the ligand is followed by ^{1}H, ^{13}C and ^{125}Te NMR (Figure 2.6 for **203**): the signals of the coordinated and of the released diols appear shifted in the NMR spectra, and this effect is particularly remarked in the ^{13}C NMR for the two carbons bound to the two donor oxygen of the diols (Figure. 2.6 center for compound **203** and Figures 2.28–2.32 at end of chapter).

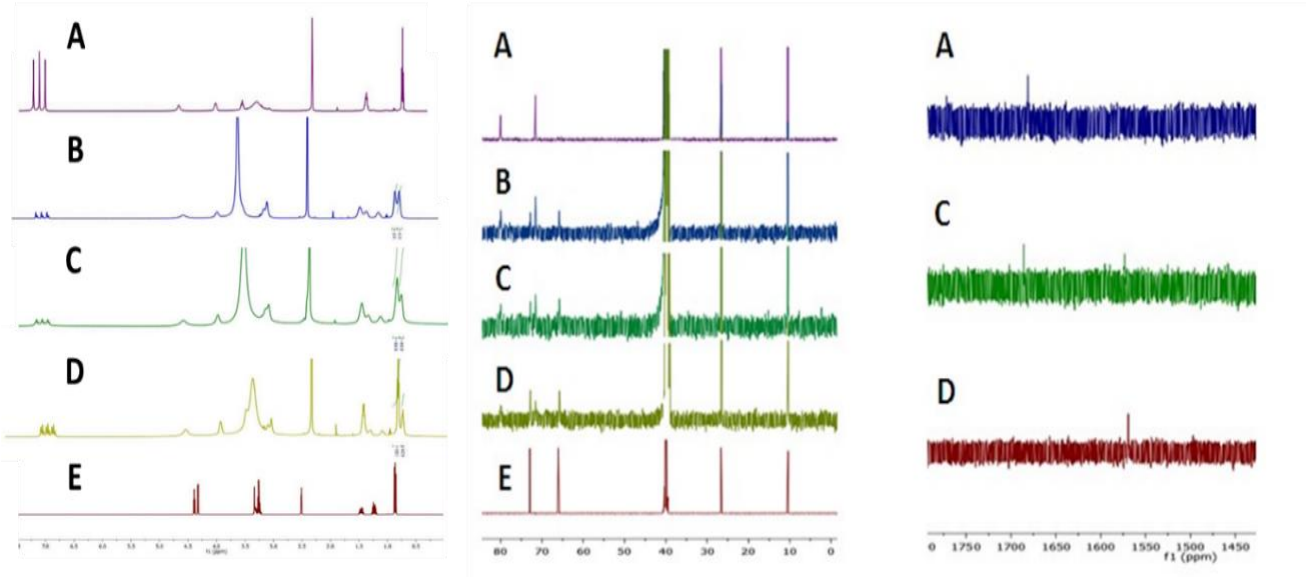

Figure 2.6. ^{1}H (left), ^{13}C (center) and ^{125}Te (right) NMR of: A) **203** (0.5 mM in DMSO-d_6); B) **203** + 10 µL D_2O (10 eq.); C) **203** + 20 µL D_2O (20 eq.); D) **203** + 30 µL D_2O (30 eq.); E) free ligand.

After addition of 10, 20 and 30 equivalents of water, the free diol is displaced with the formation of $NH_4[TeOCl_3]$, visible in the ^{125}Te NMR at δ 1560 ppm (Figure 2.6 right). To confirm the nature of the decomposed product, 20 mg of compound **203** were dissolved in 1 mL of CH_3CN and 5 mL of H_2O and, after 2 h, the solution was dried under vacuum. The white solid obtained was washed with cold CH_3CN, H_2O and diethyl ether and further dried under high vacuum pressure. Mass

spectrometry (Figure 2.7), peak at (−) *m*/*z* 250.81 corresponding to $[Cl_3OTe]^-$) and Elem. Analysis confirm the nature of the product as $NH_4[Cl_3OTe]$ (Elem. Anal. %H (1.50), %N (5.23); found H (1.91), N (5.04)).

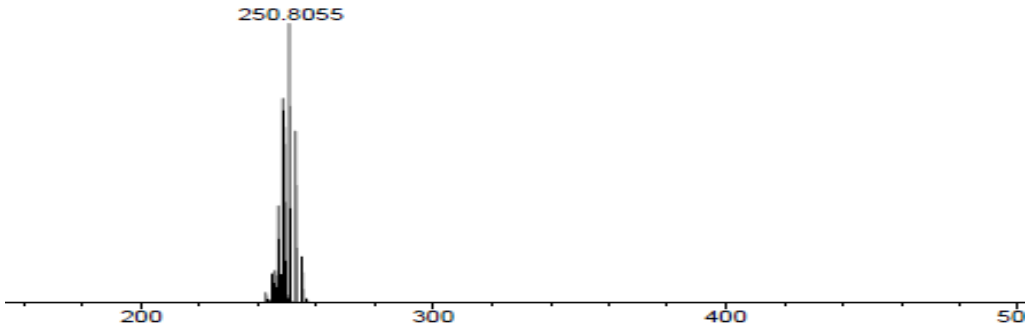

Figure 2.7. ESI-Mass spectra (-) of the decomposed product $[TeOCl_3]^-$

Analyzing the integrals of the released ligand *vs* the integrals of the starting compound with respect the equivalents of water, it is possible to estimate on the stability of the complexes.

The data show that there was an evident direct proportion between the alkyl chain of the diol and the stability of the Te complexes; an increase of the chain length corresponds to an increase of the stability, with complex **206** more stable than **205**, **204**, **203**, **202** and **201** (Figure 2.8). After addition of 30 eq. of water, compound **201** is almost completely decomposed while **206** is more resistant (55% not decomposed). Complex **207** with a Cl electro-withdrawing substituent is the least stable (it completely decomposes upon addition of 20 eq. of H_2O) while, unfortunately, it was not possible to evaluate the stability of complex **208**, since it was not obtained pure.

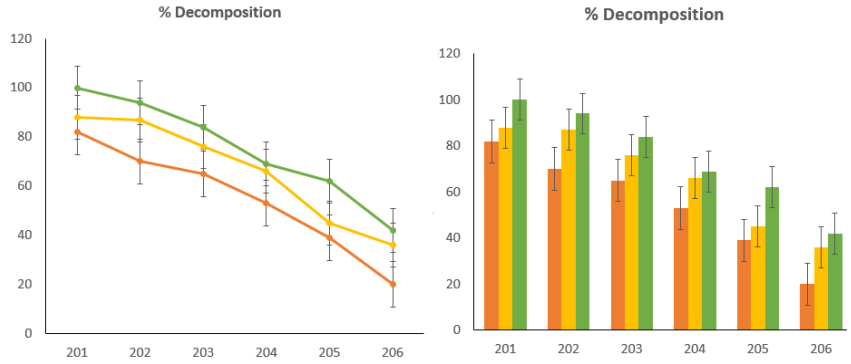

Figure 2.8. Decomposition of complexes **201-206** with addition of water. Left, marked line representation; right, 2D column representation. 10 equiv D_2O, 20 equiv D_2O and 30 equiv D_2O

2.2.2. Theoretical Investigation

To gain a molecular understanding of the factors affecting the stability of the complexes we modelled at the quantum mechanical level complex **201** and complex **205**, representing the limiting case of short and long alkyl-chain substituent, respectively, and complex **207** with the chloro-methyl substituent. The optimized equilibrium geometries and the analysis of the electronic structures in terms of atomic charges[33, 34] are reported in Figure 2.9.

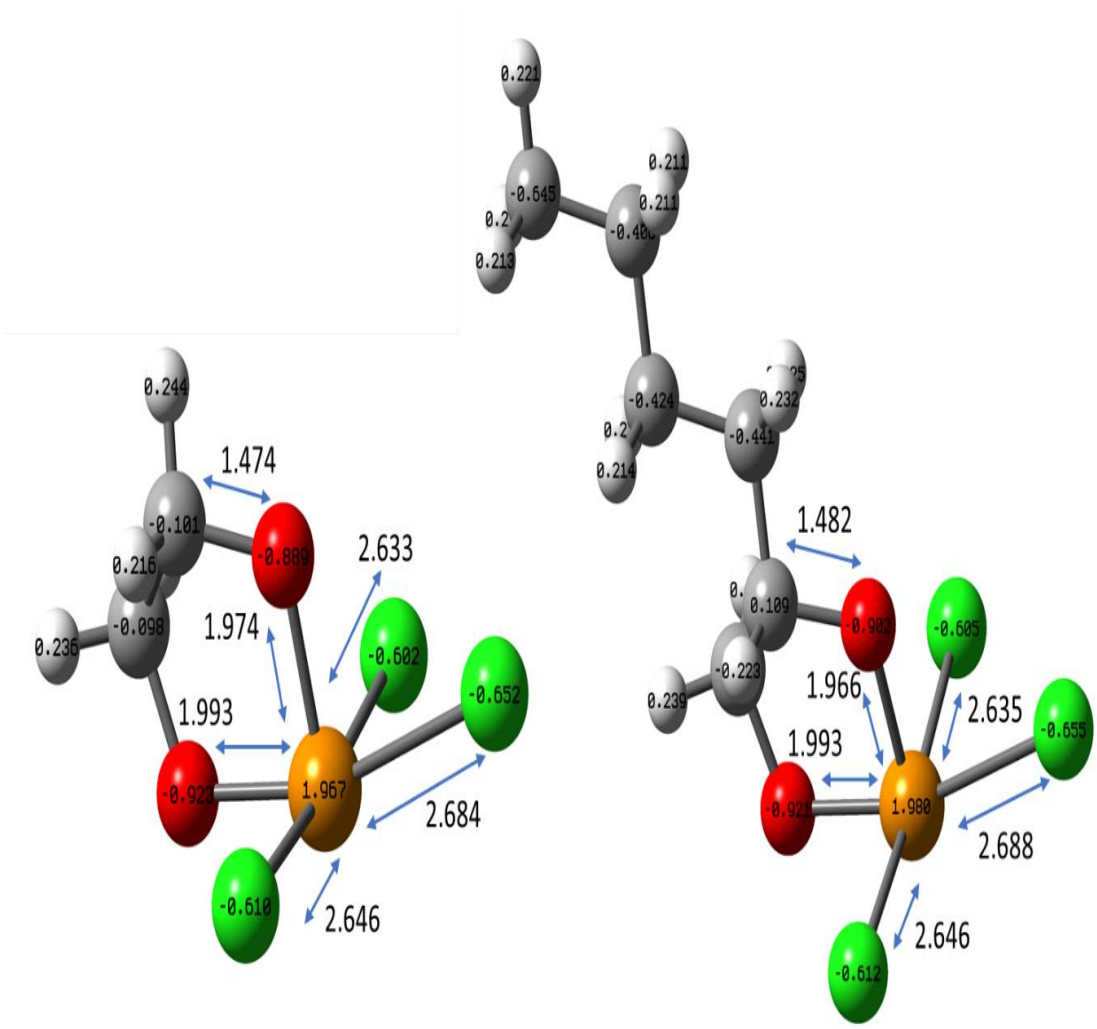

Figure 2.9. Optimized equilibrium geometries of complex **201** (left) and complex **205** (right) in implicit DMSO. The complexes are anions with charge -1 and singlet spin multiplicity. The colour code is Te in orange, Cl in green, O in red, C in grey and H in white. The atomic charge from Natural Population Analysis are reported for each atom (as fraction of the elementary electronic charge |e|) and the main distances are given in Angstrom (Å).

Both atomic charges and structural parameters of the Te center are not significantly affected by the change in the alkyl chain length nor by the chlorination of the substituent, it can therefore be inferred that the source of the complexes 'slightly different stability' does not arise from the different strengths of the Te-O bonds. As it also emerges from the stability studies, the solvating environment plays a central role in establishing the equilibrium of the decomposition reaction of the complexes. Computationally, there are several approaches to treat solvation and we will use two of them in the following to elucidate the energetics of the complex decomposition. In the first approach (*implicit solvation*), the solvent is treated as a continuous, uniform dielectric medium characterized by its dielectric constant Ɛ. The solute molecules are placed inside an empty cavity within the dielectric medium and the interactions between solvent and solute consists primarily of electrostatic interactions, that is the mutual polarization of the solute and the solvent. We use the Solvation Model based on Density (SMD) which was found to perform well for predicting reaction energies in solution[35]. The reaction free energy, ΔG_r, obtained for the decomposition of the three complexes, **201**, **205** and **207**, by considering the free energy of reactants and products implicitly solvated in acetonitrile, DMSO and water are reported in table 2.1, together with the free energy of the same reactions in gas-phase. Positive values of free energy of reactions reflect a stable complex which does not undergo significant decomposition.

Table 2.1. Free energy of the decomposition reaction of compounds **201**, **205** and **207**. The table reports the gas-phase energy and the set of energies calculated with an implicit solvent model of acetonitrile, dimethyl sulfoxide (DMSO) and water. The reaction considered in gas-phase and in implicit solvent was $[(RC_2H_3O_2)Cl_3Te]^- + H_2O = [RC_2H_3(OH)_2] + [Cl_3OTe]^-$ where reactants and products were considered as non-interacting molecules each species was solvated separately. The second set of energies are calculated by explicit consideration of a hydration shell composed of five water molecules. The labels R1, R2 and R3 refers to three different conformers of the hydrated reactant differing by the positions of the water molecules, see Figures 2.10 and 2.11 for the structures of reactants and products.

ΔG_r (kcal/mol)		Implicit solvation			Explicit microsolvation shell		
	Gas phase	*Acetonitrile (ε=35.688)*	*DMSO (ε=46.826)*	*Water (ε=78.3553)*	*R1*	*R2*	*R3*
201	16.6	18.4	18.1	16.0	-1.6	-4.7	-5.4
205	17.5	19.4	19.4	17.2	4.9	-1.3	-2.8
207	23.3	18.2	17.9	15.9	-4.0	-11.5	-13.5

From the analysis of the values of the reaction free energy in implicit solvent we can draw two main conclusions.

● We do see consistent trend in how the relative gas-phase stability of the three complexes is changed by solvation. Complex **205** is less prone to decomposition than complex **201** in all the considered solvents and complex **207** is the most destabilized by solvation. This can be understood by considering the solvation energies of the different species involved in the reactions (see Table 2.2) which show that the chloro-methyl substituted glycol is considerably more stabilized by solvation than the corresponding reactant complex.

Table 2.2. Solvation free energies of isolated reactants and products of the complex decomposition reaction for Complexes **201**, **205** and **207**. The free energy of solvation is calculated as the difference between the free energy of the gas-phase and the free energy of the solvated ground state geometries. The label R indicates the complexes (reactant) and P the free substituted glycol resulting from the decomposition reaction. A water molecule which reacts with the complexes has a solvation energy of -6.8 kcal/mol in Acetonitrile, -6.3 kcal/mol in DMSO and -12.0 kcal/mol in water. The Tellurium(IV) oxide $[OCl_3Te]^-$ has a solvation energy of -52.6 kcal/mol in Acetonitrile, -52.3 kcal/mol in DMSO and - 55.6 kcal/mol in water.

Solvation Energy (kcal/mol)	**201**		***ΔGsolv***	**205**		***ΔGsolv***	**207**		***ΔGsolv***
	R	**P**		**R**	**P**		**R**	**P**	
Acetonitrile	-57.0	-9.4	1.8	-58.8	-11.1	1.9	-54.8	-13.9	-4.9
DMSO	-56.1	-8.6	1.5	-57.3	-9.4	1.9	-53.7	-13.0	-5.2
Water	-58.3	-15.3	-0.6	-57.6	-14.2	-0.2	-54.6	-18.2	-7.2

A word of caution must be given since the calculated difference in the reaction free energies between complex **201** and **205** ($\Delta\Delta G_r$ of about 1–1.3 kcal/mol) is small and falls within the error of the numerical method. On the other hand, such a small difference is consistent with the experimental results which report a decomposition of 0.8% for **201** and 0.4% for **205** in the case of 10 eq. of water (Figure 2.8), corresponding to a difference in the reaction free energies of the two complexes of about 2 kcal/mol.

● Because of the active involvement of water molecules in the decomposition reaction, the implicit solvent calculations fail to predict the spontaneous decomposition of the reactants in water. Indeed, the use of a cavity model assumes that the solute electron density is not changed by specific interactions with individual solvent molecules and the reaction does not itself involve specific solvent molecules. The limitations resulting from these assumptions can be addressed

by including explicit solvent molecules inside the cavity. We introduce an explicit micro-solvation environment by considering the complexes interacting with five water molecules (see the reactants in Figure 2.8). The solute and its hydration shell are then considered solvated in DMSO with the implicit model to better reproduce the experimental condition of the NMR experiments. Multiple equilibrium geometries of reactants and products were generated. We reported in Figures 2.10 and 2.11 the structures of the three lower lying energy structures of the hydrated complex and the most stable structure of the products resulting from the decomposition of compound **201**, **205** and **207**.

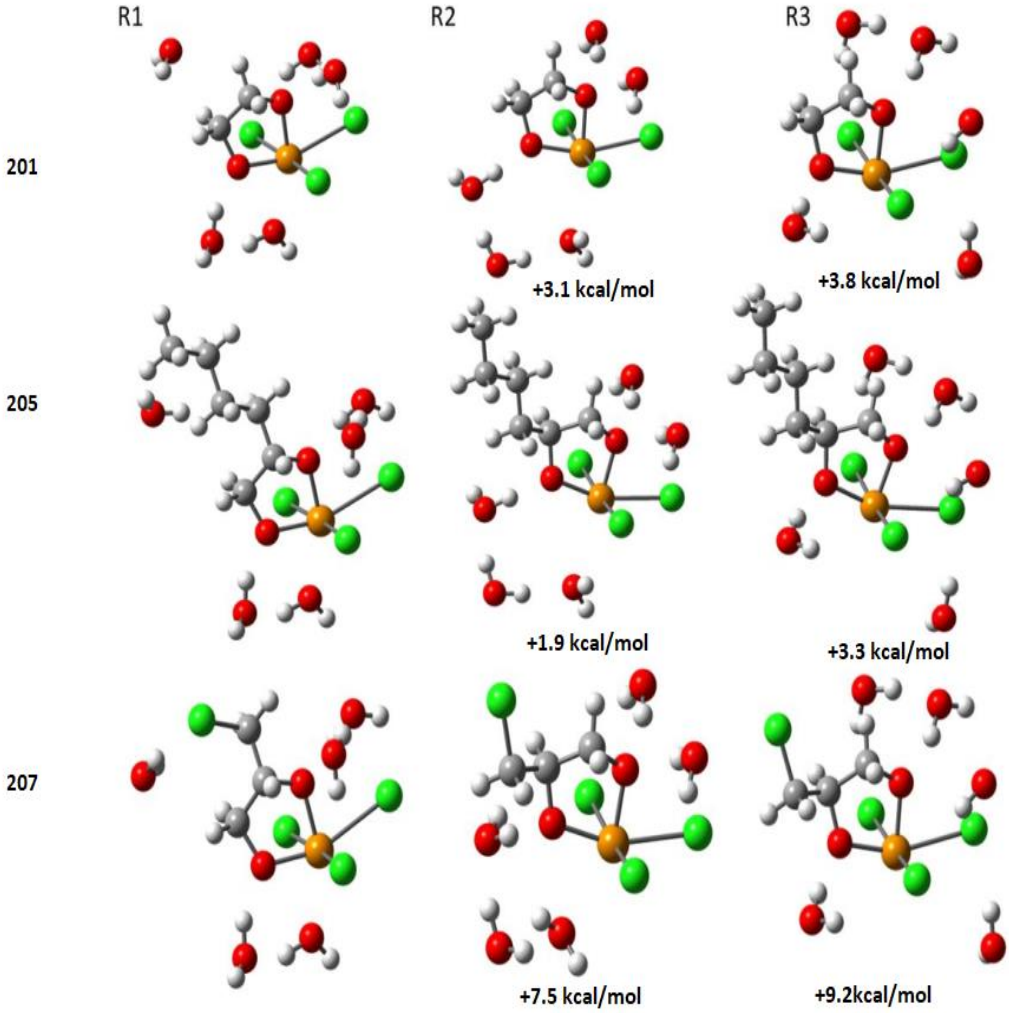

Figure 2.10. Optimized equilibrium geometries of complex **201** (upper row), **205** (central row) and complex **207** (bottom row) hydrated with five water molecules. The structures are optimized in implicit DMSO, they have an overall negative charge and a singlet spin multiplicity. The leftmost geometries are the most

stable, the other conformers have relative energies of +3.1 kcal/mol and +3.8 kcal/mol for complex **201** and +1.9 kcal/mol and 3.3 kcal/mol for complex **205**. and +7.5 kcal/mol and +9.2 kcal/mol for **207**.

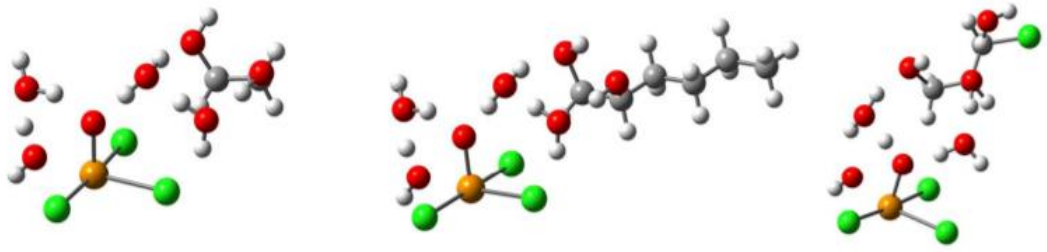

Figure 2.11. Optimized equilibrium geometries of the products of the decomposition reaction of complex **201** (left) and complex **205** (middle) and complex **207** (right). The structures include four water molecules and they are optimized in implicit DMSO. Structures have an overall negative charge and a singlet spin multiplicity.

The reaction free energies are reported in (table 2.1) for the different conformers of the reactants R1–R3 (Figure 2.11). We recover the spontaneous decomposition of the complexes and an increased stability of the complex substituted with the longer alkyl chain in good agreement with the experimental findings. By defining the solvation contribution to the free energy of reaction as the difference between the ΔG_r calculated with the explicit micro-solvation shell model and its gas-phase value we find that these contributions are −27.3 kcal/mol, −18.2 kcal/mol and −12.6 kcal/mol for complex **207**, complex **201** and complex **205**, respectively. These results suggest that the trend in the stability of the complexes increasing with the length of the alkyl chain results from a less efficient hydration of the structure of the reactants relative to the decomposition products. Indeed, the mechanism of the decomposition reaction involves multiple steps of proton transfer requiring the active involvement of clusters of water molecules. Mechanistic insights into the decomposition reaction are shown in Figure 2.12 and they were obtained by investigating the reaction path starting from the most stable structure of the hydrated compound **201** (Reactant in Figure 2.12).

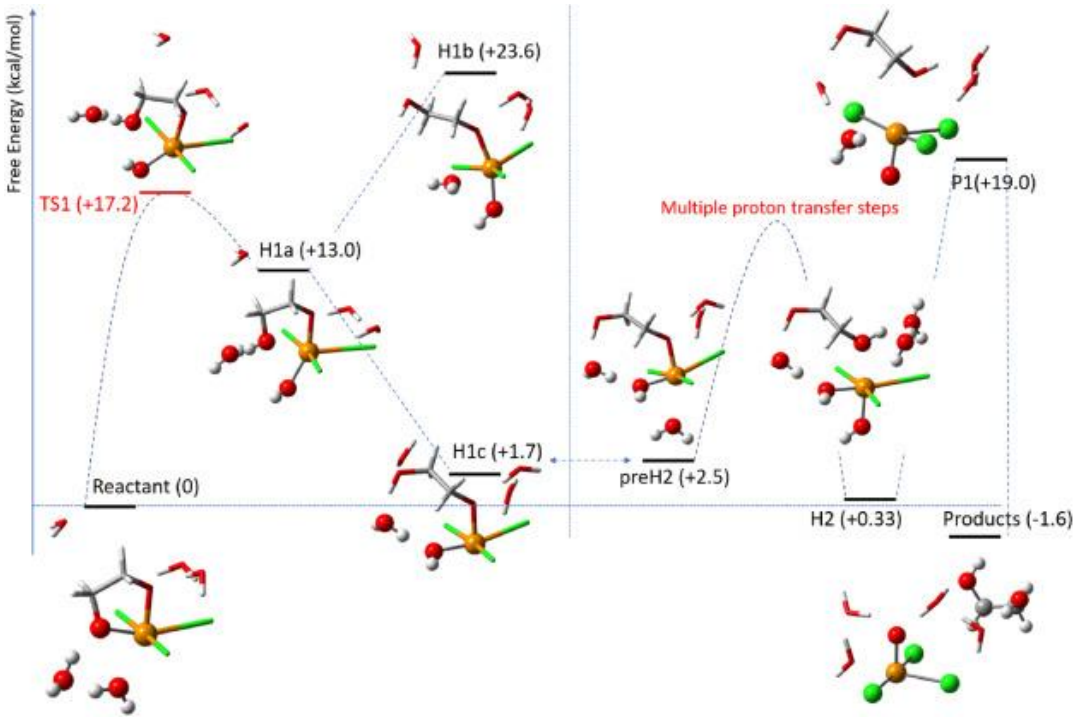

Figure 2.12. Mechanistic insights into the decomposition reaction of **201** by considering an explicit micro-solvation shell formed by 5 molecules of water. The free energy of the structures relative to the reactant complex is reported in parenthesis (in unit of kcal/mol). Geometries corresponding to black lines are minima of the potential energy surface while TS1 is a transition state with an imaginary frequency of 131 cm^{-1}. The vertical line in the middle of the picture divides the hydrolysis of the fist Te-O bond from the hydrolysis of the second Te-O bond which leads to the formation of the free glycol.

Structures with real frequencies corresponds to minima of the potential energy surface that are equilibrium geometries of reactants, products and reaction intermediates. Geometries of transition states correspond to a saddle point of the Potential Energy Surface (PES) and are characterized by an imaginary frequency for the mode identifying the reaction coordinate. The mechanism of the decomposition reaction was assumed to consist of two subsequent hydrolysis steps. We identify a transition state (TS1 in Figure 2.12) corresponding to the rupture of the first Te-O bond at a free energy of +17.2 kcal/mol from the reactant complex. Breaking this bond requires both a nucleophilic attack of a water molecule to the Te center together with a proton transfer from the water to the forming glycol molecule. Following the intrinsic reaction coordinate corresponding to the imaginary frequency of TS1 we find a reaction intermediate where a -OH group is coordinated to the Te center at an angle of about 120° from the plane of the $-TeCl_3$ moiety (H1a in Figure 2.12). This structure can rearrange in other conformers (H1b and H1c in Figure 2.12) where the most stable (+1.7 kcal/mol from the reactant) is

characterized by the -OH group coordinated to Te in equatorial position. The hydrolysis of the second Te-O bond to form the free glycol molecules again requires the coordination of a second water molecule to the Te centre. This second nucleophilic attack to the Te centre comes most probably from the side opposite to the Te-O bond to break (see structure preH2 in Figure 2.12). This geometry implies that the water molecule attacking the Te centre transfers its protons to other acceptors and the protonation of the glycol is operated by a separate species (which might be a second water molecule or even a H_3O^+ ion). Most probably there are many possible paths for these multiple proton transfer steps and the mechanistic details depends on the relative position of the hydrating water molecules. The increasing of the decomposition ratio with the numbers of water equivalents observed experimentally is readily explained by considering that clusters formed by a higher number of water molecules are more efficient in mediating proton transfer steps trough the more extended H-bond network. From the intermediate structure where two -OH groups are coordinated to the Te centre (H2 in Figure 2.12) a further proton transfer step leads to the formation of the trichloro Tellurium(IV) oxide $[OCl_3Te]^-$ (Products in Figure 2.12) where one of the vertexes of the square pyramid is occupied by a coordinated water molecule, at least in solution. In the mass spectrum of the decomposed product, as described before, the coordinated water molecule is not visible due to the ESI conditions.

2.2.3. Antimicrobial Activity

Since AS-101 and Te(IV) species showed antimicrobial activity against *Enterobacter cloacae* and Pseudomonas aeruginosa, some of the complexes synthesized, **(203**, **204** and **205**), together with the free ligands, were selected and screened for antimicrobial activity against the most common and representative bacteria, including *Escherichia coli* (Gram negative), *Staphylococcus aureus* (Gram positive), methicillin resistant *Staphylococcus aureus* (MRSA), *Pseudomonas aeruginosa*, and the yeast *Candida albicans* (fungi representative). These compounds showed interesting activity against the Gram negative bacterium *E. coli* (MIC_{50} values between 15 and 20 μM as reported in Table 2.3) while they were less active or inactive against the other bacteria and *C. albicans*. The free diol ligands that are displaced in physiological conditions, have been analyzed and they do not show any activity. We conclude that the similar activity of the complexes is probably due to the hydrolyzed product $[Cl_3OTe]^-$. Interesting, a black metallic, granular layer

was visible in the assay medium of *E. coli* treated plates and it is probably due to the reduction of the Te(IV) by the bacteria, as already observed by Yang and co-workers (Figure 2.13)[39].

Table 2.3. MIC_{50} and MIC_{80} values for compounds **203-205** against *E-Coli*

Compound	MIC_{50} (μM)	MIC_{80} (μM)
203	19.8 ± 0.5	40.5 ± 0.6
204	18.4 ± 0.4	37.8 ± 0.7
205	17.1 ± 0.6	35.7 ± 0.8

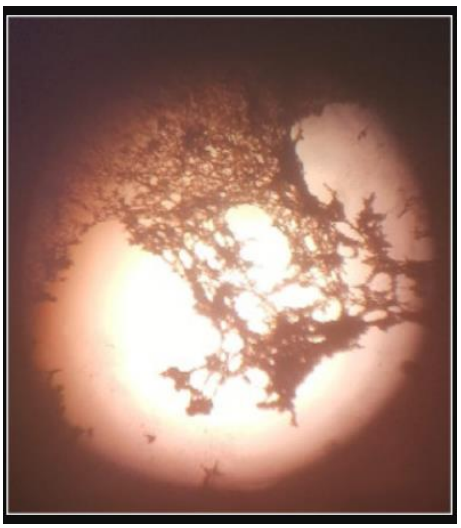

Figure 2.13. Black precipitate observed at the bottom of the plate of *E. coli* treated with **203**.

2.3. Experimental

2.3.1 Material and methods

$TeCl_4$ and all the diol ligands have been purchased from Sigma-Aldrich or TCI Europe. All solvents were used without further purification except for CH_3CN which was kept dry over molecular sieves under inert atmosphere. All NMR spectra were recorded on a Bruker Advance spectrometer with the probe at 293 K, operating at 500 MHz for the ^{1}H, at 125 MHz for the ^{13}C and at 158 MHz for the ^{125}Te nucleus, respectively. Spectra were recorded in DMSO-d_6 using Me_4Si as the internal standard for ^{1}H and ^{13}C while diphenyl ditelluride was used as external reference for ^{125}Te. All chemical shifts δ are reported in ppm. FT-IR spectra were recorded (compounds **201** and **203**) from either CsI disks (solid samples) or KRS-5 thallium bromoiodide cells (neat liquid samples) at r.t on a Perkin Elmer Frontier FT-IR/FIR spectrophotometer in the range 4000–600 cm^{-1} (32 scans, resolution 4 cm^{-1}) and in the range 600–200 cm^{-1} (32 scans, resolution 2 cm^{-1}). Data processing was carried out using OMNIC version 5.1 (Nicolet Instrument Corporation). For all the other compounds Infrared (IR) spectra were recorded in the region 4000–400 cm^{-1} on a Perkin Elmer ATR (Attenuated Total Reflectance) precisely spectrum 100 FT/IR spectrometer. Elemental analysis (carbon, hydrogen and nitrogen) were performed with a PerkinElmer 2400 series II analyzer. ESI (Electro Spray Ionization) mass spectra were recorded in negative mode with a Waters LCT Premier XE Spectrometer. The stability of the complexes has been evaluated following the decomposition reaction by ^{1}H, ^{13}C and ^{125}Te NMR. Each compound was accurately weighted and dissolved in 400 µL of DMSO-d_6 to obtain 125 mM solution (0.05 mmoles). 10 µL of D_2O were added in three consecutive aliquots and the NMR spectra were recorded 1 h after each addition (each addition corresponds to 10 equivalents of water with respect the complex). The experiments were run in triplicate.

2.3.2. Effect of compounds on growth of *E. coli*

To each well of a 96-well plate (Sarstedt), 100 µL of fresh nutrient broth medium were added. A serial dilution of each compound was performed on the plate to give a concentration range of (150–0.59 µM). Cells suspension (100 µL) of *E. coli* (1 × 106 cells/mL) was added to each well and the plates were incubated at 37 °C for 24 h. The experiments were carried out in duplicate. The OD570nm of the cultures was determined using a microplate reader (Bio-Tek, Synergy HT) and all growth was expressed as a percentage of that in the control. The MIC_{50} and MIC_{80} (Minimum

Inhibition Concentration) are defined as the lowest concentration to inhibit growth by 50% and 80%, respectively. Since being the first time, the antibacterial activity was studied in these complexes, the most common and representative bacteria of each family were selected: Escherichia coli is gran negative, Staphylococcus aureus is gran positive, Staphylococcus aureus (MRSA) is methicillin resistant, yeast Candida albicans as a fungi representative.

2.3.3. Computational method

Structures and energetics were modelled by Density Functional Theory (DFT) at the wB97XD/lanL2DZ level of theory, which performs well in prediction of reaction geometries and energies.[40] Implicit solvation was introduced with the *Solvation Model based on Density* (SMD) parametrization software Gaussian09 with explicit solvents of acetonitrile, DMSO and water. The ground state geometry of each compound was optimized in implicit solvent by including the effect of the polarizable continuum in the self-consistent field procedure. The explicit micro-solvation model was built by adding five water molecules to the reactant complex, the whole hydrated complex was then re-optimized in implicit DMSO. The initial positions of the water molecules were selected manually by maximizing the possibility of forming hydrogen bonds between water molecules and the compounds in order to find the most stable structures of reactants and products upon optimizations. The initial models were optimized, for the analysis we retained the three lower energy structures of the reactants (Figure 2.10) and the lowest energy structure of the hydrated products (Figure 2.11). Frequency calculations allowed the characterization of the potential energy surface and the evaluation of the thermochemistry of the involved compounds. All computations were performed with Gaussian16.

2.3.4. Synthesis and Characterization

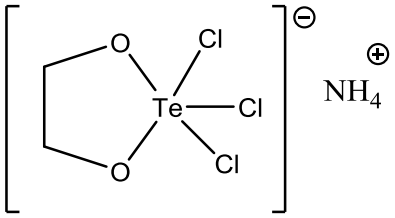

201. 201 was obtained following the procedure of Albeck with a slight modification. $TeCl_4$ (0.27 g, 1 mmol) was refluxed with dry ethylene glycol (0.15 g, 2.6 mmol) in dry CH_3CN (2ml) for 4 h at 80°C. A white crystalline solid precipitated out after cooling the reaction at r.t and it was recovered by filtration, washed with cold CH_3CN and Et_2O and dried under vacuum. Yield (46%).

Elem. Anal. %C (7.70), %H (2.58), %N (4.49); found C (7.85) H (2.38) N (4.79)

^{1}H NMR (DMSO-d_6): δ 4.37(s, 4H, $(CH_2)_2$): 7.20(t,4H, NH_4)

^{13}C NMR (DMSO-d_6): δ 67.44 $(CH_2)_2$

^{125}Te (DMSO-d_6): δ = 1680

IR cm^{-1} (ATR): 3189: 2932: 1398: 1334: 1217: 1106: 1017: 991: 865 cm^{-1}

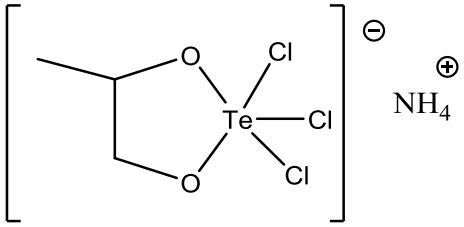

202. $TeCl_4$ (0.28 g, 1 mmol) was refluxed with dry 1,2 Propanediol (0.18 g, 2.3 mmol) in dry CH_3CN (2ml) for 4 h at 80°C. A white crystalline solid precipitated out after cooling the reaction at r.t. and it was recovered by filtration, washed with cold CH_3CN and Et_2O and dried under vacuum. Yield (52%).

Elem. Anal. %C (11.05), %H (3.09), %N (4.30); found C (10.83) H (3.21) N (4.49).

^{1}H NMR (DMSO-d_6): δ = 1.21 (d, 3H, CH_3): 3.65 (t, CH), 4.33 (t, 1H, CH), 4.84 (t, 1H, CH), 7.33 (t, 4H, NH_4)

^{13}C NMR (DMSO-d_6): δ = 18.70 (CH_3), 72.72 (CH_2), 74.31 (CH)

^{125}Te (DMSO-d_6): δ = 1692.

(-) ESI mass: peak at m/z 307.83 corresponding to $[C_3H_6Cl_3O_2Te]^-$.

IR cm^{-1} (ATR): 3158: 2937: 1397: 1336: 1235: 1122: 1068: 979: 837 cm^{-1}

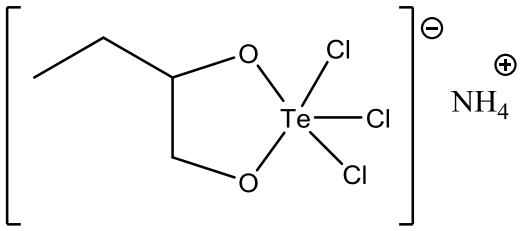

203. $TeCl_4$ (0.28 g, 1 mmol) was refluxed with 1,2 Butanediol (0.21 g, 2.4 mmol) in dry CH_3CN (2ml) for 24 h at 80°C. A white crystalline solid precipitated after addition of diethyl ether at r.t. and it was recovered by filtration, washed with cold CH_3CN and Et_2O and dried under vacuum. Yield (72%).

Elem. Anal. %C (14.13), %H (3.56), %N (4.12); found C (14.52) H (3.69) N (4.49).

^{1}H NMR (DMSO-d_6): δ 0.93 (t, 3H, CH_3), 1.56 (m, 2H, CH_2), 3.71 (t, 1H, CH), 4.17 (t, 1H, CH), 4.82 (s, 1H, CH), 7.33 (t, 4H, NH_4).

^{13}C NMR (DMSO-d_6): δ 10.01 (CH_3), 26.19 (CH_2), 71.10 (CH_2), 79.55 (CH).

^{125}Te (DMSO-d_6): δ = 1692.

(-) ESI mass: peak at m/z 321.85 corresponding to $[C_4H_8Cl_3O_2Te]^-$.

IR cm^{-1} (ATR): 3160: 2965: 1402: 1332: 1118: 1081: 1029: 975: 960: 934: 858: 774 cm^{-1}

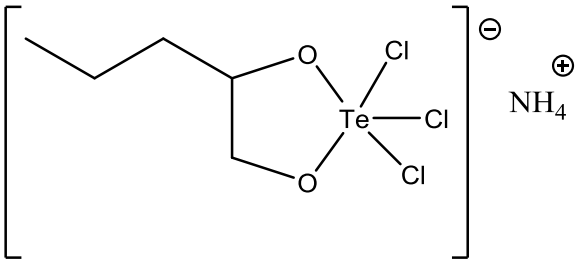

204. $TeCl_4$ (0.36 g, 1.2 mol) was refluxed with 1,2 Pentanediol (0.32 g, 3 mmol) in dry CH_3CN (2ml) for 120 h at 80°C. A white crystalline solid precipitated after addition of diethyl ether at r.t. and recovered by filtration, washed with cold CH_3CN and Et_2O and dried under vacuum. Yield (61%).

Elem. Anal. %C (16.96), %H (3.96), %N (3.99); found C (16.85), H (4.09), N (4.29).

^{1}H NMR (DMSO-d_6): δ = 0.89 (t, 3H, CH_3), 1.40 (m, 2H, CH_2), 1.51 (m, 2H, CH_2), 3.69 (t, 1H, CH), 4.24 (t, 1H, CH), 4.81 (s, 1H, CH), 7.26 (t, 4H, NH_4).

^{13}C NMR (DMSO-d_6): δ = 14.08 (CH_3), 18.57 (CH_2), 35.28 (CH_2), 71.37(CH_2), 78.03 (CH).

^{125}Te (DMSO-d_6): δ = 1690.

(-) ESI mass: peak at m/z 335.87 corresponding to $[C_5H_{10}Cl_3O_2Te]^-$.

IR cm^{-1} (ATR): 3145: 3046: 2961: 1403: 1083: 994: 964: 892: 838: 678 cm^{-1}

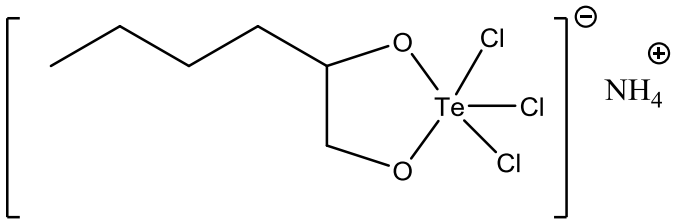

205. $TeCl_4$ (0.44 g, 1.5 mmol) was refluxed with 1,2 Hexanediol (0.35 g, 3 mmol) in dry CH_3CN (2ml) for 120 h at 80°C. A white crystalline solid precipitated after addition of diethyl ether at r.t. and it was recovered by filtration, washed with cold CH_3CN and Et_2O and dried under vacuum. Yield (56%).

Elem. Anal. %C (19.58), %H (4.38), %N (3.80); found C (19.40), H (4.08), N (4.05).

^{1}H NMR (DMSO-d_6): δ = 0.87 (d, 3H, CH_3): 1.30 (m, 2H, CH_2), 1.39 (m, 2H, CH_2), 1.54 (m, 2H, CH_2) 3.70 (t,1H, CH), 4.23 (t,1H, CH), 4.85 (t,1H, CH), 7.23 (t, 4H, NH_4).

^{13}C NMR (DMSO-d_6): δ = 13.88 (CH_3), 22.23 (CH_2), 27.44 (CH_2), 32.81 (CH_2), 71.44 (CH_2), 78 (CH).

^{125}Te (DMSO-d_6): δ = 1692.

IR cm^{-1} (ATR): 3154: 2958: 1401: 1084: 1051: 999: 963: 858: 782: 680 cm^{-1}

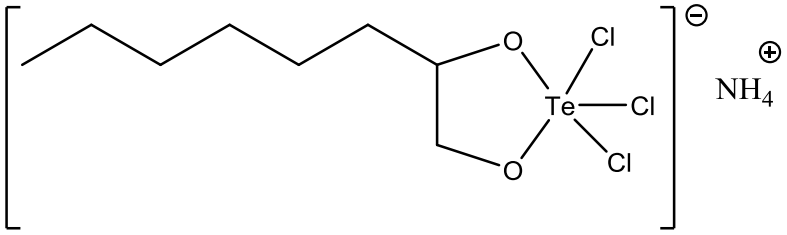

206. $TeCl_4$ (1.09 g, 3.7 mmol) was refluxed with 1,2 Octanediol (1.35 g, 9.2 mmol) in dry CH_3CN (15ml) for 120 h at 80°C. A white crystalline solid precipitated after addition of diethyl ether at r.t. and it was recovered by filtration, washed with cold CH_3CN and Et_2O and dried under vacuum. Yield (53%)

Elem. Anal. %C (24.25), %H (5.09), %N (3.54); found C (24.40), H (5.32), N (3.25).

^{1}H NMR (DMSO-d_6): δ = 0.85 (t, 3H, CH_3), 1.25 (m, 6H, $(CH_2)_3$), 1.38 (m, 2H, CH_2), 1.51 (m, 2H, CH_2), 3.68 (t, 1H, CH), 4.21 (t, 1H, CH), 4.79 (t, 1H, CH), 7.29 (t, 4H, NH_4).

^{13}C NMR (DMSO-d_6): δ = 13.93 (CH_3), 22.01 (CH_2), 25.22 (CH_2), 28.79 (CH_2), 31.18 (CH_2), 33.20 (CH_2) 71.33 (CH_2), 78.25(CH).

^{125}Te (DMSO-d_6): δ = 1687.

IR cm^{-1} (ATR): 3151: 2929: 1402: 1073: 1012: 961: 885: 849: 789: 722: 688 cm^{-1}

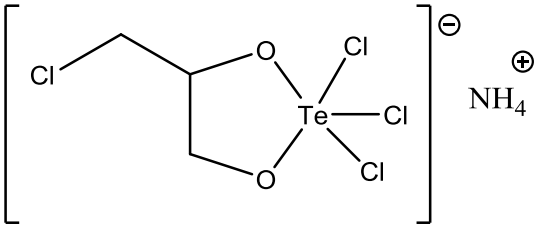

207. $TeCl_4$ (0.97 g, 3.3 mol) was refluxed with 3-Chloro-1,2 Propanediol (0.7 g, 8.2 mmol) in dry CH_3CN (15ml) for 120 h at 80°C. A yellow/white solid precipitated after addition of diethyl ether at r.t. and it was recovered by filtration, washed with cold CH_3CN and Et_2O and dried under vacuum. Yield 30%.

Elem. Anal. %C (10.00), %H (2.52), %N (3.89); found C (10.13), H (2.28), N (3.64).

^{1}H NMR (DMSO-d_6): δ = 3.70 (m, 2H, CH2), 4.03 (t, 1H, CH), 4.51 (t, 1H, CH), 4.72 (t, 1H, CH), 7.29 (t, 4H, NH_4).

^{13}C NMR (DMSO-d_6): δ = 45.81 (CH_2), 68.28 (CH_2), 78.15 (CH).

^{125}Te (DMSO-d_6): δ = 1673.

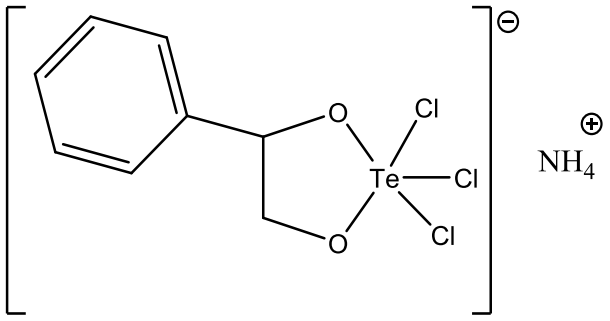

208. $TeCl_4$ (0.97 g, 3.3 mol) was refluxed with 1-phenyl-1,2-ethandiol (1.14 g, 8.2 mmol) in dry CH_3CN (15ml) for 120 h at 80°C. The solution turned a slight red colour at first and after 1 hr a green solution was formed. After 4 h, diethyl ether was added to but no solid precipitated. A

black/green oil was obtained after drying the solution under vacuum but from the NMR it was a mixture of several different species.

2.3.5. Figures

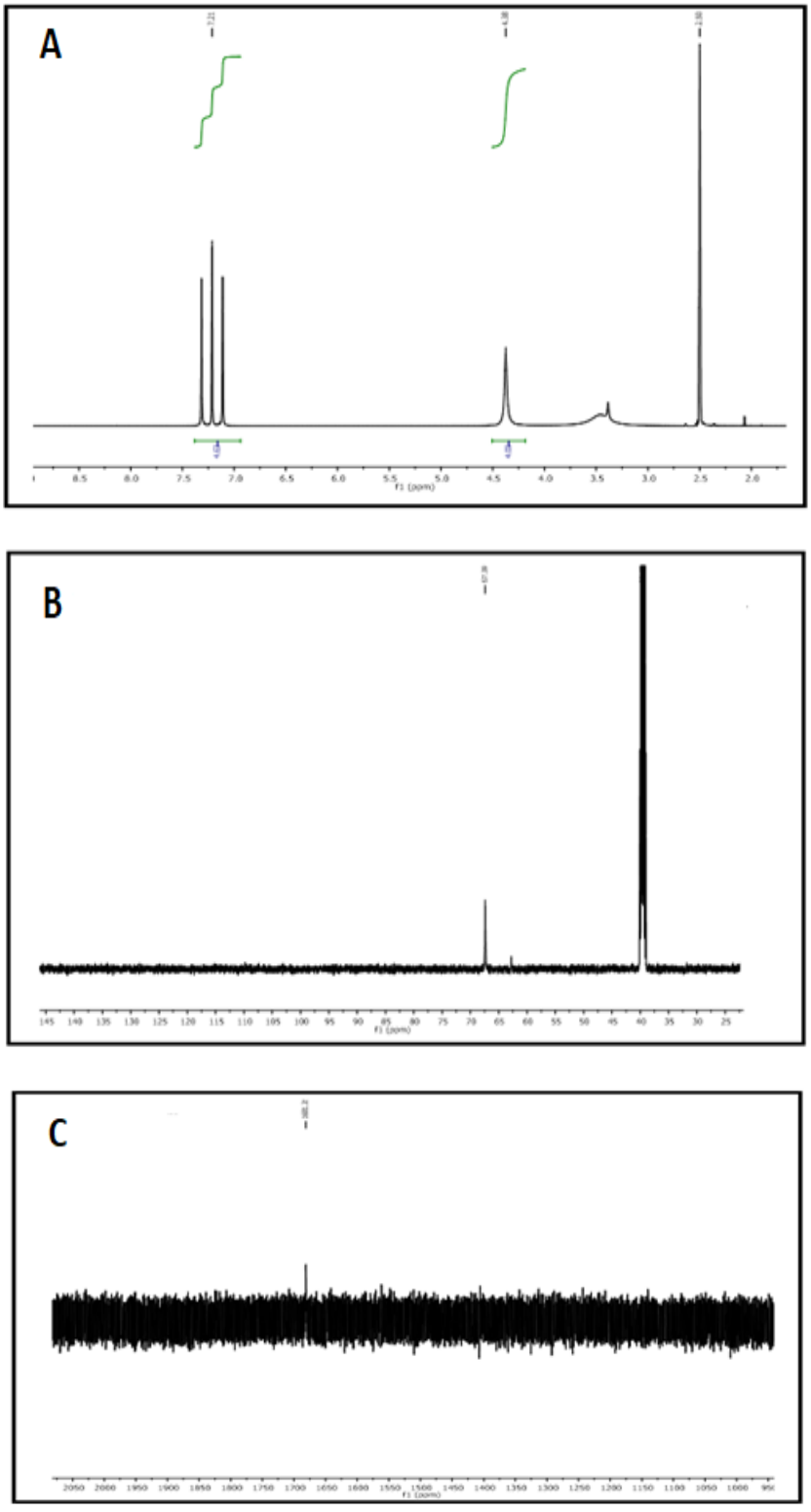

Figure 2.14. NMR spectra of **201;** A: ^{1}H, B: ^{13}C and C: ^{125} Te NMR in DMSO-d_6

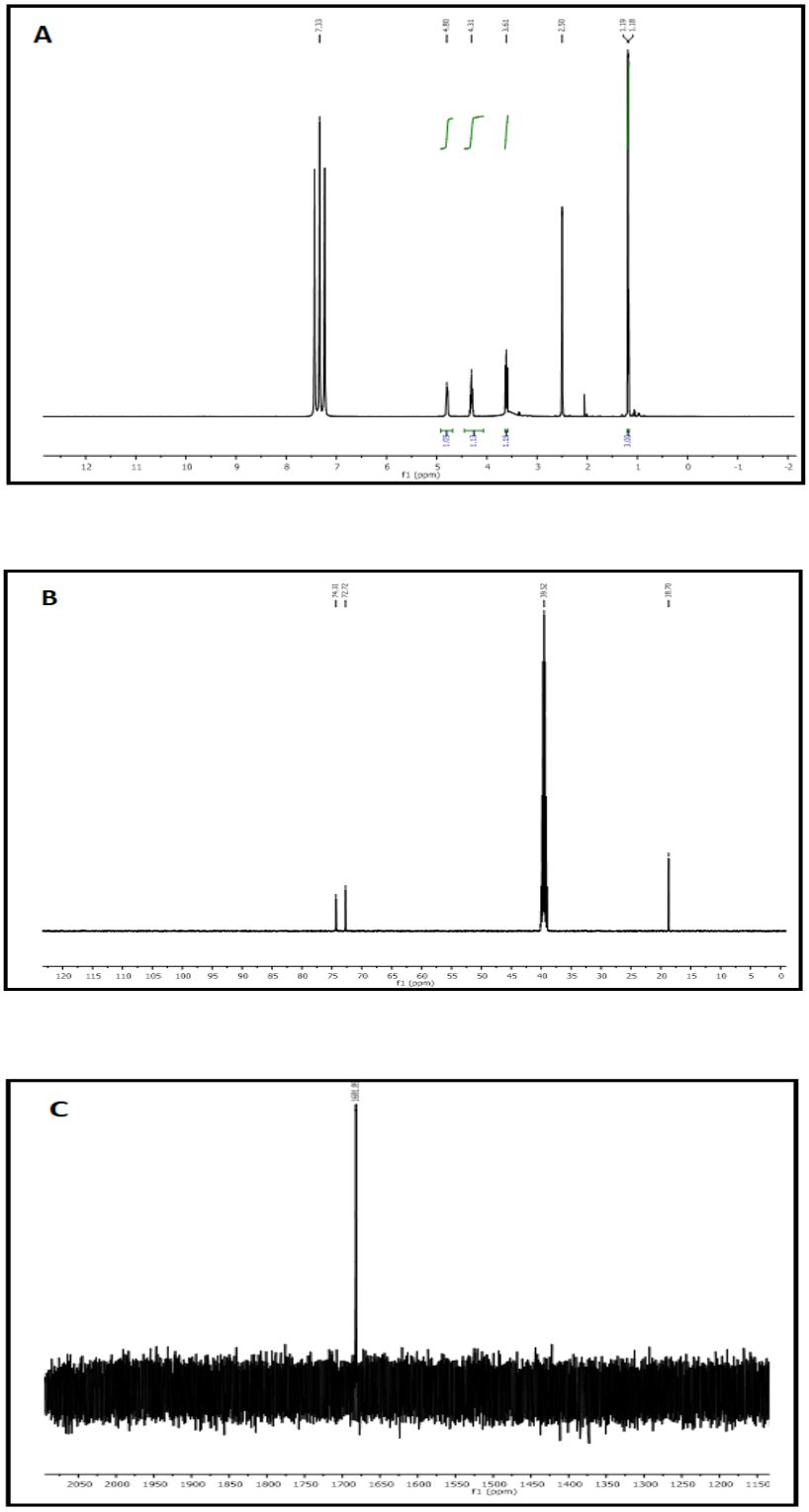

Figure 2.15. NMR spectra of **202;** A: ^{1}H, B: ^{13}C and C: ^{125} Te NMR in DMSO-d_6

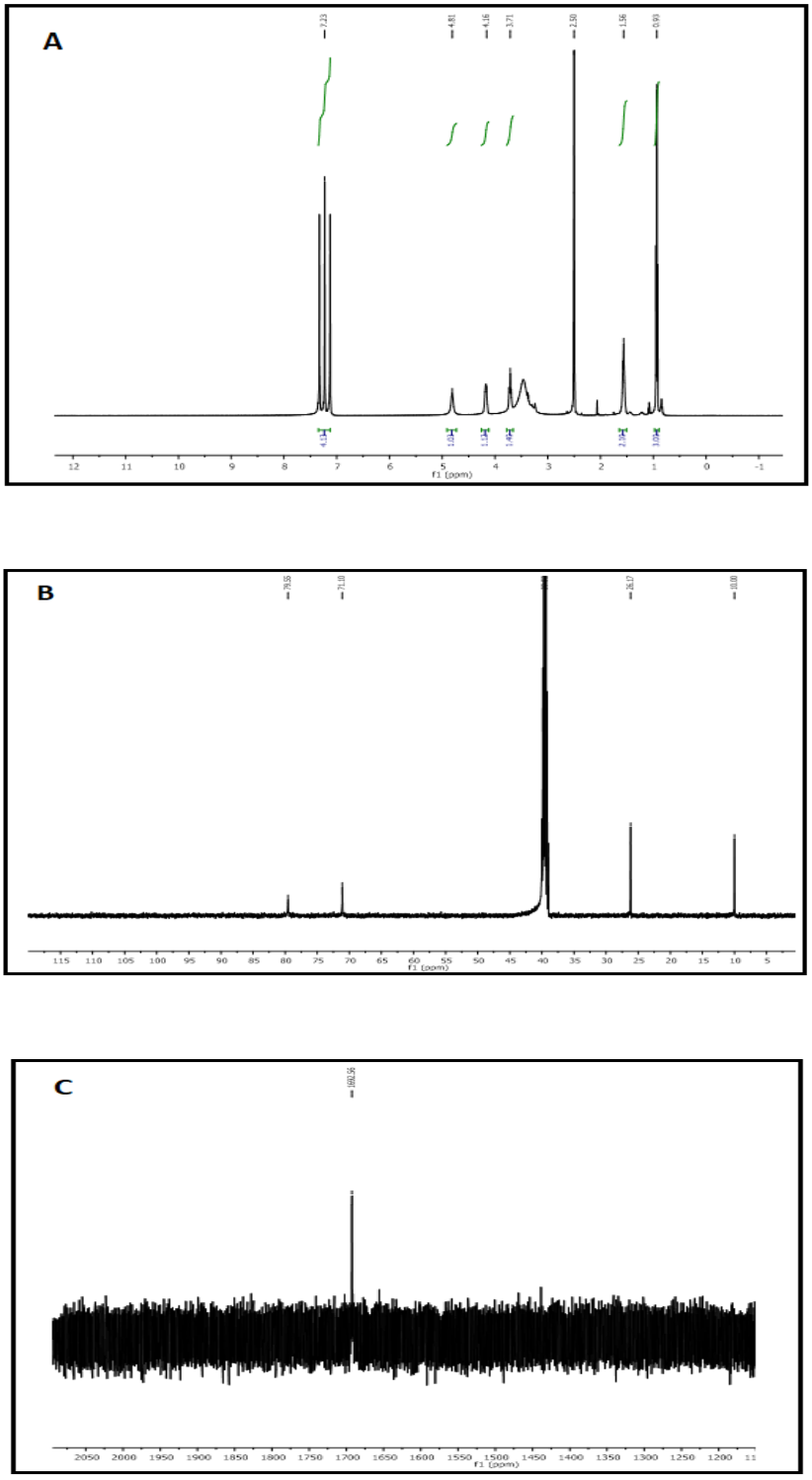

Figure 2.16. NMR spectra of **203**; A: ^{1}H, B: ^{13}C and C: ^{125} Te NMR in DMSO-d_6

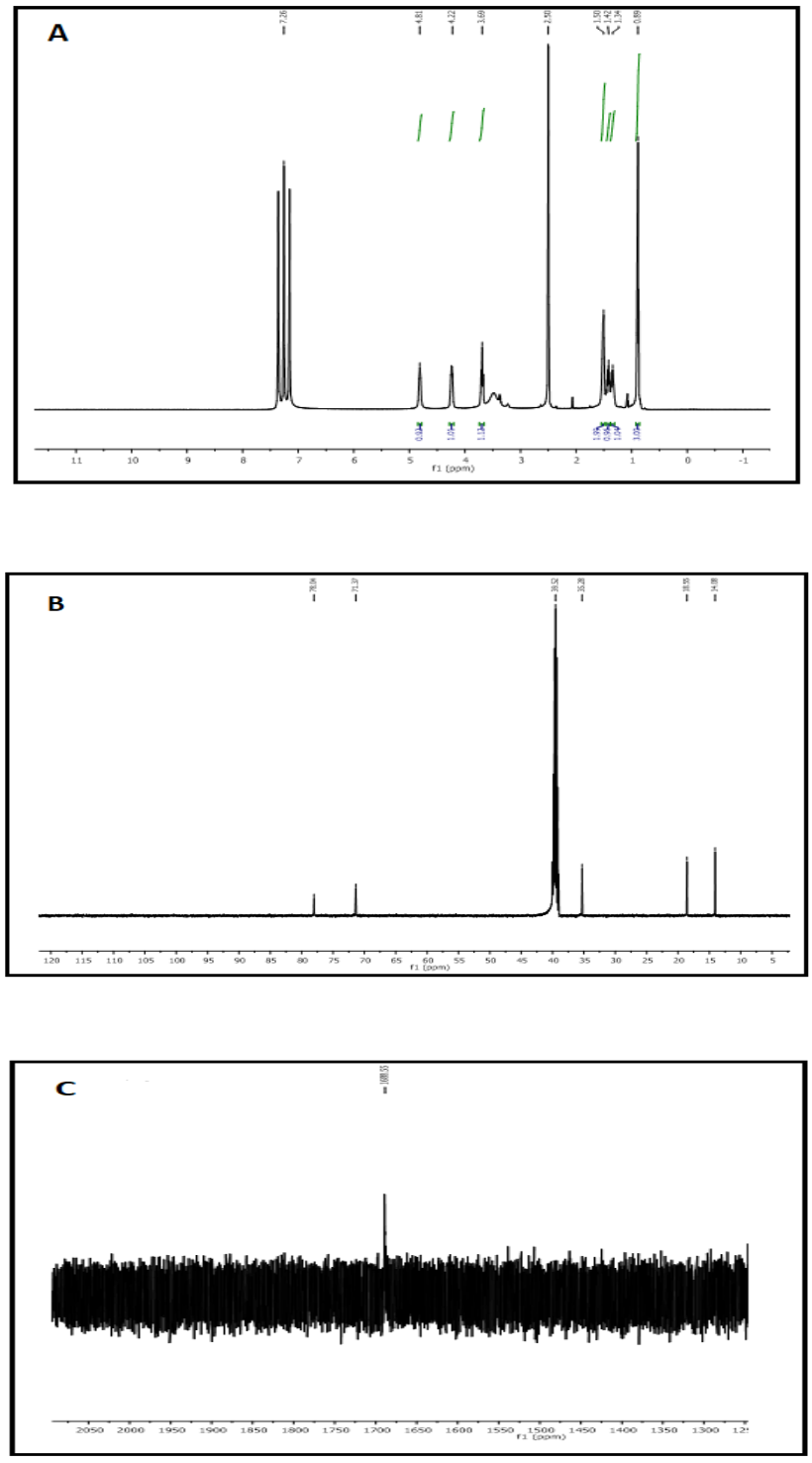

Figure 2.17. NMR spectra of **204**; A: ^{1}H, B: ^{13}C and C: ^{125} Te NMR in DMSO-d_6

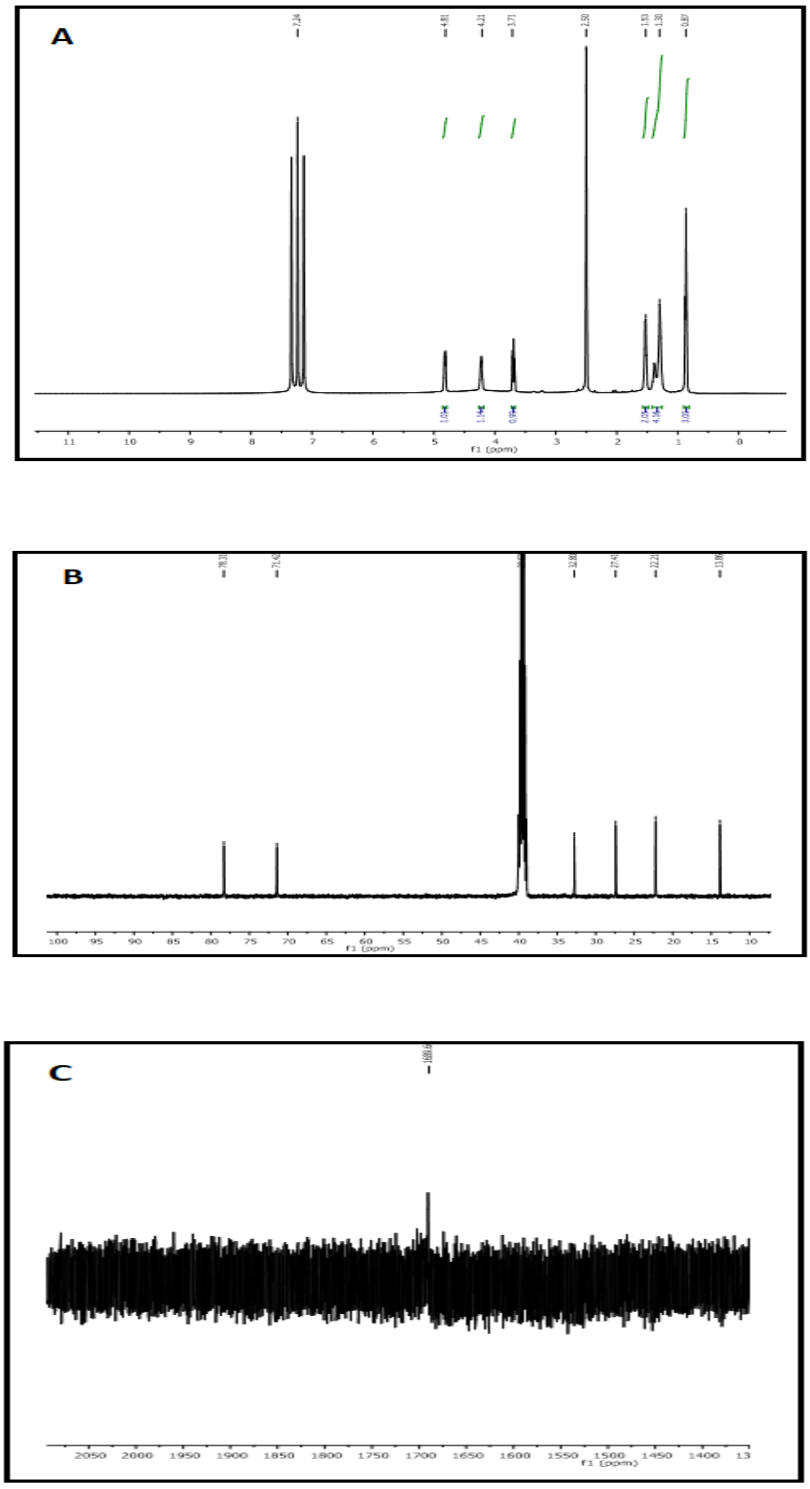

Figure 2.18. NMR spectra of **205**; A: ^{1}H, B: ^{13}C and C: ^{125} Te NMR in DMSO-d_6

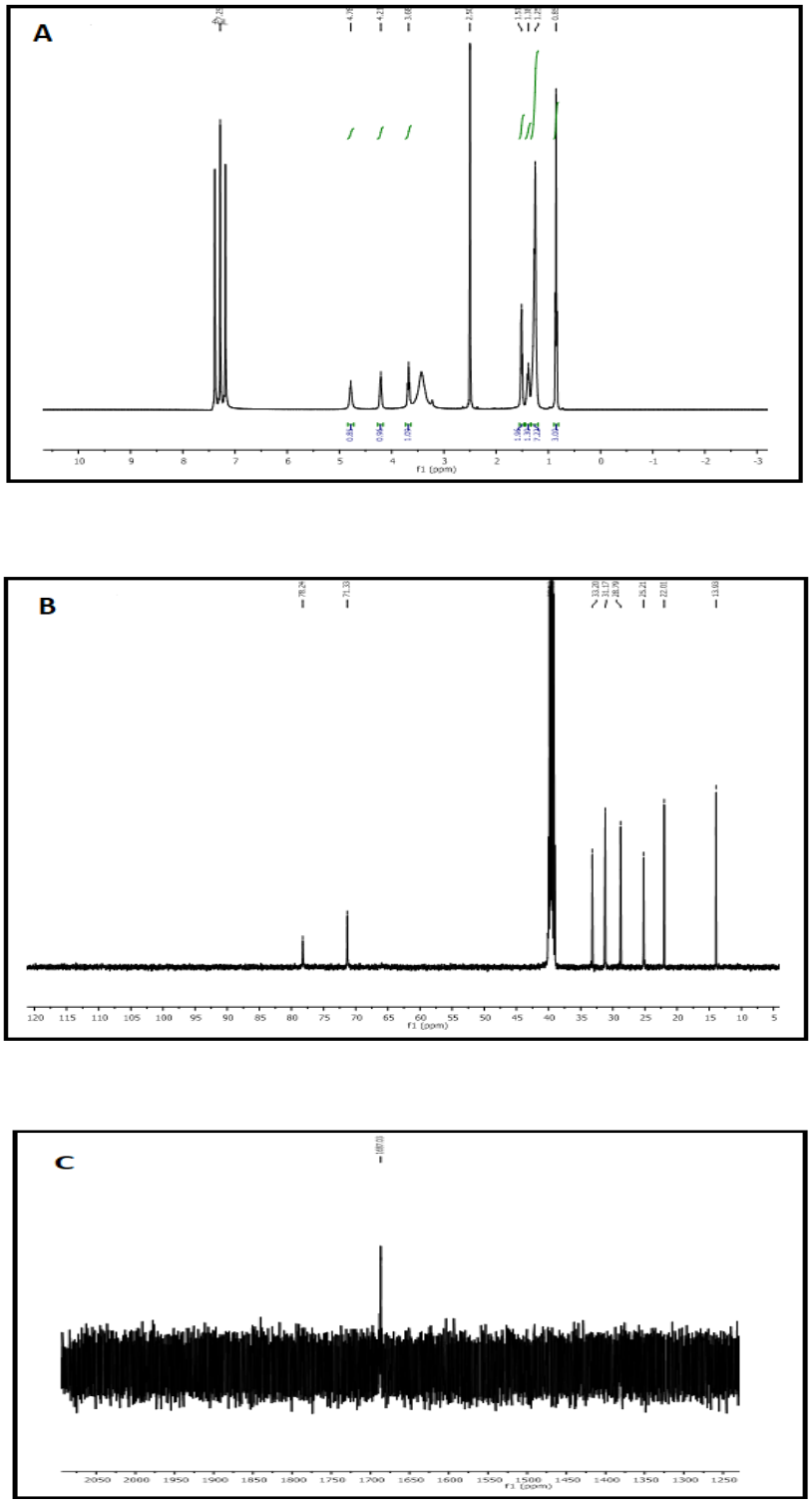

Figure 2.19. NMR spectra of **206**; A: ^{1}H, B: ^{13}C and C: ^{125} Te NMR in DMSO-d_6

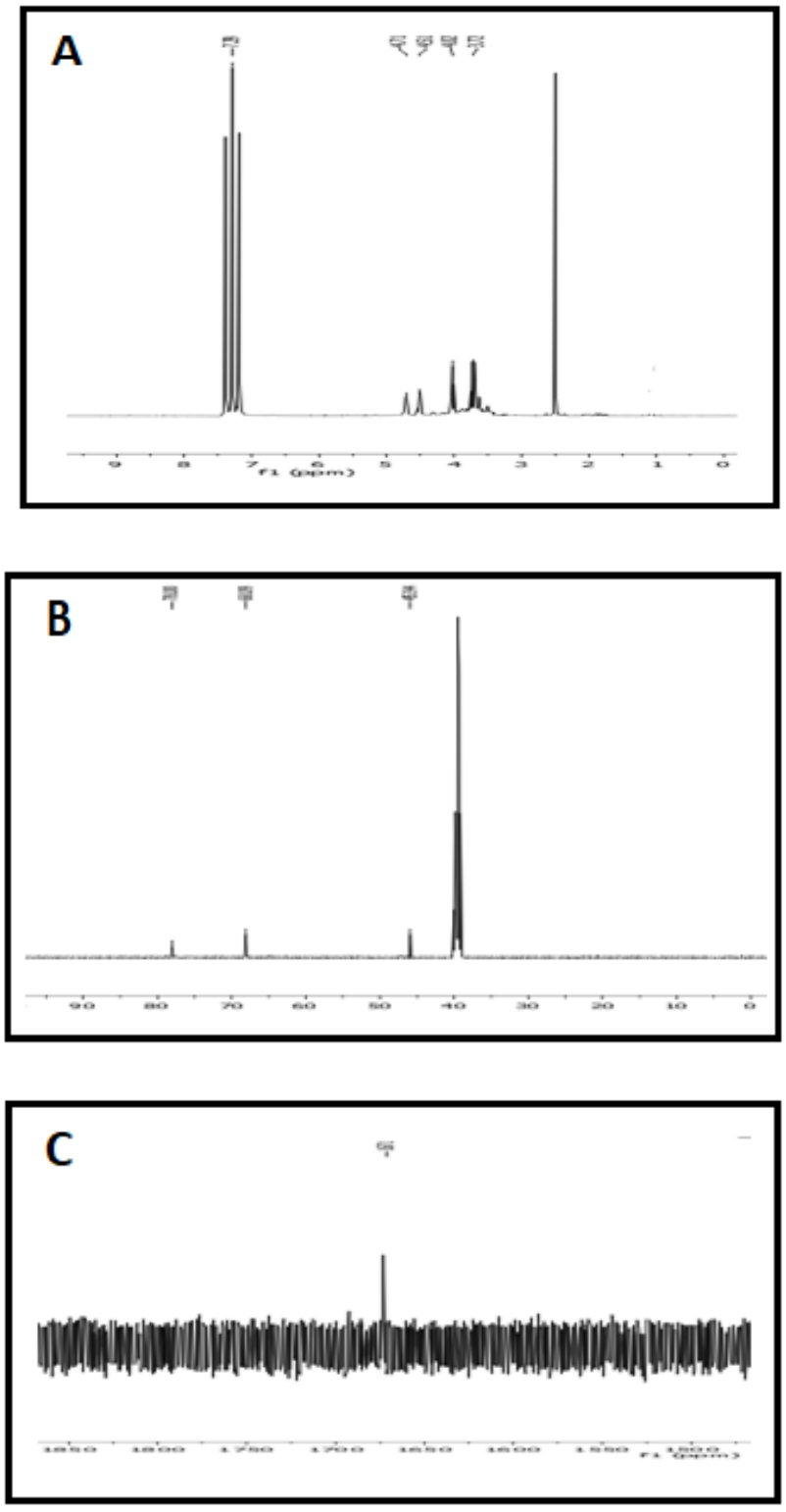

Figure 2.20. NMR spectra of **207**; A: ^{1}H, B: ^{13}C and C: ^{125} Te NMR in DMSO-d_6

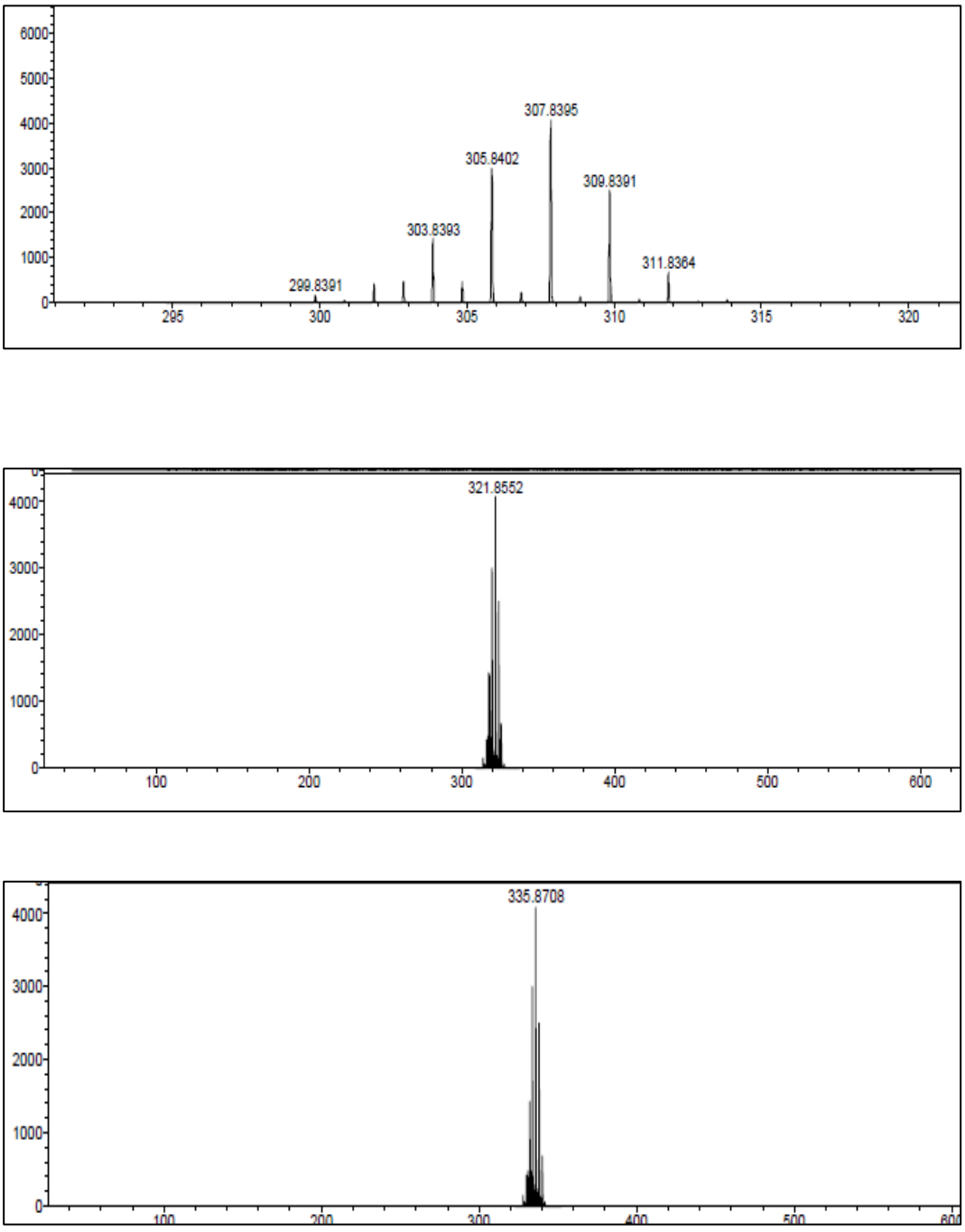

Figure 2.21. ESI-Mass spectra (-) of (top to bottom) of **202**, **203** and **204**.

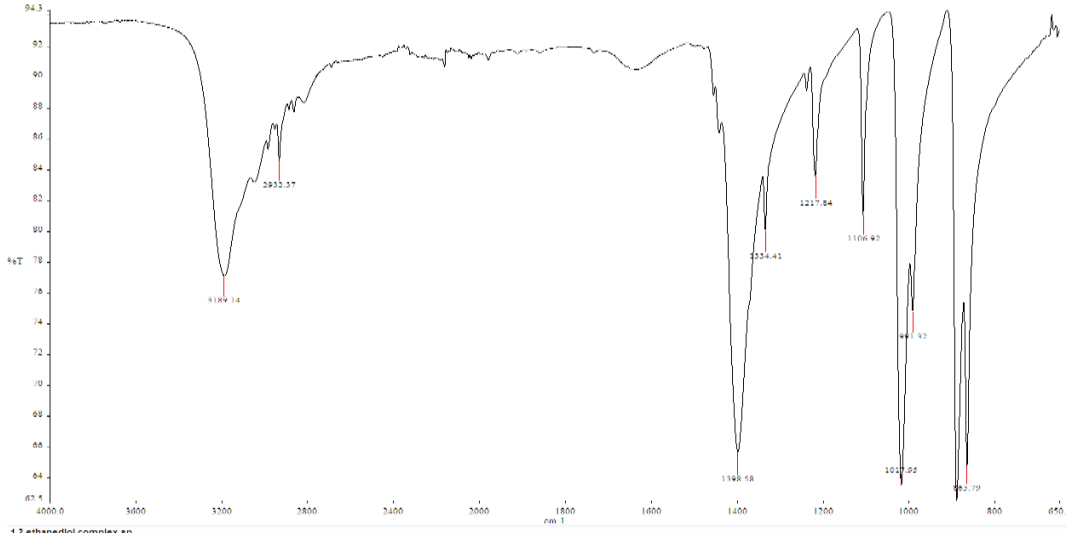

Figure 2.22. IR spectrum of compound **201**

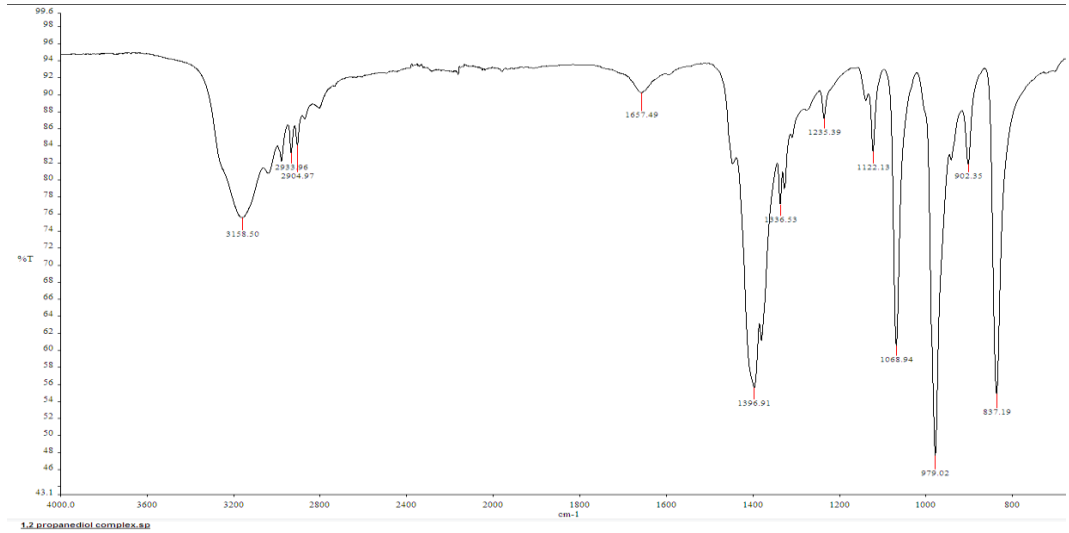

Figure 2.23. IR spectrum of compound **202**

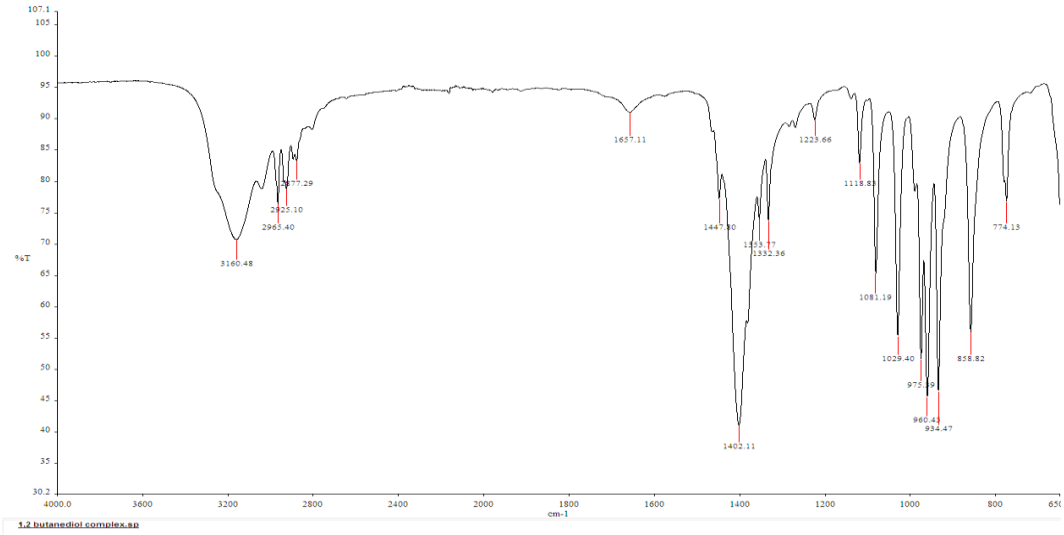

Figure 2.24. IR spectrum of compound **203**

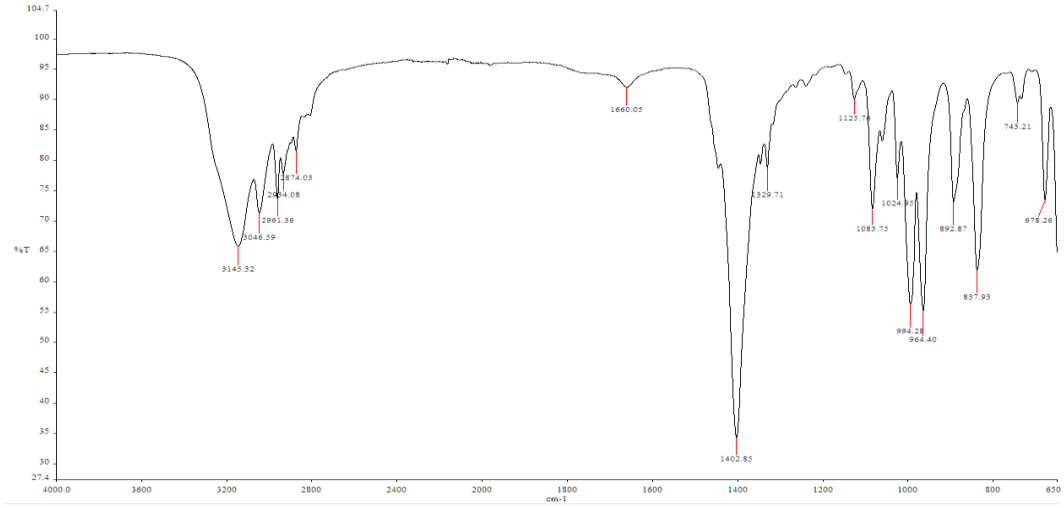

Figure 2.25. IR spectrum of compound **204**

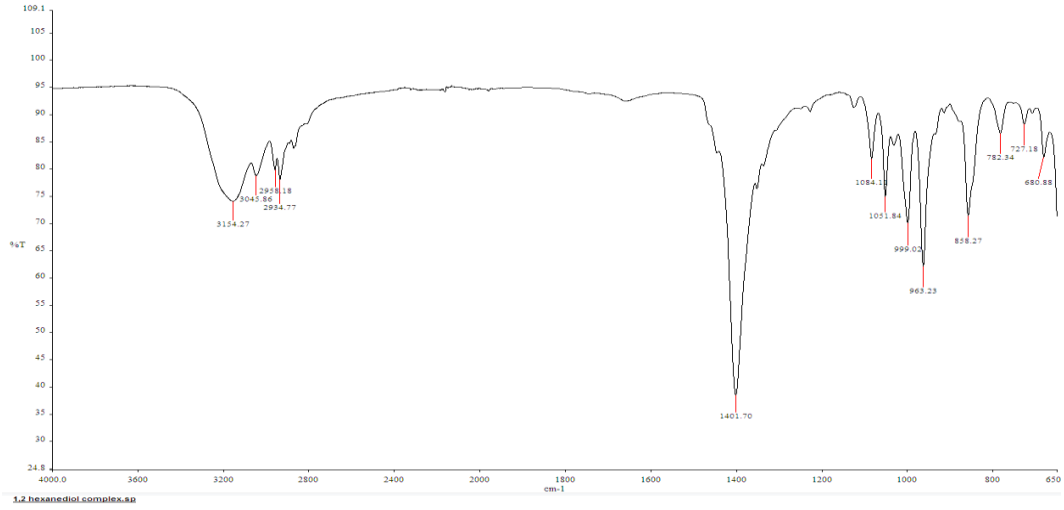

Figure 2.26. IR spectrum of compound **205**

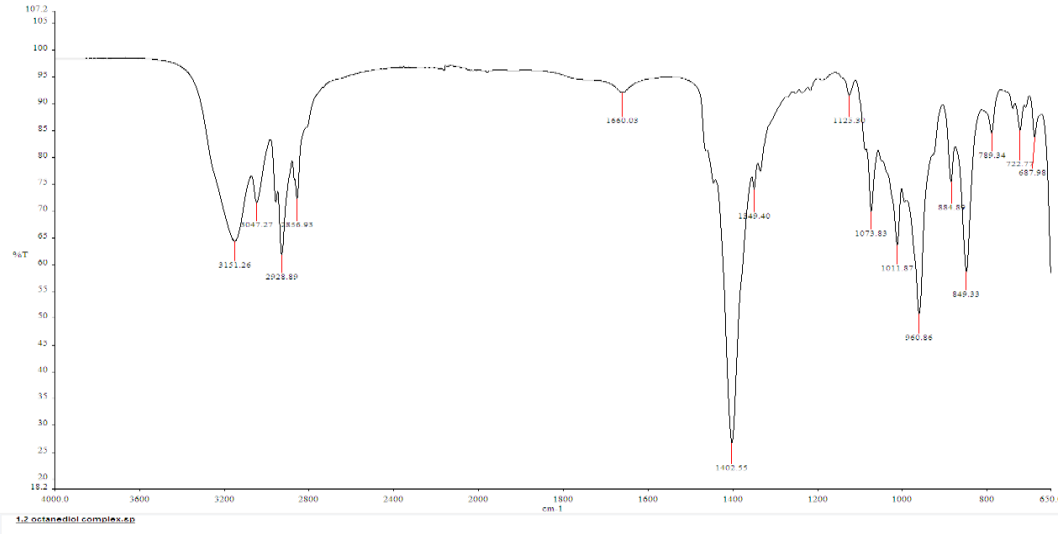

Figure 2.27. IR spectrum of compound **206**

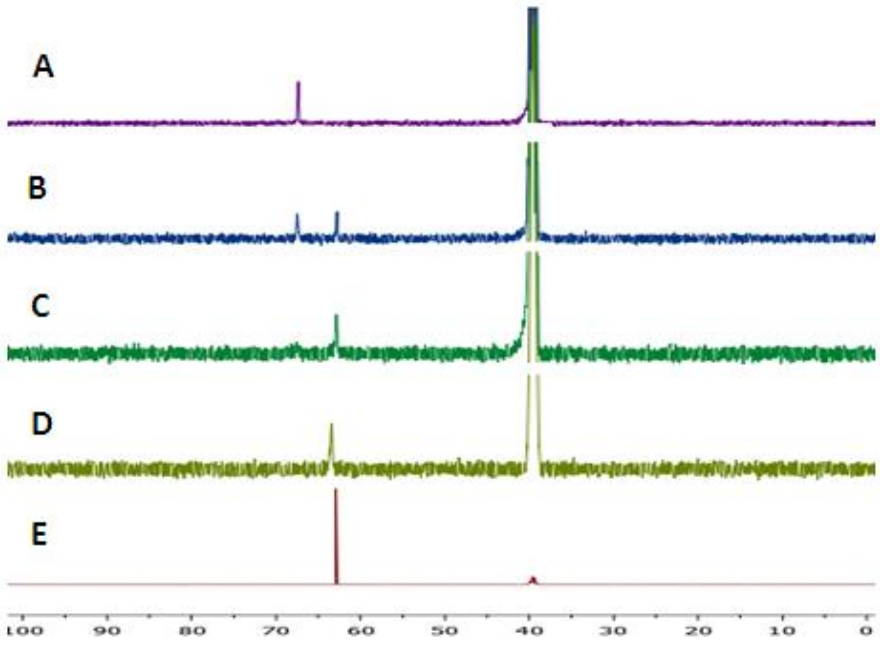

Figure 2.28. A: ^{13}C NMR of **201** (0.5 mM in DMSO-d_6), B: **201** + 10uL D_2O (10 equivalents), C: **201** + 20uL D_2O (20 equivalents), D: **201** + 30uL D_2O (30 equivalents) and E: **free ligand.**

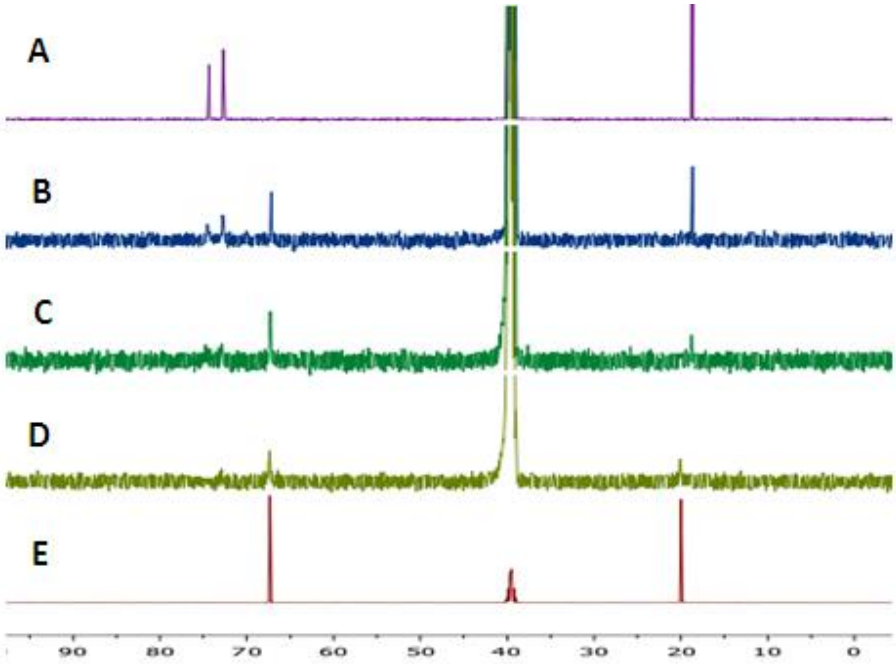

Figure 2.29. A: ^{13}C NMR of **202** (0.5 mM in DMSO-d_6), B: **202** + 10uL D_2O (10 equivalents), C: **202** + 20uL D_2O (20 equivalents), D: **202** + 30uL D_2O (30 equivalents) and E: **free ligand.**

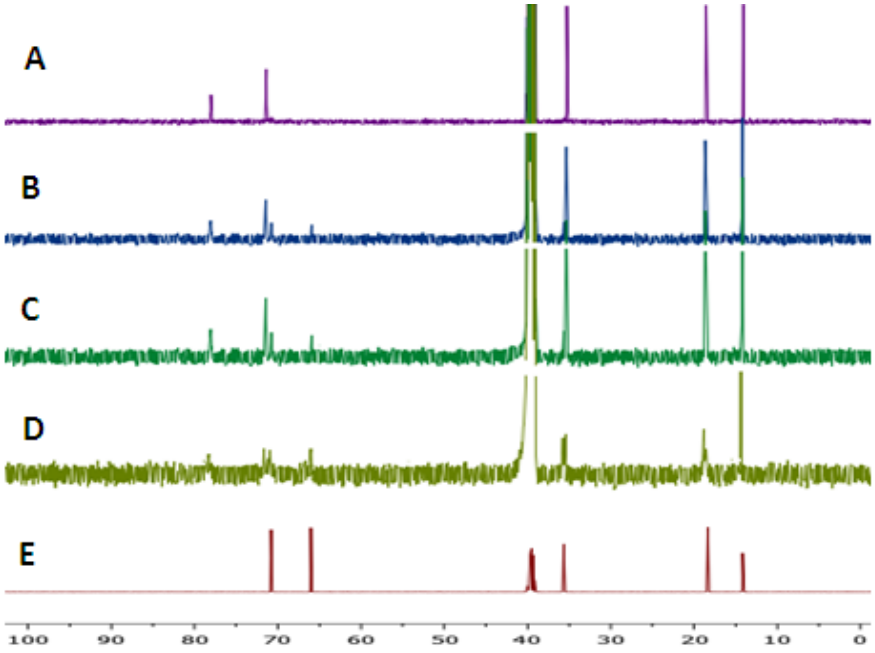

Figure 2.30. A: ^{13}C NMR of **204** (0.5 mM in DMSO-d_6), B: **204** + 10uL D_2O (10 equivalents), C: **204** + 20uL D_2O (20 equivalents), D: **204** + 30uL D_2O (30 equivalents) and E: **free ligand.**

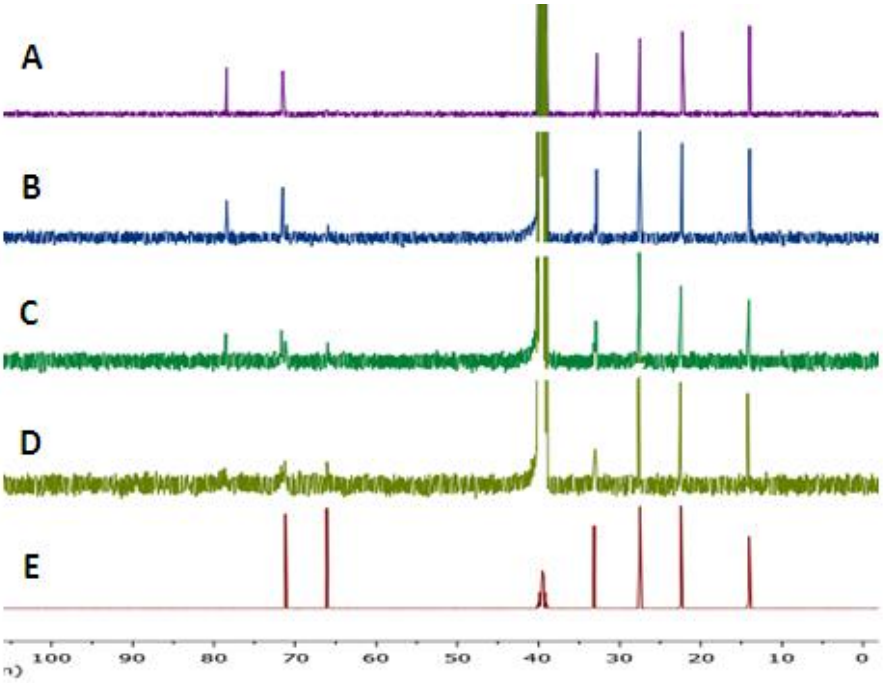

Figure 2.31. A: ^{13}C NMR of **205** (0.5 mM in DMSO-d_6), B: **205** + 10uL D_2O (10 equivalents), C: **205** + 20uL D_2O (20 equivalents), D: **205** + 30uL D_2O (30 equivalents) and E: **free ligand.**

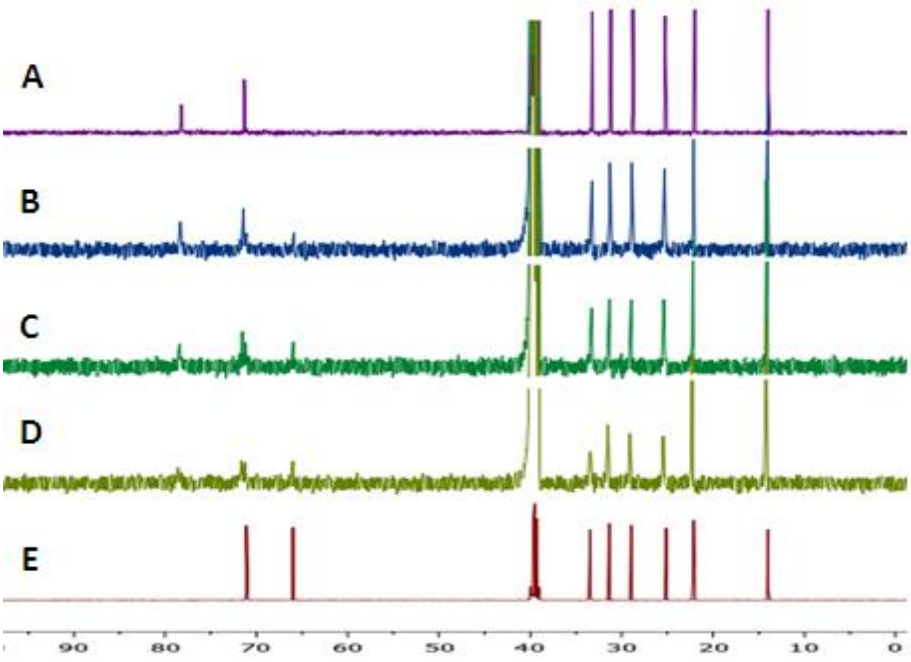

Figure 2.32. A: ^{13}C NMR of **206** (0.5 mM in DMSO-d_6), B: **206** + 10uL D_2O (10 equivalents), C: **206** + 20uL D_2O (20 equivalents), D: **206** + 30uL D_2O (30 equivalents) and E: **free ligand**.

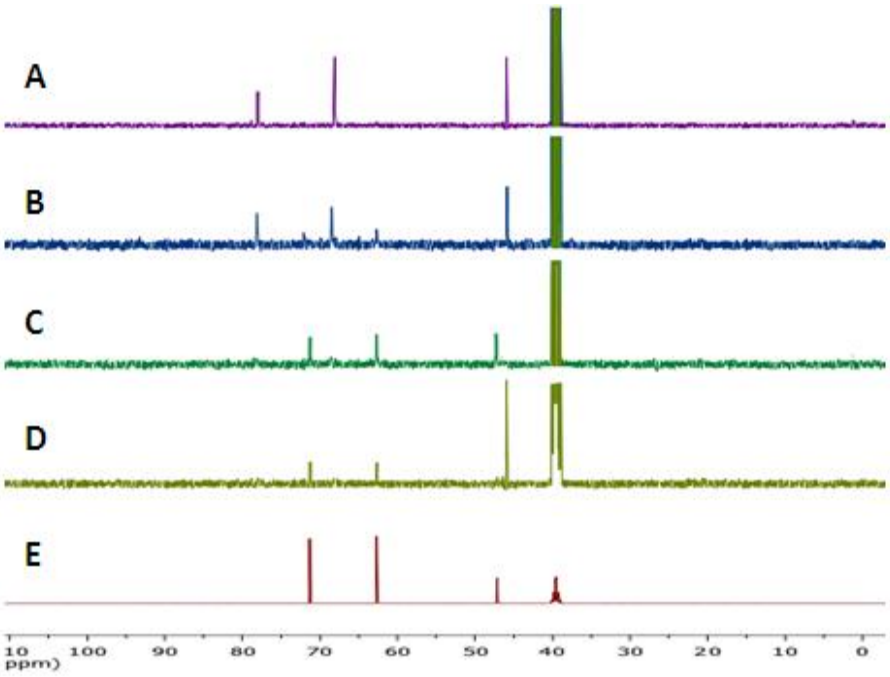

Figure 2.33. A: ^{13}C NMR of **207** (0.5 mM in DMSO-d_6), B: **207** + 10uL D_2O (10 equivalents), C: **207** + 20uL D_2O (20 equivalents), D: **207** + 30uL D_2O (30 equivalents) and E: **free ligand.**

2.4 References:

1. B. S. Sekhon, *Research in pharmaceutical sciences*, 2013, **8**, 145-158.
2. S. E. Ramadan, A. A. Razak, A. M. Ragab and M. el-Meleigy, *Biological trace element research*, 1989, **20**, 225-232.
3. Y. Kalechman, A. Shani, I. Sotnik-Barkai, M. Albeck and B. Sredni, *Cancer research*, 1993, **53**, 5962.
4. A. Silberman, Y. Kalechman, S. Hirsch and Z. Erlich, *Chembiochem : a European journal of chemical biology*, **17**, 918-927.
5. R. L. O. R. Cunha, M. E. Urano, J. R. Chagas, P. C. Almeida, C. Bincoletto, I. L. S. Tersariol and J. V. Comasseto, *Bioorganic & Medicinal Chemistry Letters*, 2005, **15**, 755-760.
6. H.-L. Seng, H. L. Seng and E. R. T. Tiekink, *Applied organometallic chemistry*, **26**, 655-662.
7. B. Sredni, *Seminars in Cancer Biology*, 2012, **22**, 60-69.
8. M. Brodsky, G. Halpert, M. Albeck and B. Sredni, *Journal of Inflammation*, 2010, **7**, 3-3.
9. B. Sredni, R. R. Caspi, A. Klein, Y. Kalechman, Y. Danziger, M. Benya'akov, T. Tamari, F. Shalit and M. Albeck, *Nature*, 1987, **330**, 173-176.
10. B. Sredni, R. Geffen-Aricha, W. Duan, M. Albeck, F. Shalit, H. M. Lander, N. Kinor, O. Sagi, A. Albeck, S. Yosef, M. Brodsky, D. Sredni-Kenigsbuch, T. Sonino, D. L. Longo, M. P. Mattson and G. Yadid, *FASEB journal : official publication of the Federation of American Societies for Experimental Biology - Journal Article*, 2007, **21**, 1870.
11. M. Albeck, T. Tamari and B. Sredni, *Synthesis*, 1989, **8**, 635-636.
12. H. Rosenblatt-Bin, Y. Kalechman, A. Vonsover, R. H. Xu, J. P. Da, F. Shalit, M. Huberman, A. Klein, G. Strassmann, M. Albeck and B. Sredni, *Cellular Immunology*, 1998, **184**, 12-25.
13. A. Albeck, H. Weitman, B. Sredni and M. Albeck, *Inorganic Chemistry*, 1998, **37**, 1704-1712.
14. E. Okun, T. V. Arumugam, S. C. Tang, M. Gleichmann, M. Albeck, B. Sredni and M. P. Mattson, *Journal of Neurochemistry*, 2007, **102**, 1232-1241.
15. P. Bhattacharyya, *Annual reports on the progress of chemistry. Section A. Inorganic chemistry*, 2005, **101**, 117-127.
16. B. Sredni, R.-H. Xu, M. Albeck, U. Gafter, R. Gal, A. Shani, T. Tichler, J. Shapira, I. Bruderman, R. Catane, B. Kaufman, J. K. Whisnant, K. L. Mettinger and Y. Kalechman, *International Journal of Cancer*, 1996, **65**, 97-103.
17. M. Daniel-Hoffmann, B. Sredni and Y. Nitzan, *Journal of Antimicrobial Chemotherapy*, 2012, **67**, 2165-2172.
18. A. Silberman, M. Albeck, B. Sredni and A. Albeck, *Inorganic Chemistry*, 2016, **55**, 10847-10850.
19. C. R. Princival, M. V. L. R. Archilha, A. A. Dos Santos, M. P. Franco, A. A. C. Braga, A. F. Rodrigues-Oliveira, T. C. Correra, R. L. O. R. Cunha and J. V. Comasseto, *ACS Omega*, 2017, **2**, 4431-4439.
20. M. P. Vázquez-Tato, A. Mena-Menéndez, X. Feás and J. A. Seijas, *International journal of molecular sciences*, 2014, **15**, 3287-3298.
21. F. Mavandadi and P. Lidström, *Curr Top Med Chem*, 2004, **4**, 773-792.

22. B. Sredni, M. Weil, G. Khomenok, I. Lebenthal, S. Teitz, Y. Mardor, Z. Ram, A. Orenstein, A. Kershenovich, S. Michowiz, Y. I. Cohen, Z. H. Rappaport, I. Freidkin, M. Albeck, D. L. Longo and Y. Kalechman, *Cancer Research*, 2004, **64**, 1843-1852.
23. D. B. Denney, D. Z. Denney, P. J. Hammond and Y. F. Hsu, *Journal of the American Chemical Society*, 1981, **103**, 2340-2347.
24. H. E. Gottlieb, S. Hoz, I. Elyashiv and M. Albeck, *Inorganic Chemistry*, 1994, **33**, 808-811.
25. K. Krishnan and R. S. Krishnan, *Proceedings of the Indian Academy of Sciences - Section A*, 1966, **64**, 111-122.
26. K. Nakamoto, *Infrared and Raman spectra of inorganic and coordination compounds*, Wiley-Blackwell, 2009.
27. K. Büscher, S. Heuer and B. Krebs, *Zeitschrift fur Naturforschung - Section B Journal of Chemical Sciences*, 1981, **36**, 307-312.
28. A. Kovács, K.-G. Martinsen and R. J. M. Konings, *Journal of the Chemical Society, Dalton Transactions*, 1997, 1037-1042.
29. N. N. Greenwood and B. P. Straughan, *Journal of the Chemical Society A: Inorganic, Physical, Theoretical*, 1966, 962-964.
30. D. M. Adams and D. M. Morris, *Journal of the Chemical Society A: Inorganic, Physical, and Theoretical Chemistry*, 1967, 2067-2069.
31. N. S. Dance and W. R. McWhinnie, *Journal of the Chemical Society, Dalton Transactions*, 1975, 43-45.
32. C. W. Brown, *Journal*, 1992, **64**, 889A.
33. A. E. Reed, R. B. Weinstock and F. Weinhold, *The Journal of Chemical Physics*, 1985, **83**, 735-746.
34. B. Fresch, H. G. Boyen and F. Remacle, *Nanoscale*, 2012, **4**, 4138-4147.
35. A. V. Marenich, C. J. Cramer and D. G. Truhlar, *The Journal of Physical Chemistry B*, 2009, **113**, 6378-6396.
36. M. Daniel-Hoffmann, M. Daniel-Hoffmann, B. Sredni and Y. Nitzan, *Journal of antimicrobial chemotherapy*, **67**, 2165-2172.
37. Z.-H. Lin, C.-H. Lee, H.-Y. Chang and H.-T. Chang, *Chemistry – An Asian Journal*, 2012, **7**, 930-934.
38. R. C. Molina-Quiroz, C. M. Muñoz-Villagrán, E. de la Torre, J. C. Tantaleán, C. C. Vásquez and J. M. Pérez-Donoso, *PloS one*, 2012, **7**, e35452.
39. S. L. Chua, K. Sivakumar, M. Rybtke and M. Yuan, *Scientific reports*, **5**.
40. Y. Zhao and D. G. Truhlar, *Journal of Chemical Theory and Computation*, 2011, **7**, 669-676.

Chapter 3

Te(IV)-pinacol salts compounds

3.1 Introduction

In the previous chapter, the tellurium compound AS101 and its derivatives were studied, where only one of the two vicinal carbons of the diol was substituted with an alkyl chain. All these complexes possessed one secondary and one tertiary carbon in the main chain of the diol ligand. In this chapter, we decided to explore if the same class of compounds could be formed substituting both the diol vicinal carbons. The following diol ligands were explored whose structure are shown in Figure 3.1 (in brackets the corresponding Te-compounds):

- pinacol, 1,1,2,2 tetramethyl-1,2 ethanediol (**301-309**);
- 1,1,2,2 tetraphenyl 1,2-ethanediol (**310**);
- catechol (**311**);
- hexafluoro 2,3 bis(trifluoromethyl) 2,3 butanediol (**312**);
- 2,3-butandiol (**313**).

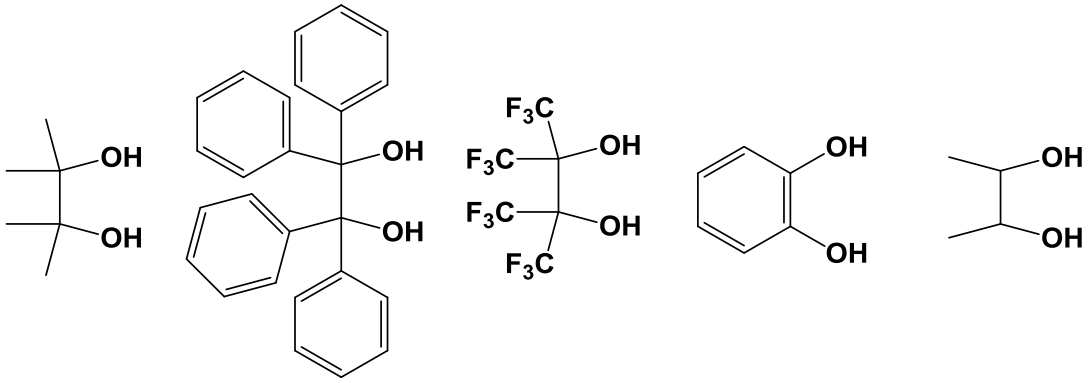

Figure 3.1. Structures of the diol ligands studied in this chapter. From left to right: pinacol, 1,1,2,2 tetramethyl-1,2 ethanediol; 1,1,2,2 tetraphenyl 1,2-ethanediol; hexafluoro 2,3-bis(trifluoromethyl) 2,3 butanediol; cathecol; 2,3-butandiol.

These Tellurium(IV) compounds, were obtained by reacting the corresponding diol with $TeCl_4$ in nitrile solutions, in a similar way as the reaction performed in chapter 2. Compounds can be extracted as solids, by filtration after the solution was concentrated by rotary evaporation or by the addition of Et_2O, as oil or can be purified by column chromatography. Complexes **301** and **302** were also synthesised in microwave similar to those of the AS101 analogues (chapter 2), thus reducing the reaction time from several hours to 40 mins.

Unfortunately, only with pinacol, 1,1,2,2 tetramethyl-1,2 ethanediol, it has been possible to isolate and completely characterise the tellurium compounds, while with all the other ligands the nature of the final products are still not clear.

3.2 Results and Discussion

3.2.1. Synthesis and Characterisation

The first reaction that was attempted was between pinacol and $TeCl_4$ in acetonitrile. The reaction was conducted following the procedure of the AS-101 derivatives described in chapter 2. By addition of Et_2O to the acetonitrile solution cooled at r.t after several hours of reflux, a nice yellow powder was isolated (See Experimental Part 3.5). Surprisingly, the product obtained was completely different from the analogues of AS-101. From multinuclear NMR studies (^{1}H, ^{13}C and ^{125}Te), IR spectroscopy and X-Ray structure analyses, it was possible to identify the new compound **301** as a salt where $TeCl_6^{2-}$ is the anion and an oxazoline derivative (formed by reaction between pinacol and acetonitrile) is the cation (Scheme 3.1).

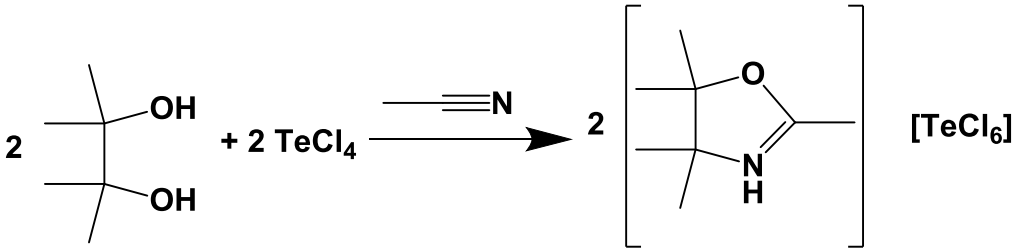

Scheme 3.1. Synthetic pathway for the synthesis of **301.**

Unfortunately, even if X-Ray analyses, NMR and IR spectra were in agreement with the structure proposed, the elemental analyses did not match with the final formula of the salt, $C_{16}H_{32}Cl_6N_2O_2Te$. Furthermore, it was evident that the reaction in Scheme 3.1 was not stoichiometric; together with **301**, another species was formed, $[TeCl_2(OH)_2]$ that precipitated together with the salt after addition of Et_2O (Scheme 3.2).

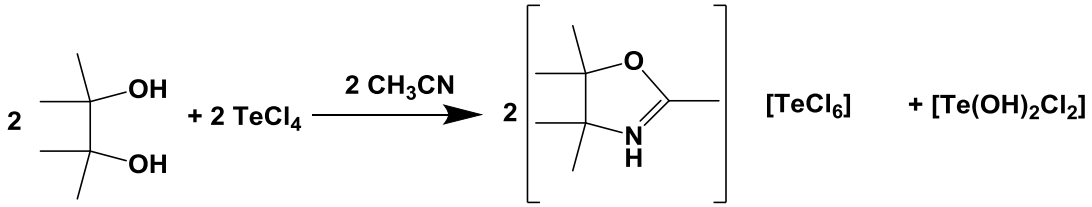

Scheme 3.2. Stoichiometric synthetic pathway for the synthesis of **301.**

The Elemental Analyses did match somewhat with the mixture of the two compounds (El. Anal. % Calcd. For $C_{16}H_{34}Cl_8N_2O_4Te_2$ C: 22.42, H: 4.00; N: 3.27; found C: 22.02, H: 4.32; N: 3.57). From NMR and IR spectra the presence of the second species $[TeCl_2(OH)_2]$ in the mixture was not easy to identify. Nevertheless, the two species can be separated by dissolving the mixture in a minimum amount of MeOH and by removal of $[TeCl_2(OH)_2]$, that crashed out by addition of water, while **301** remains in solution. The Elemental Analyses of the purified **301** was found with the formula (El. Anal. % Calcd. For $C_{16}H_{32}Cl_6N_2O_2Te$ C: 30.76, H: 5.16; N: 4.48; found C: 30.25, H: 5.62; N: 4.87). We decided to investigate if the same class of compounds could have been formed modifying the nitrile nature; analogues have been isolated and characterized with X-Ray structure analysis with benzonitrile (**302**) and 4-trifluoromethyl-benzonitrile (**303**), as shown in Scheme 3.3.

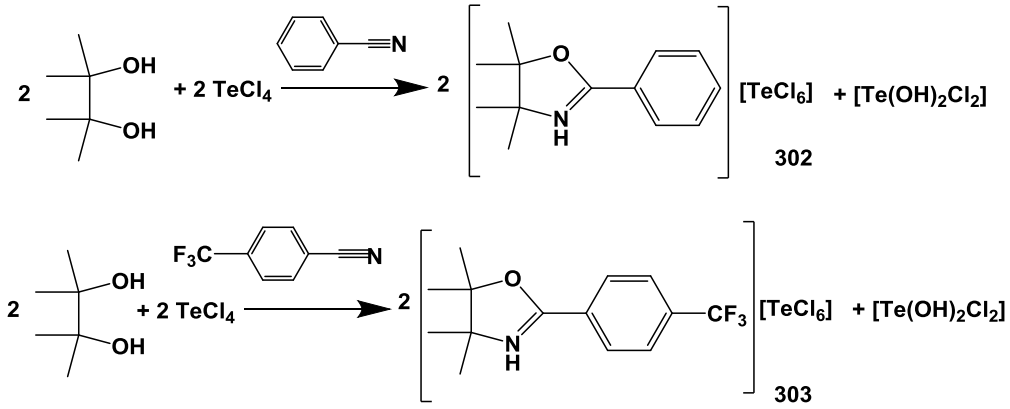

Scheme 3.3. Stoichiometric synthetic pathway for the synthesis of **302** (top) and **303** (bottom).

The reaction was explored also with different nitriles, including 3-trifluoro-methylbenzonitrile (**304**), fluoroacetonitrile (**305**), 2,3Dimethoxybenzonitrile (**306**), trichloroacetonitrile (**307**), cyclohexene-nitrile (**308**) and naphto-nitrile (**309**). Only with fluoroacetonitrile (**305**) and 2,3

Dimethoxybenzonitrile (**306**) analogues compounds were isolated; the reaction using the other nitriles did not produce clear and pure compounds (See Experimental Part 3.5).

Compounds **301, 302** and **303** were characterised by X-Ray crystallography.

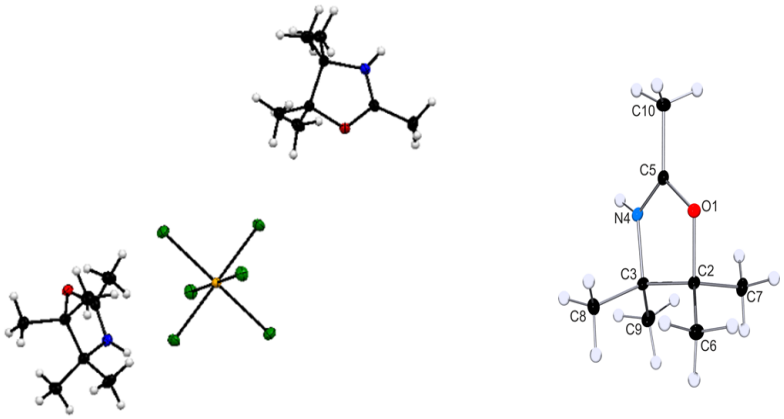

Figure 3.2. X-Ray structure of **301**. Left: the full salt; right the TMO tetramethyloxozolium cation (molecules of DMF removed for clarity).

301. The crystals were obtained by diffusion of Et_2O into a DMF solution of 3.1. The asymmetric unit of the dimethylformamide-solvated salt $[CH_3\text{-TMO}]_2[TeCl_6]\cdot 2DMF$ (**301**) encloses a CH_3-TMO cation (TMO = TetraMethylOxazolium), a DMF solvate molecule (not shown) and half hexachlorotelurate anion. The Te(IV) ion is located at the crystallographic inversion center (origin of the unit cell), and displays the expected bond distances (Te1–Cl1, 2.5431(4) Å; Te1–Cl2, 2.5380(4) Å; Te1–Cl3, 2.5494(4) Å) and angles (maximal deviation from right angle: Cl2–Te1–Cl3, 91.102(13)°). The molecular ring of the pentamethyloxazolium cation (Table 1) exhibits an expected distortion, as the C3–N4–C5 angle (111.31(12)°) widens upon protonation. In addition, the O1–C2–C3–N4 torsion angle was found to be 23.32(12)°. This is probably due to the steric accommodation of the four methyl substituents at the endocyclic C–C bond. The N1H site is involved in hydrogen bonding with the oxygen atom of a neighboring DMF molecule (2.6872(16) Å). Crystal data for Compound **301**: $[C_{22}H_{46}Cl_6N_4O_4Te]$, orthorhombic, *Pbca*, a = 15.5390(14) Å, b = 12.2853(11) Å, c = 17.8374(16) Å, Z = 4, M_r = 770.93, V = 3405.2(5) Å^3, D_{calcd} = 1.504 g cm^{-3}, λ(Mo Kα) = 0.71073 Å, T = 100 K, μ = 1.377 mm^{-1}, 74355 reflections collected, 4631 unique (R_{int} = 0.0454), 3948 observed, $R1(F_o)$ = 0.0208 [$I > 2\sigma(I)$], $wR2(F_o^2)$ = 0.0550 (all data), GOF = 1.051.

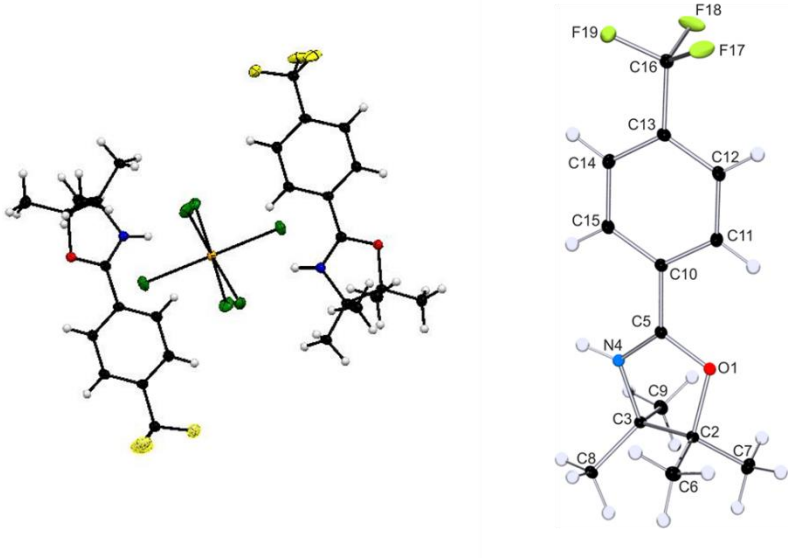

Figure 3.3. X-Ray structure of **303**. Left: the full salt; right the TMO tetramethyloxozolium cation.

303. Crystals were obtained by diffusion of Et_2O into a 4-trifluoromethyl-benzonitrile solution. The compound $[CF_3Ph\text{-}TMO]_2[TeCl_6]$ (**303**) crystallizes in the monoclinic C2/c space group, and the unit cell encloses half $TeCl_6^{2-}$ anion, and an oxazolium derivative cation, namely, 4,4,5,5-tetramethyl-2-(p-trifluoromethyl-phenyl)oxazolium. Two Te–Cl distances of the anion differ significantly from those observed in **301** (Te1–Cl1, 2.4557(4) Å; Te1–Cl2, 2.5341(4) Å; Te1–Cl3, 2.6432(4) Å), whereas bond angles remain unaltered (Table 1). As in the case of **301**, cation **303** exhibits a wide C3–N4–C5 angle (110.72(11)°) and a pronounced O1–C2–C3–N4 twist angle (26.64(11)°). The intramolecular hydrogen bonding pattern could be responsible for the hexafluorotelurate anion distortion, a the N4 site H-binds a Cl3 ligand (N4(H)···Cl3, 3.2495(12) Å). Thus, each $TeCl_6^{2-}$ anion is connected to two $CF_3Ph\text{-}TMO^+$ cations. Crystal data for Compound **303**: $[C_{28}H_{34}Cl_6F_6N_2O_2Te]$, monoclinic, *C2/c*, a = 19.5893(16) Å, b = 7.4413(6) Å, c = 23.8477(19) Å, β = 90.8384(12)°, Z = 4, M_r = 884.87, V = 3475.9(5) Å^3, D_{calcd} = 1.691 g cm^{-3}, λ(Mo Kα) = 0.71073 Å, T = 100 K, μ = 1.379 mm^{-1}, 19515 reflections collected, 4829 unique (R_{int} = 0.0188), 4499 observed, $R1(F_o)$ = 0.0198 [$I > 2\sigma(I)$], $wR2(F_o^2)$ = 0.0487 (all data), GOF = 1.036.

Table 1. Endocyclic ring angles [°] and distances [Å] of cations in **301** and **303**.

	301	**303**
O1–C2	1.5111(17)	1.4938(16)
C2–C3	1.5577(19)	1.5548(18)
C3–N4	1.4817(17)	1.4938(16)
N4–C5	1.2887(19)	1.2953(17)
O1–C5	1.3191(17)	1.3138(16)
C5–O1–C2	107.36(10)	107.31(10)
O1–C2–C3	101.41(10)	101.38(9)
N4–C3–C2	99.64(11)	98.66(9)
C5–N4–C3	111.31(12)	110.72(11)
N4–C5–O1	114.03(13)	113.77(12)

By diffusion of Et_2O into a benzonitrile solution of **302**, crystals were obtained but the X-ray structure is not of good quality, even if the nature of the compounds is clearly identified (Figure 3.4).

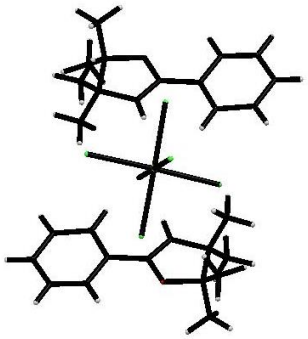

Figure 3.4. X-Ray structure of **302**.

All the compounds **301-313** were characterised by elemental analysis, IR spectroscopy, ^{1}H, ^{13}C, ^{125}Te and ^{19}F NMR (all the spectra are reported at the end of this chapter in the section 3.5). All the compounds show a unique ^{125}Te NMR peak in DMSO-d_6 around 1525 ppm, the region of $TeCl_6^{2-}$ species. In the IR spectra is clearly visible the stretching of the C=N between 1618-1671 cm^{-1}. When comparing IR spectra of that of starting ligand pinacol and compounds **301-303**, the stretching at 3439cm^{-1} (OH) disappeared in the IR of **301–303** and new peaks are seen at 1500-1656 cm^{-1} (C=N); 2979 cm^{-1} (CH_3). Compounds containing CF_3 group show the characteristic CF_3 symmetrical stretching at 1100 cm^{-1} and symmetrical CF_3 deformation at 700 cm^{-1} in the IR spectra.[1] Compounds **301**, **302**, **303**, **305** and **306** are very stable in deuterated

DMSO. The ^{1}H NMR spectrum of the free pinacol ligand shows two signals corresponding to the two OH groups (3.52 ppm, broad singlet) and to the methyl groups at 1.06 ppm (singlet) and the ^{13}C NMR spectrum shows the equivalent *C*H_3 groups at 25.8 ppm (singlet) and the two vicinal carbons at 74.4 ppm (singlet). In **301**, the methyl groups and the vicinal carbons are no more equivalent; the ^{13}C NMR spectrum of **301** shows six peaks corresponding to the *C*H_3 group of acetonitrile at 14 ppm, the CH_3 groups of pinacol at 22.4 and 22.6 ppm, the vicinal carbons at 65.5 and 97.0 ppm and the quaternary carbon of CH_3*C*N at 173.0 ppm (all the assignments were done *via* 2D-COSY/TOCSY/HMBC/HSQC spectra). The ^{1}H NMR for compound **301** shows three peaks, two corresponding to the two sets of CH_3 of the pinacol at 1.36 and 1.49 ppm and the CH_3 of the acetonitrile at 2.34 ppm. The NH protonated is visible as a broad singlet at 6.7 ppm. The ^{125}Te NMR shows one single peak at 1523 ppm corresponding to the $TeCl_6^{2-}$ anion. Analogues spectra are obtained for **302**, **303**, **305** and **306**.

^{1}H NMR of **302** shows five peaks, two singlets of the two sets of CH_3 of the pinacol at 1.47 and 1.60 ppm and three multiplets associated to the aromatic protons of the benzene ring at 7.67, 7.86 and 8.10 ppm (integrals 2:2:1). The ^{13}C NMR spectrum for **302** shows 9 signals: 22.3 and 22.7 (two sets of CH_3 pinacol), 66.5 and 97.2 ppm for the two vicinal carbons, 167.0 ppm (quaternary carbon of the benzonitrile) and four peaks of the aromatic benzene ring at 129. 7, 129.5, 121.2 and 129.5 ppm. The ^{125}Te NMR shows a peak at 1524ppm.

^{1}H NMR of **303** was similar to that of **301** and **302** in that it shows the two sets of methyl groups of pinacol (no more equivalent) at 1.46 and 1.58 ppm and two multiplets at 8.06 and 8.28 ppm of the aromatic protons. ^{13}C NMR of **303** is a little more complex due to the coupling between the carbons and the ^{19}F of the CF_3 group. The two sets of methyl groups of pinacol appear at 22.4 and 22.9 ppm; the vicinal carbons are at 67.0 and 96.5 ppm and the quaternary carbon of the nitrile at 165 ppm. All the carbons of the benzene ring are coupling with different constants with the ^{19}F of the CF_3 and show three different quartets at 126.0, 130.0 and 136.6 ppm. The carbon of the CF_3 appear as a quartet at 124 ppm. The ^{125}Te NMR shows again a broad peak at 1521 ppm, very close to the other ^{125}Te peaks. Finally, ^{19}F NMR shows one peak at -62 ppm for the CF_3 group. ^{1}H NMR spectrum of **305** with fluoro-acetonitrile, shows similar pattern as the previous three compounds with the two sets of pinacol methyl groups at 1.27 and 1.51 ppm and one doublet at 5.52 ppm corresponding to the CH_2 protons (coupling with ^{19}F). The ^{13}C NMR spectrum for **305** show peaks at 22.5, 22.6, 66.4, 77.21, 76.0 and 169.7 ppm. The ^{125}Te NMR shows a peak

at 1523 and the ^{19}F NMR shows a peak at -20.4 ppm for the CF_3 group. The last compound that formed analogues Te(IV) species is with the 2,3-dimethoxy benzonitrile, **306**. The ^{1}H NMR spectrum shows the same pattern for the peaks of the methyl groups of pinacol at 1.27 and 1.40 ppm, two multiplets between 7-7.25 ppm of the aromatic protons and one broad peak at 3.85 of the methoxy groups. ^{13}C NMR spectrum of **306** shows 13 peaks, the first two are assign again to those of the methyl groups of pinacol at 22.9 and 24.2 ppm, two peaks to the vicinal carbons at 69.5 and 88.5 ppm, one peak at 160 ppm of the quaternary carbon of the nitrile, six aromatic carbons at 153.2, 148.4, 124.4, 122.4, 115.2 and 110.1 ppm and two methoxy carbons at 61.4 and 56.3 ppm. The ^{125}Te NMR shows a peak at 1523 ppm. As mentioned before, unfortunately, with all the other nitriles (**304**, **307**, **308** and **309**) or replacing pinacol with other diols (**310**, **311**, **312**, and **313**) no clear compounds were obtained and characterised. Nevertheless, the NMR spectra did not show the same pattern of the previous species and the integrals did not match with the hypothetical structure. Theoretical calculations will be conducted in order to understand the mechanism of formations of these species and to understand the effect of the steric/electronic properties of the diol/nitrile in the formation of these species. All the spectra are reported in the experimental part 3.5.

3.2.2. Stability in aqueous conditions.

As mentioned before, the nature of these new class of compounds was quite surprising. The cation was a protonated oxazoline, a cyclic five member ring with an endo-imino ether (-N=C-O-) group. The chemistry of oxazoline has been extensively studied and reviewed.[1] Several ways are known for the syntheses of oxazoline, including cyclisation of 2-amino-alcohol[2], reaction between acyl-chlorides and amino-alcohol, the Appeal reaction and reaction between nitriles and amino-alcohol catalysed by $ZnCl_2$ (Pinner reaction)[3]. Oxazolines have been synthesised since the early 19th century and since their discovery, their chemistry has been investigated intensively.[3-8]

It must also be noted that the same reaction did not happen if $TeCl_4$ was replaced by other Lewis Acids, such as $AlCl_3$, $ZnCl_2$ or $MgCl_2$. Reacting $TeCl_4$ with an excess of pinacol (10 equivalents) in acetonitrile, afforded the same compound **301**. This could suggest that $TeCl_4$ could act as a catalyst and a catalytic mechanism is proposed in Figure 3.5. This is only a hypothesis and will be

confirmed and combined by theoretical calculations. Another important advantage with respect the common zinc-catalysed reactions, is that the formation of these oxazoline derivatives also happens at r.t. without refluxing conditions.

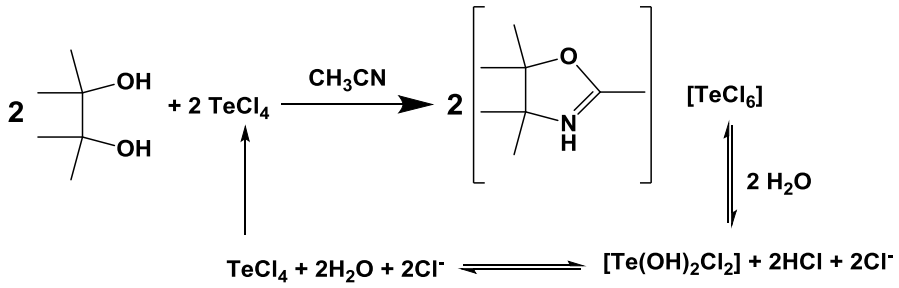

Figure 3.5. Catalytic mechanism proposed for the syntheses of Te-catalysed oxazolines**.**

Milne showed that $[TeCl_6]^{2-}$ in water is in equilibrium with different Te(IV)-hydroxo-chloride species (Figure 3.5), including $[Te(OH)Cl_4]^-$ and $[Te(OH)_2Cl_2]$.[9, 10] ^{125}Te NMR shows a broad peak around 1250 ppm demonstrating a rapid exchange of all the Te species in solution. **301**, **302** and **303** compounds were selected to study their stability in aqueous environment. The compounds were accurately weighted in a NMR tube, dissolved in DMSO-*d*$_6$ and aliquots of D_2O were added were added (10, 20, 30, 40 and 50 equivalents, see Experimental). The ^{1}H, ^{13}C, ^{125}Te and ^{19}F NMR were collected after each addition and after one week after each addition, in order to allow the systems to reach the equilibrium. All the compounds were not stable after addition of water and they decomposed forming new species with a very similar NMR pattern compared to the parent species, with all the peaks shifted up-field.

An accurate integration of the ^{1}H-NMR peaks, allowed the determination of the stability performance of **301**, **302** and **303** (Figure 3.6 for compound **301**, see Experimental Part 3.5 for **302** and **303**).

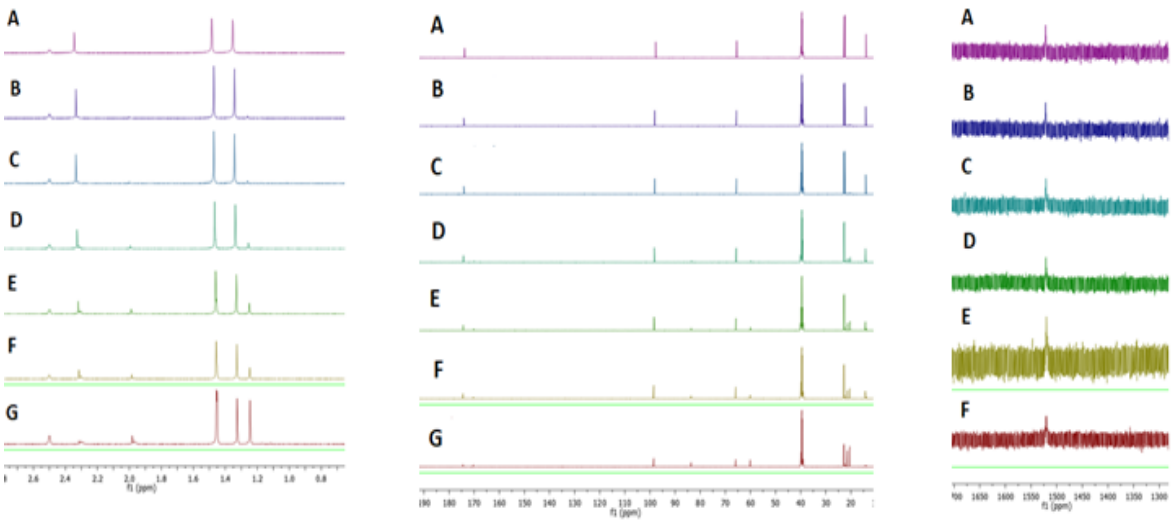

Figure 3.6. ^{1}H (left), ^{13}C (centre) and ^{125}Te (right) NMR of: A) **301** (0.5 mM in DMSO-d_6); B) **301** + 10 µL D_2O (10 eq.); C) **301** + 20 µL D_2O (20 eq.); D) **301** + 30 µL D_2O (30 eq.); E) **301** + 40 µL D_2O (40 eq.); F) **301** + 50 µL D_2O (50 eq.); F) **301** + 50 µL D_2O (50 eq.) after 3 weeks.

Figure 3.7 and Table 3.2 show the plot of the stability data for the three compounds analysed, **301**, **302** and **303**. **303** containing a CF_3 group is the least stable, decomposing of almost 85% after addition of 50 equivalents of D_2O. The acetonitrile derivative, **301**, is the most stable, with a decomposition of only 50 % after addition of 50 equivalents.

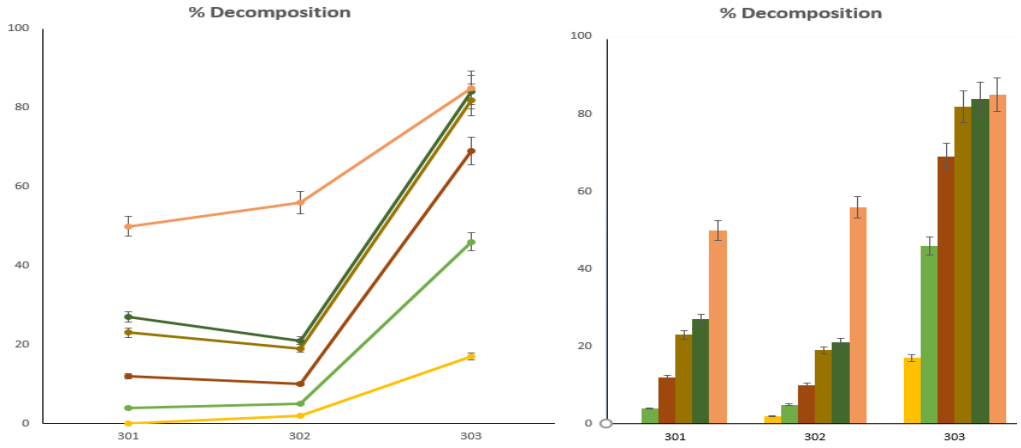

Figure 3.7. Decomposition of compounds **301, 302** and **303** with addition of water. Left, marked line representation; right, 2D column representation. 10 equiv D_2O, 20 equiv D_2O, 30 equiv D_2O, 40 equiv D_2O, 50 equiv D_20, 50 equiv D_2O after 3 weeks.

Table 3.2. Percentage of decomposition of compounds **301, 302** and **303** after addition of 10-50 equivalents of D_2O.

equivalents of D_2O	**301**	**302**	**303**
0	0	0	0
10	0	2±1	17±1
20	4±1	5±1	46±2
30	12±1	10±1	69±2
40	23±2	19±2	82±3
50	27±2	21±2	84±3
50 after 3 weeks	50±3	56±3	85±3

Makino and co-workers[11] reported that oxazolines, in the presence of acidic solution and nucleophiles (H-X), decomposes as shown in Figure 3.8[11]. We speculate that the product that is forming upon addition of D_2O could be a similar species, due to the presence of an acidic environment (Figure 3.5, confirmed also by litmus paper). The reason for the different stability performance, will be investigated by theoretical calculations, but we can hypothesise that the presence of electro-withdrawing groups, such as CF_3, will increase the polarisation of C and make it more amenable to nucleophilic attack of X^- (Figure 3.8).

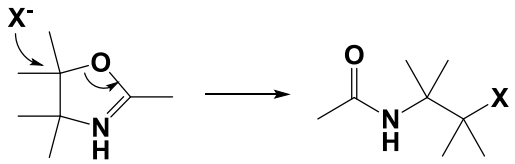

Figure 3.8. Mechanism proposed for the decomposition of the oxazoline cations in **301, 302** and **303**.

3.3 Experimental

3.3.1. Material and methods

$TeCl_4$, all the diol ligands and all the nitriles have been purchased from Sigma-Aldrich or TCI Europe. All solvents were used without further purification except for CH_3CN which was kept dry over molecular sieves under inert atmosphere. All NMR spectra were recorded on a Bruker Advance spectrometer with the probe at 293 K, operating at 500 MHz for the ^{1}H, at 125 MHz for the ^{13}C, 470 MHz for ^{19}F and at 158 MHz for the ^{125}Te nucleus, respectively. Spectra were recorded in DMSO-d_6 using Me_4Si as the internal standard for ^{1}H and ^{13}C while diphenyl ditelluride was used as external reference for ^{125}Te. All chemical shifts δ are reported in ppm. Infrared (IR) spectra were recorded in the region 4000–400 cm^{-1} on a Perkin Elmer ATR (Attenuated Total Reflectance) precisely spectrum 100 FT/IR spectrometer. Elemental analysis (carbon, hydrogen and nitrogen) were performed with a PerkinElmer 2400 series II analyser. The stability of the complexes has been evaluated following the decomposition reaction by ^{1}H, ^{13}C and ^{125}Te NMR. Each compound was accurately weighted and dissolved in 400 µL of DMSO-d_6 to obtain 125 mM solution (0.05 mmoles). 10 µL of D_2O were added in three consecutive aliquots and the NMR spectra were recorded 1 h after each addition (each addition corresponds to 10 equivalents of water with respect the complex). The experiments were run in triplicate.

3.3.2. Synthesis and Characterization

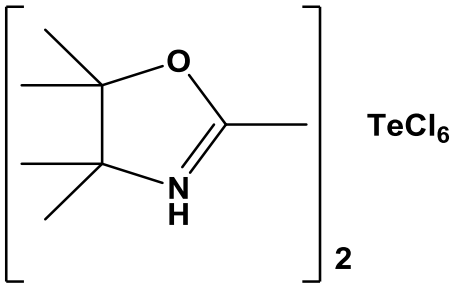

301. $TeCl_4$ (1g, 3.4mmol) was refluxed with Pinacol $C_6H_{14}O_2$ (0.8g, 6.77mmol) in 8ml of dry acetonitrile for 4hrs at 80°C. After 4hrs a yellow solution remained. A light yellow crystalline solid precipitated after addition of diethyl ether at r.t. and it was recovered by filtration, washed with cold CH_3CN and Et_2O and dried under vacuum. The powder was re-dissolved in 3 mL of

MeOH and 25 mL of water were added. A white solid formed, $[Te(OH)_2Cl_2]$ that was removed by filtration. The filtrate was dried, washed with MeOH and Et_2O and dried in vacuum, obtaining a yellow solid.

Yield 76%. M.W: 624.3g/mol

Elem. Anal. %C (30.75), %H (5.13), %N (4.49); found C (30.25), H (5.62), N (4.87.

^{1}H NMR (DMSO-d_6): δ = 1.36 (s, 6H, CH_3), 1.49 (s, 6H, (CH_3), 2.34 (s, 3H, CH_3)

^{13}C NMR (DMSO-d_6): δ = 14.05 (CH_3), 22.36 (CH_3, CH_3), 22.62 (CH_3, CH_3), 65.50 (C-N), 97.81 (C-O), 173.8 (O-C=N)

^{125}Te (DMSO-d_6): δ = 1523.

IR cm^{-1} (ATR): 3213, 2979, 1656, 1503, 1468, 1401, 1379, 1247, 1168, 1120, 1078, 1013, 955, 907, 801cm^{-1}

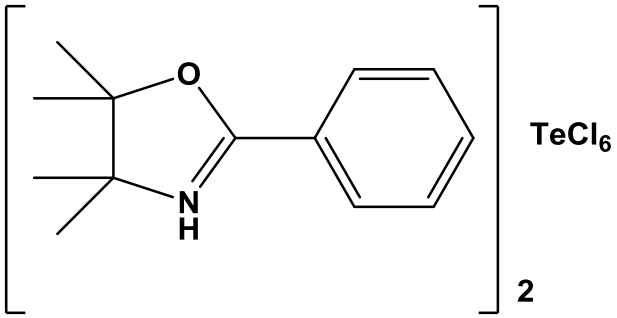

302. $TeCl_4$ (0.5357g, 1.81mmol) was refluxed with Pinacol $C_6H_{14}O_2$ (0.2136g, 1.81mmol) in 8ml of benzonitrile for 4hrs at 80°C. After 4hrs a yellow solution remained. A light green crystalline solid precipitated after addition of diethyl ether at r.t. and it was recovered by filtration, washed with cold Et_2O and dried under vacuum. The powder was re-dissolved in 3 mL of MeOH and 25 mL of water were added. A white solid formed, $[Te(OH)_2Cl_2]$ that was removed by filtration. The filtrate was dried, washed with MeOH and Et_2O and dried in vacuum, obtaining a yellow/green solid. Yield 49%. M.W: 748.3g/mol

Elem. Anal. %C (41.7), %H (4.81), %N (3.70); found C (40.1), H (4.67), N (3.4).

^{1}H NMR (DMSO-d_6): δ = 1.47 (s, 6H, CH_3), 1.60 (s, 6H, (CH_3), 7.67 (d, 2H, CH_2), 7.86 (d, 1H, CH), 8.10 (d, 2H, CH_2)

^{13}C NMR (DMSO-d_6): δ = 22.33 (CH_3, CH_3), 22.75 (CH_3, CH_3), 22.62, 66.52 (C-N), 97.21 (C-O), 167.25 (O-C=N), 121.18, 129.47, 129.65, 136.16

^{125}Te (DMSO-d_6): δ = 1525.

IR cm^{-1} (ATR): 3142, 1618, 1459, 1377, 1356, 1268, 1167, 1167, 1143, 1095, 1041, 775, 670cm^{-1}

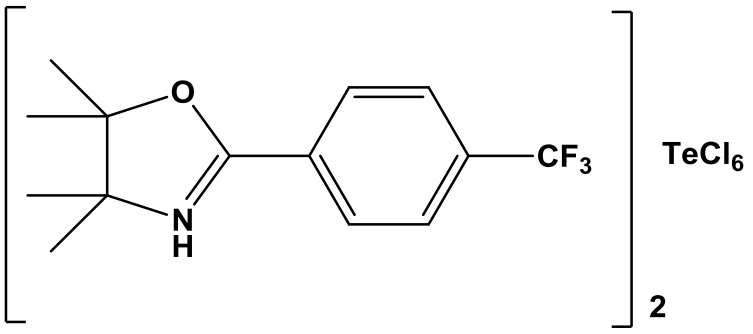

303. $TeCl_4$ (0.4129g, 1.39mmol) was refluxed with Pinacol $C_6H_{14}O_2$ (0.1646g, 1.39mmol) and 4-trifluoro-methylbenzonitrile (1.12g, 6.6mmol) for 4hrs at 80°C. The nitrile started off as solid but when 40°C turned to liquid. After 30mins the solution turned from yellow to dark brown solution. After 4hrs reaction stopped and flask cooled on ice bath. A green brown crystalline solid precipitated after addition of diethyl ether at r.t. and it was recovered by filtration, washed with cold Et_2O and dried under vacuum. The powder was re-dissolved in 3 mL of MeOH and 25 mL of water were added. A white solid formed, $[Te(OH)_2Cl_2]$ that was removed by filtration. The filtrate was dried, washed with MeOH and Et_2O and dried in vacuum, obtaining a green solid. Yield 38%. M.W: 884.9g/mol

Elem. Anal. %C (38.01), %H (3.87), %N (3.17); found C (37.7), H (3.51), N (2.90).

^{1}H NMR (DMSO-d_6): δ = 1.46 (s, 6H, CH_3), 1.58 (s, 6H, (CH_3), 8.02 (d, 2H, CH_2), 8.28 (d, 2H, CH_2)

^{13}C NMR (DMSO-d_6): δ = 22.48 ($2CH_3$), 22.94 ($2CH_3$), 67.41 (quat), 95.5 (quat), 165 (-C=N), 120 (CF_3), 122 (CH), 124 (CH), 126 (CH), 130(quat), 134 (quat), 134.27 (CH).

^{125}Te (DMSO-d_6): δ = 1521.

^{19}F NMR (DMSO-d_6): δ = -61.96

IR cm^{-1} (ATR): 3142, 1618, 1459, 1377, 1356, 1268, 1167, 1167, 1143, 1095, 1041, 775, 670cm^{-1}

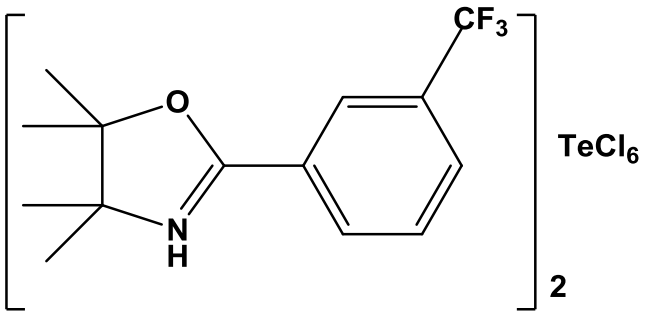

304. $TeCl_4$ (0.8801g, 2.9mmol) was refluxed with Pinacol $C_6H_{14}O_2$ (0.3427g, 2.9mmol) and 3-trifluoro-methylbenzonitrile (2.562g, 15mmol) for 4hrs at 80°C. After 60mins the solution turned from yellow to dark brown solution. After 4hrs reaction stopped and flask cooled on ice bath. A green brown crystalline solid precipitated after addition of diethyl ether at r.t. and it was recovered by filtration, washed with cold Et_2O and dried under vacuum. Yield 24%.

Elem. Anal. %C (24.25), %H (5.09), %N (3.54); found C (24.40), H (5.32), N (3.25).

^{1}H NMR (DMSO-*d*$_6$): δ = 1.38 (s, 6H, CH_3), 1.52 (s, 6H, (CH_3), 8.19 (d, 2H, CH_2), 7.85 (d, 2H, CH_2), 8.19, 8.26, 8.34

^{13}C NMR (DMSO-*d*$_6$): δ = 22.51 ($2CH_3$), 23.04 ($2CH_3$), 67.47 (quat), 96.45 (quat), 164.89 (-C=N), 112 (CF_3), 117 (CH), 122 (CH), 124 (CH), 131 (quat), 133 (quat), 136 (CH).

^{125}Te (DMSO-*d*$_6$): δ = 1525.

^{19}F NMR (DMSO-*d*$_6$): δ = -61.46

IR cm^{-1} (ATR): 3181, 2229, 1644, 1598, 1510, 1439, 1327, 1120, 919, 805, 734, 692, 659 cm^{-1}

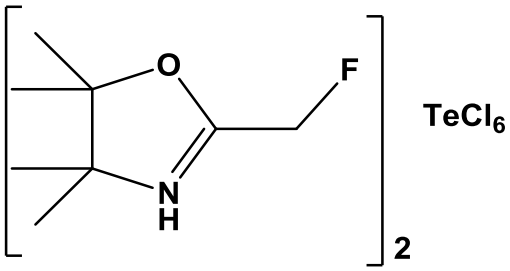

305. $TeCl_4$ (0.666g, 2.25mmol) was refluxed with Pinacol $C_6H_{14}O_2$ (0.2659g, 2.25mmol) and fluoroacetonitrile (1g, 17mmol) for 4hrs at 80°C. After 10mins the solution turned from yellow to dark brown solution. After 4hrs reaction stopped and flask cooled on ice bath. A dark brown crystalline solid precipitated after addition of diethyl ether at r.t. and it was recovered by filtration, washed with cold Et_2O and dried under vacuum. Yield 23%. M.W: 893.24g/mol

Elem. Anal. %C (21.51), %H (3.61), %N (3.14); found C (22.21), H (4.03), N (4.06).

^{1}H NMR (DMSO-d_6): δ = 1.37 (s, 6H, CH_3), 1.51 (s, 6H, CH_3), 5.47 (s, 1H, CH), 5.56 (s, 1H, CH)

^{13}C NMR (DMSO-d_6): δ = 22.49 ($2CH_3$), 22.64 ($2CH_3$), 66.40 (quat), 76 (quat), 164.70 (-C=N), 77.21 (CH)

^{125}Te (DMSO-d_6): δ = 1523.

^{19}F NMR (DMSO-d_6): δ = -20.18

IR cm^{-1} (ATR): 3154, 1671, 1513, 1379, 1243, 1162, 1073, 951, 881. 782 cm^{-1}

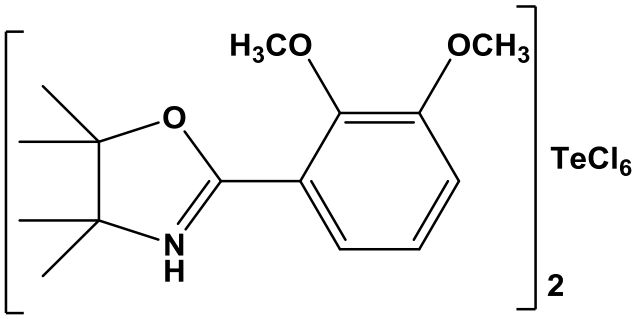

306. $TeCl_4$ (0.76g, 2.56mmol) was refluxed with Pinacol $C_6H_{14}O_2$ (0.3025g, 2.56mmol) and 2,3 Dimethoxybenzonitrile (0.8476g, 5.2mmol) for 4hrs at 120°C. After 10mins the solution turned from yellow to black solution. After 4hrs reaction stopped and flask cooled on ice bath. Dried for 1hr on rotavap and a dark crude solution remained. Product was removed through column chromatography 100:1 DCM to methanol. A dark brown oil was extracted.

^{1}H NMR (DMSO-d_6): δ = 1.27 (s, 6H, CH_3), 1.40 (s, 6H, CH_3), 3.85 (s, 6H, CH_3), 7.00 (m, 2H, CH), 7.26(t, 1H CH)

^{13}C NMR (DMSO-d_6): δ = 22.94 ($2CH_3$), 24.20 ($2CH_3$), 56.27 (OCH_3), 61.41 (OCH_3), 69.49 (quat), 88.51 (quat), 110 (CH), 115 (CH), 122 (CH), 124 (quat), 149 (quat), 153 (quat), 161 (-C=N)

^{125}Te (DMSO-d_6): δ = 1523.

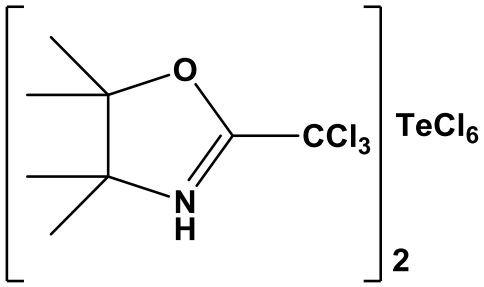

307. $TeCl_4$ (0.8963g, 3mmol) was refluxed with Pinacol $C_6H_{14}O_2$ (0.3545g, 3mmol) and trichloroacetonitrile (4.32g, 30mmol) for 4hrs at 80°C. After 30mins the solution turned from yellow to dark green solution. After 4hrs reaction stopped and flask cooled on ice bath. Dried for 1hr on rotavap and a dark crude solution remained. A dark green oil was extracted.

^{1}H NMR (DMSO-d_6): δ = 0.98 (s, 6H, CH_3), 1.09 (s, 6H, CH_3), 2.00

^{13}C NMR (DMSO-d_6): δ = 24.88 (CH_3, CH_3), 26.13 (CH_3, CH_3), 56.27, 92.9 (C-N), 113.45, 128.90, 162.95)

^{125}Te (DMSO-d_6): δ = 1526.

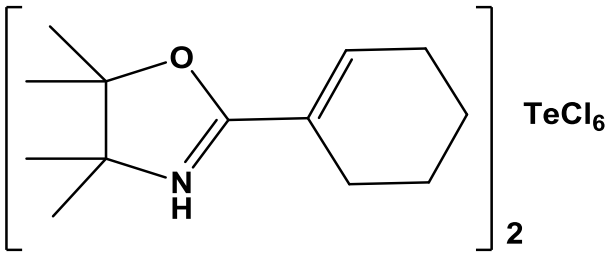

308. $TeCl_4$ (0.695g, 2.34mmol) was refluxed with Pinacol $C_6H_{14}O_2$ (0.277g, 2.34mmol) and 1-cyclohexeneacetonitrile (2.63g, 8.25mmol) for 8hrs at 130°C. After 15mins the solution turns dark brown in colour. After 8hrs reaction stopped and solution allowed to cool to r.t. Attempted to dry on rotavap to reduce solvent but would not reduce. Diethyl ether added to precipitate solid a grey fine powder achieved but analysing solid showed no product produced.

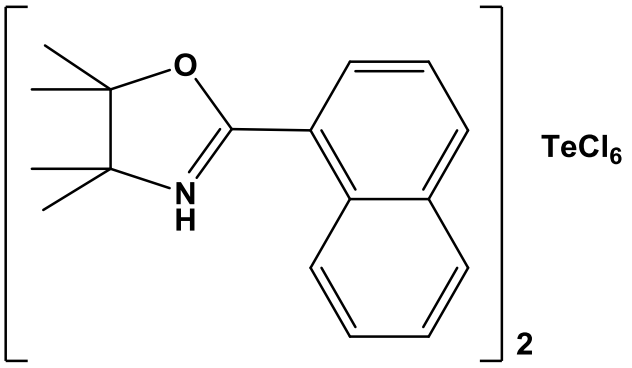

309. $TeCl_4$ (0.44g, 1.48mmol) was refluxed with Pinacol $C_6H_{14}O_2$ (0.35g, 3mmol) and 1-napthonitrile (0.44g, 3mmol) for 6hrs at 80^{o}C. After 5mins the solution changed colour from yellow to a dark solution. After 6hrs the reaction was stopped and allowed to cool to r.t. Attempts to try recover a solid by evaporation of solvent and addition of diethyl ether and petroleum ether failed to recover solid. A dark oil had formed which could not be purified.

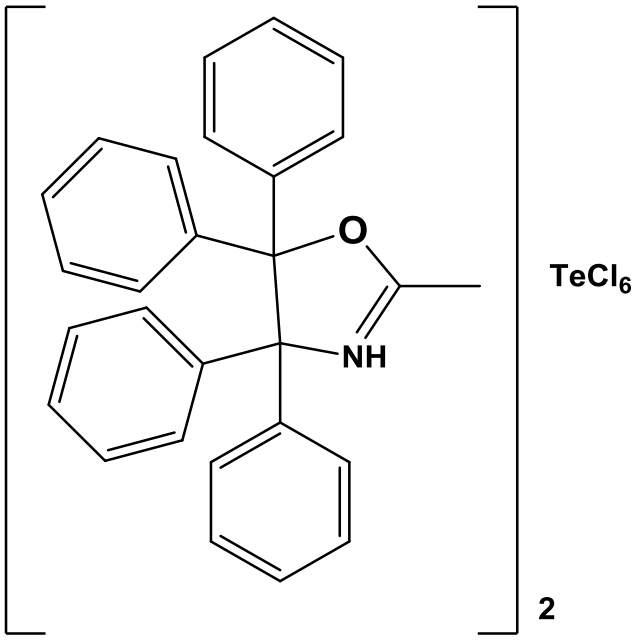

310. $TeCl_4$ (0.1513g, 0.5mmol) was refluxed with 1,1,2,2 tetraphenyl 1,2 ethanediol $C_{26}H_{22}O_2$ (0.1832g, 0.5mmol) and dry acetonitrile (10ml) for 4hrs at 80°C. The solution stayed yellow for the entire reaction. After 4hrs reaction stopped and flask cooled on ice bath. Dried for 1hr on rotavap and a yellow solid was extracted.

^{1}H NMR (DMSO-d_6): δ = 1.76 (s, 3H, CH_3), 7.16 (6H), 7.30 (1H), 7.58 (2H)

^{13}C NMR (DMSO-d_6): δ = 22.46 (CH_3), 70.60 (quat), 126 (quat), 127 (CH), 130 (CH), 132 (CH), 136 (quat), 143 (quat), 171 (-C=N), 197 (CH)

^{125}Te (DMSO-d_6): δ = 1525.

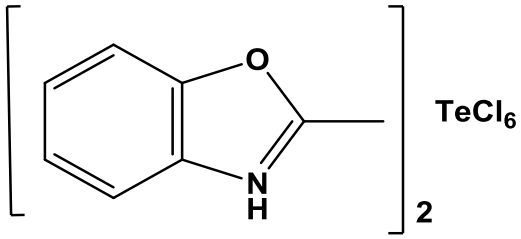

311. $TeCl_4$ (0.5893g, 2mmol) was refluxed with Catechol $C_6H_8O_2$ (0.2202g, 2mmol) and dry acetonitrile (5ml) for 4hrs at 80°C. The solution started off yellow in colour but after 1.5hrs changed to a red solution. After 4hrs reaction stopped and flask cooled on ice bath. Dried for 1hr on rotavap and a dark brown oil formed.

^{1}H NMR (DMSO-d_6): δ = 1.18 (s, 3H, CH_3), 6.69 (t, 4H)

^{13}C NMR (DMSO-d_6): δ = 8.67, 45.65, 113.9, 115.67, 119.79, 145.25, 149.16

^{125}Te (DMSO-d_6): δ = 1524.

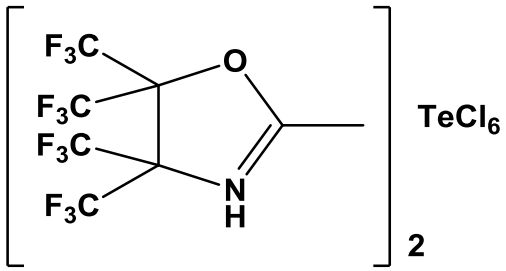

312. $TeCl_4$ (0.7651g, 2.6mmol) was refluxed with hexafluoro 2,3 bis(trifluoromethyl) 2,3 butanediol [$(CF_3)_2C(OH)_2$] (0.8686g, 2.6mmol) and dry acetonitrile (5ml) for 16hrs at 80°C. The solution started off yellow in colour for entire reaction. After 16hrs reaction stopped and flask cooled on ice bath. Dried for 1hr on rotavap and a dark brown oil formed.

^{1}H NMR (DMSO-d_6): δ = 1.23 (s, 3H, CH_3), 7.26

^{13}C NMR (DMSO-d_6): δ = 25.55, 62.86, 74.83, 77.16, 80.23

^{125}Te (DMSO-d_6): δ = 1525.65.

^{19}F NMR (DMSO-d_6): δ = -70.51

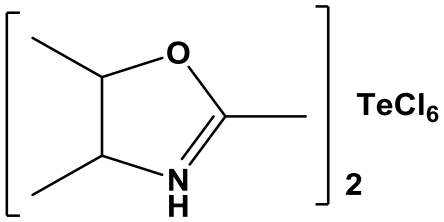

313. $TeCl_4$ (1.239g, 4.2mmol) was refluxed with 2,3 butanediol $C_4H_{10}O_2$ (0.2202g, 4.2mmol) and dry acetonitrile (10ml) for 12hrs at 80°C. The solution started off yellow in colour but after 1.5hrs changed to a red solution. After 12hrs reaction stopped and flask cooled on ice bath. Dried for 1hr on rotavap and a dark yellow oil formed. When oil analysed using NMR found that reaction did not occur.

3.3.3. Figures

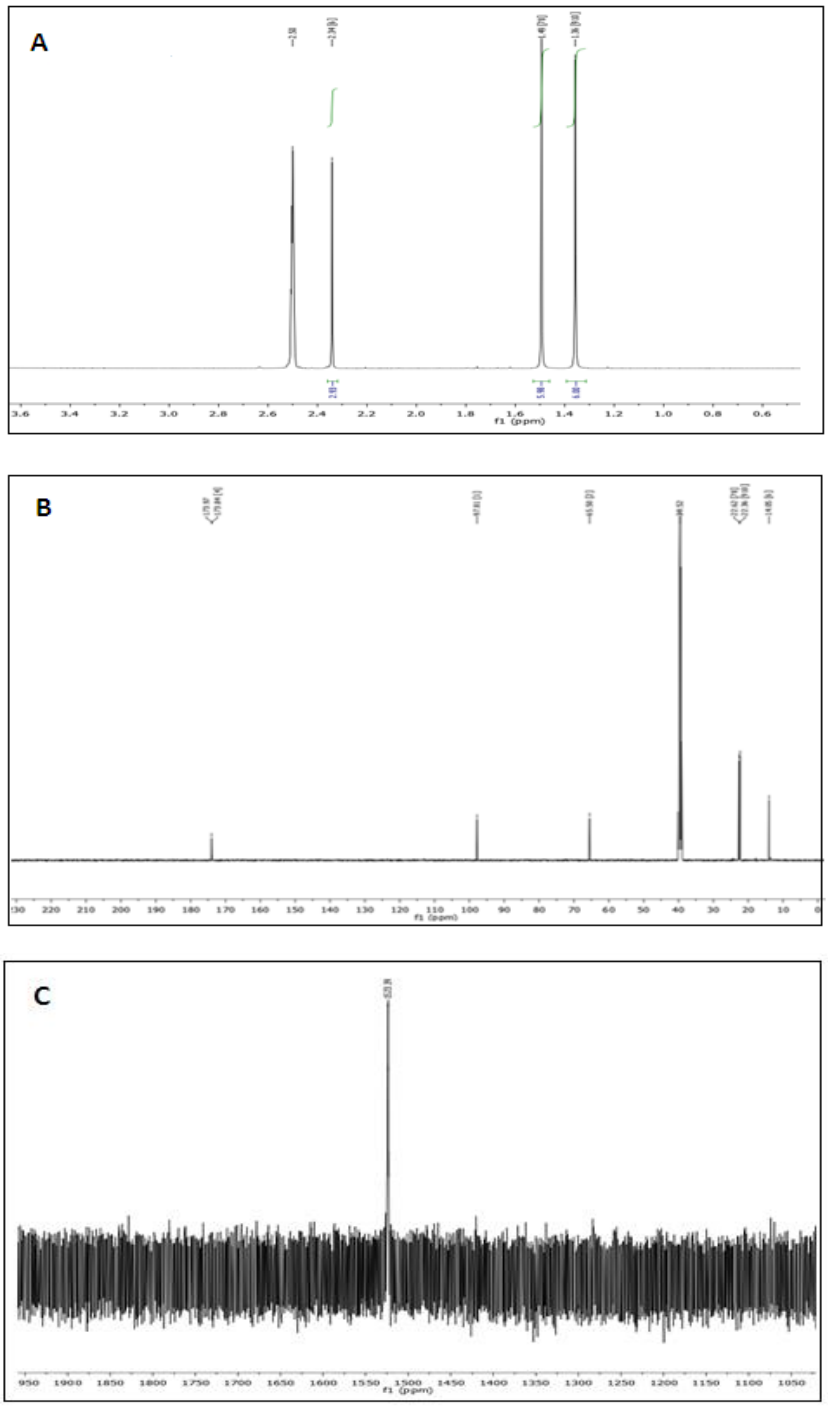

Figure 3.09. NMR spectra of compound **301**. (A) ^{1}H NMR, (B) ^{13}NMR and (C) ^{125}Te NMR

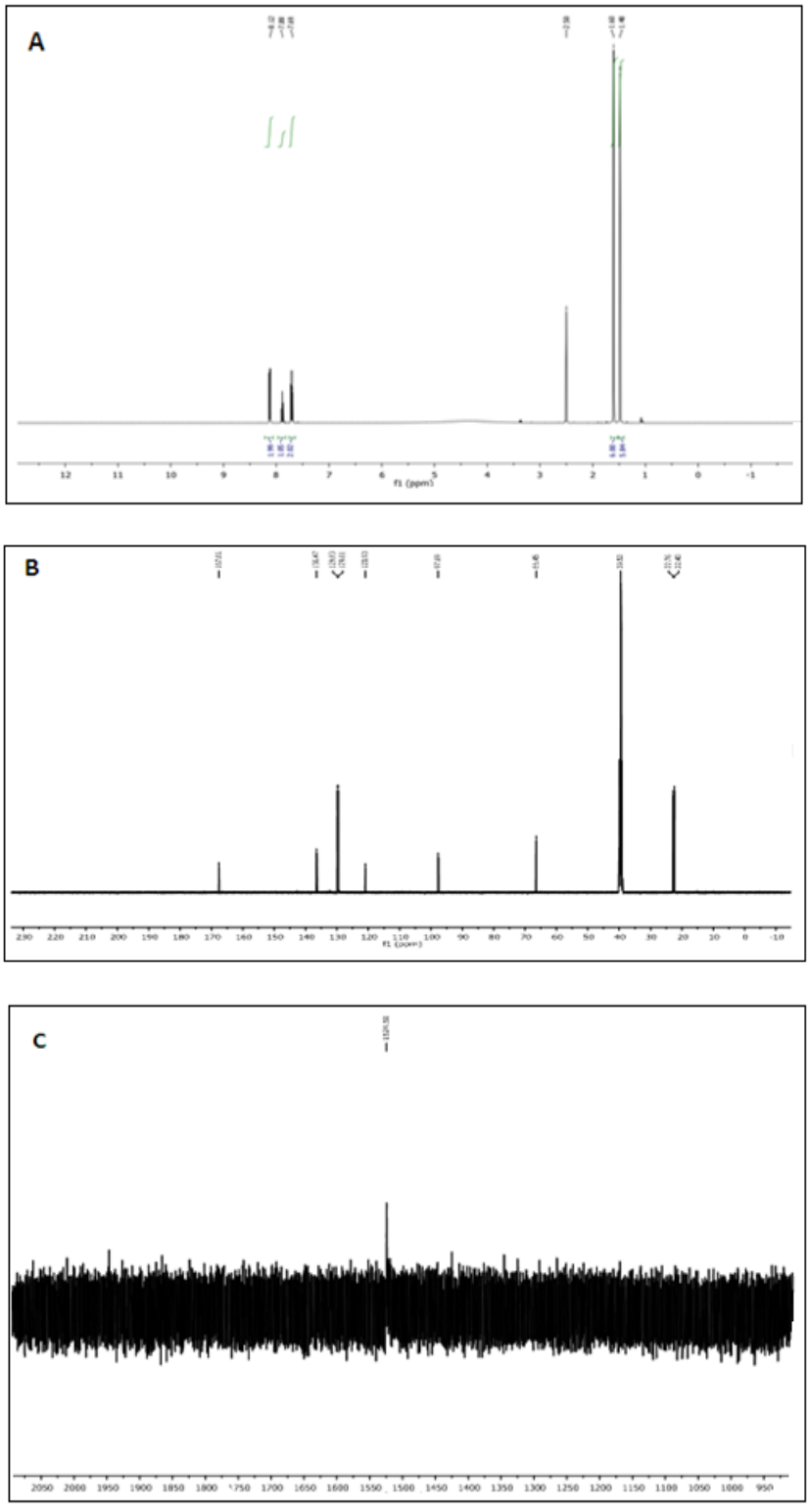

Figure 3.10. NMR spectra of compound **302**. (A) ^{1}H NMR, (B) ^{13}NMR and (C) ^{125}Te NMR

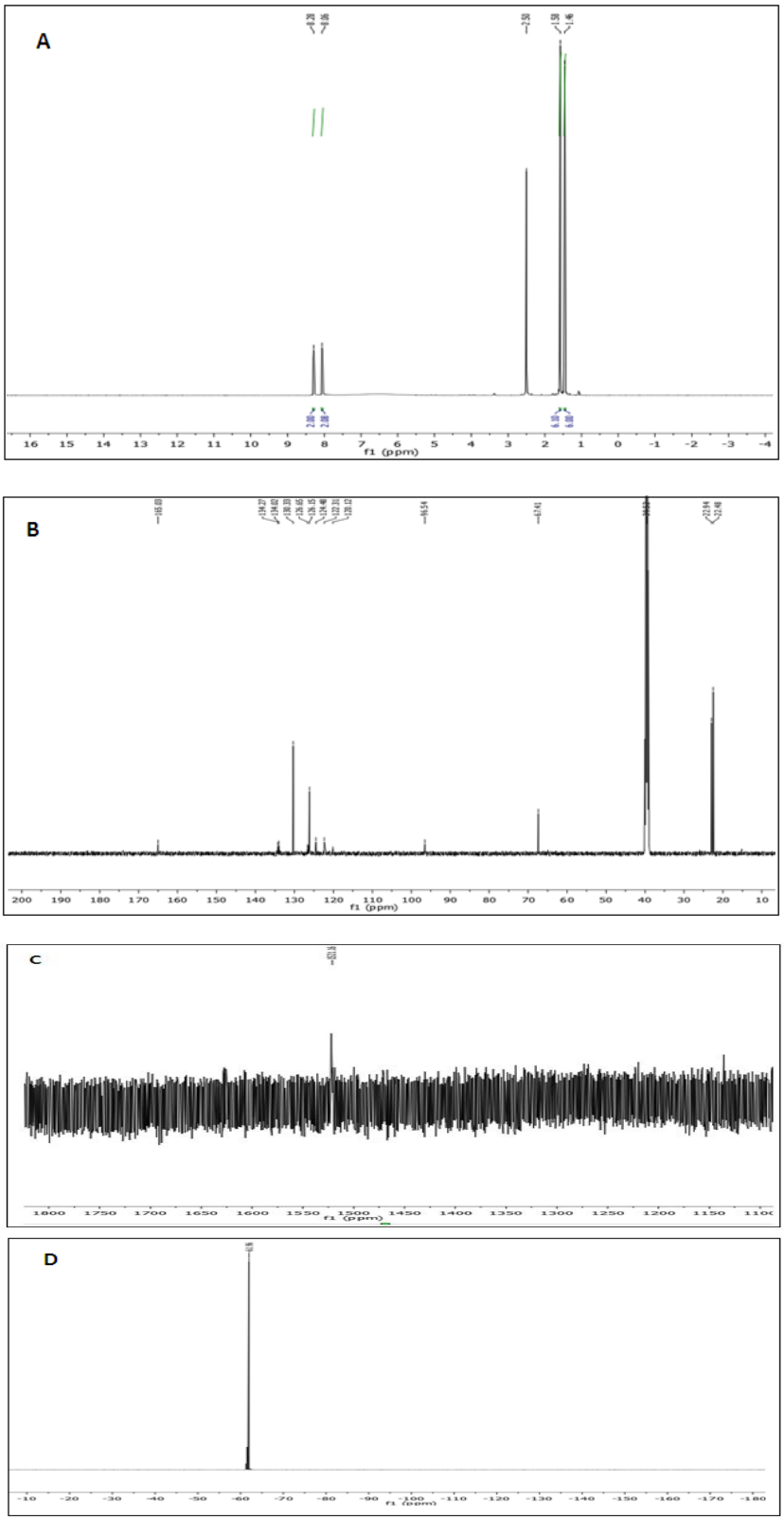

Figure 3.11. NMR spectra of compound **303**. (A) ^{1}H NMR, (B) ^{13}NMR and (C) ^{125}Te NMR

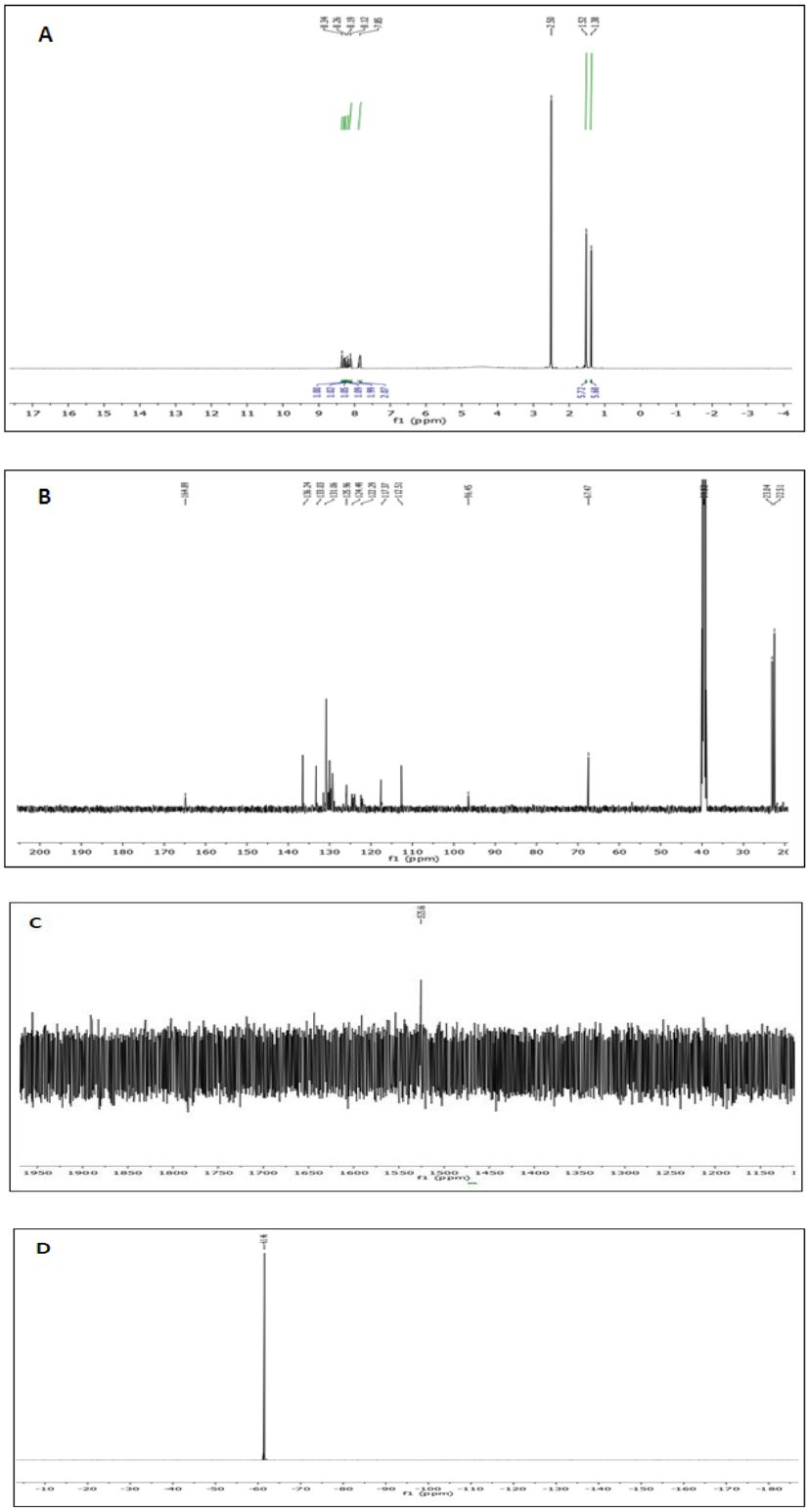

Figure 3.12. NMR spectra of compound **304**. (A) ^{1}H NMR, (B) ^{13}NMR, (C) ^{125}Te NMR and (D) ^{19}F NMR

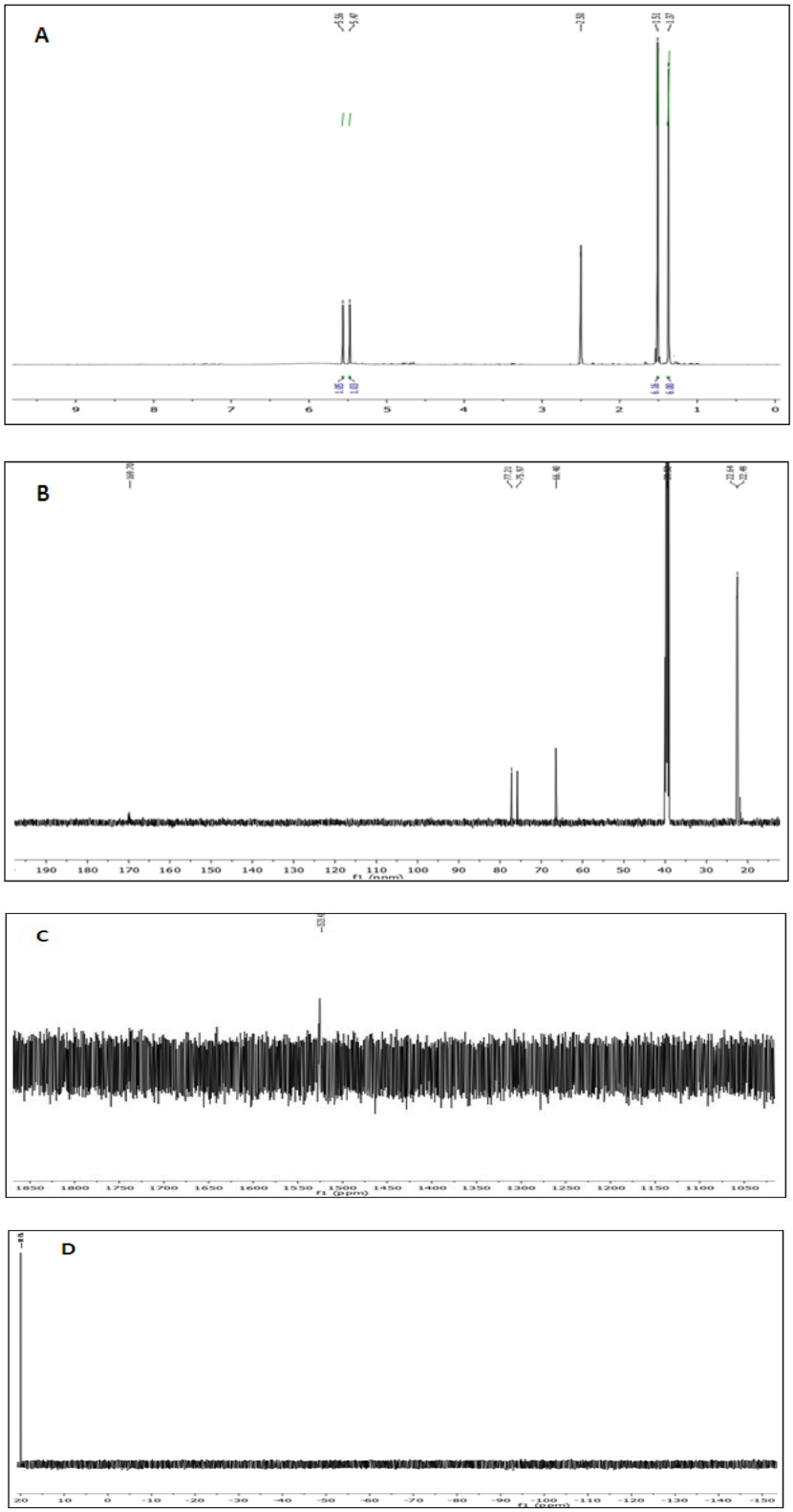

Figure 3.13. NMR spectra of compound **305**. (A) ^{1}H NMR, (B) ^{13}NMR, (C) ^{125}Te NMR and (D) ^{19}F NMR

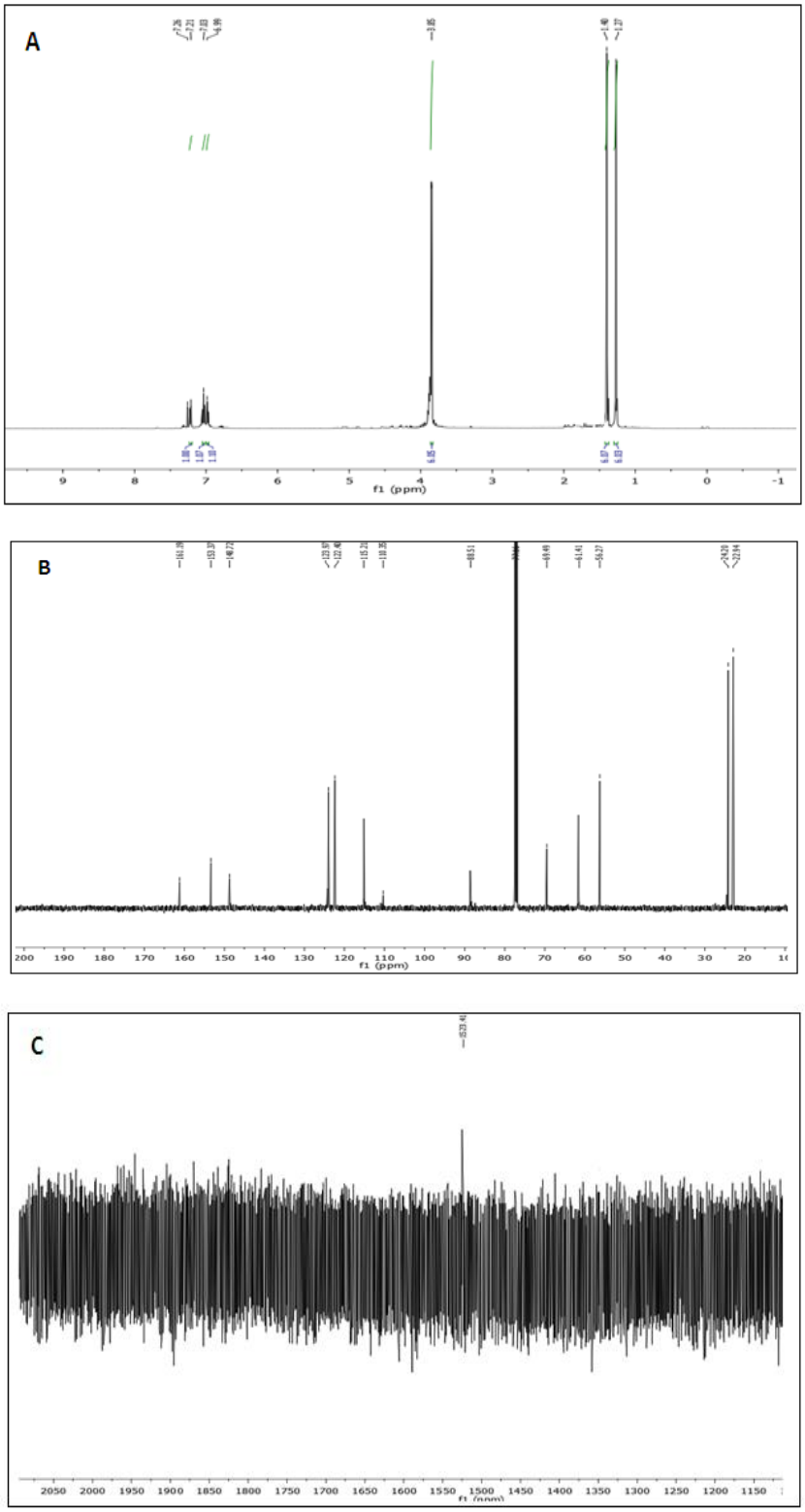

Figure 3.14. NMR spectra of compound **306**. (A) ^{1}H NMR, (B) ^{13}NMR and (C) ^{125}Te NMR

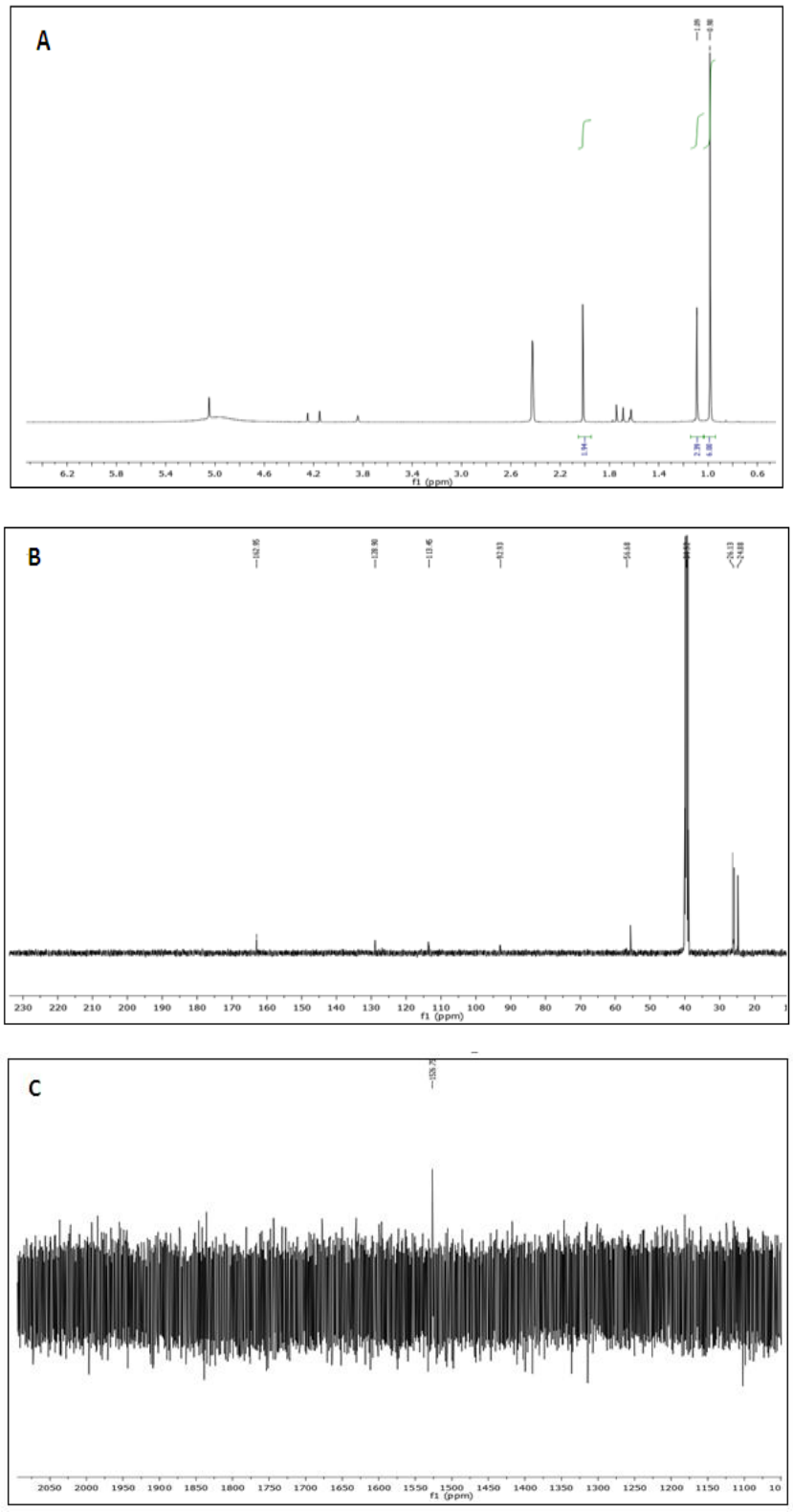

Figure 3.15. NMR spectra of compound **307**. (A) ^{1}H NMR, (B) ^{13}NMR and (C) ^{125}Te NMR

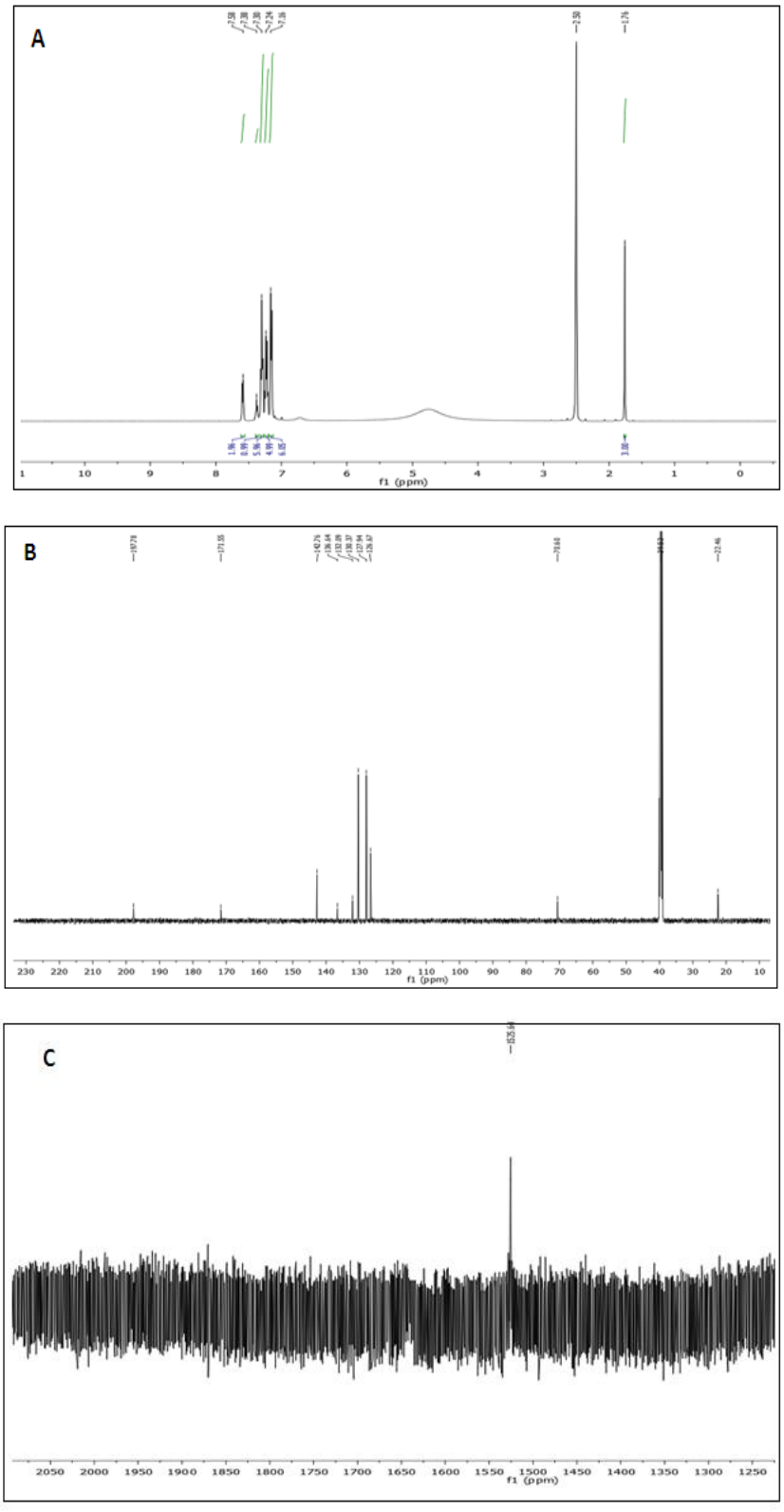

Figure 3.16. NMR spectra of compound **310**. (A) ^{1}H NMR, (B) ^{13}NMR and (C) ^{125}Te NMR

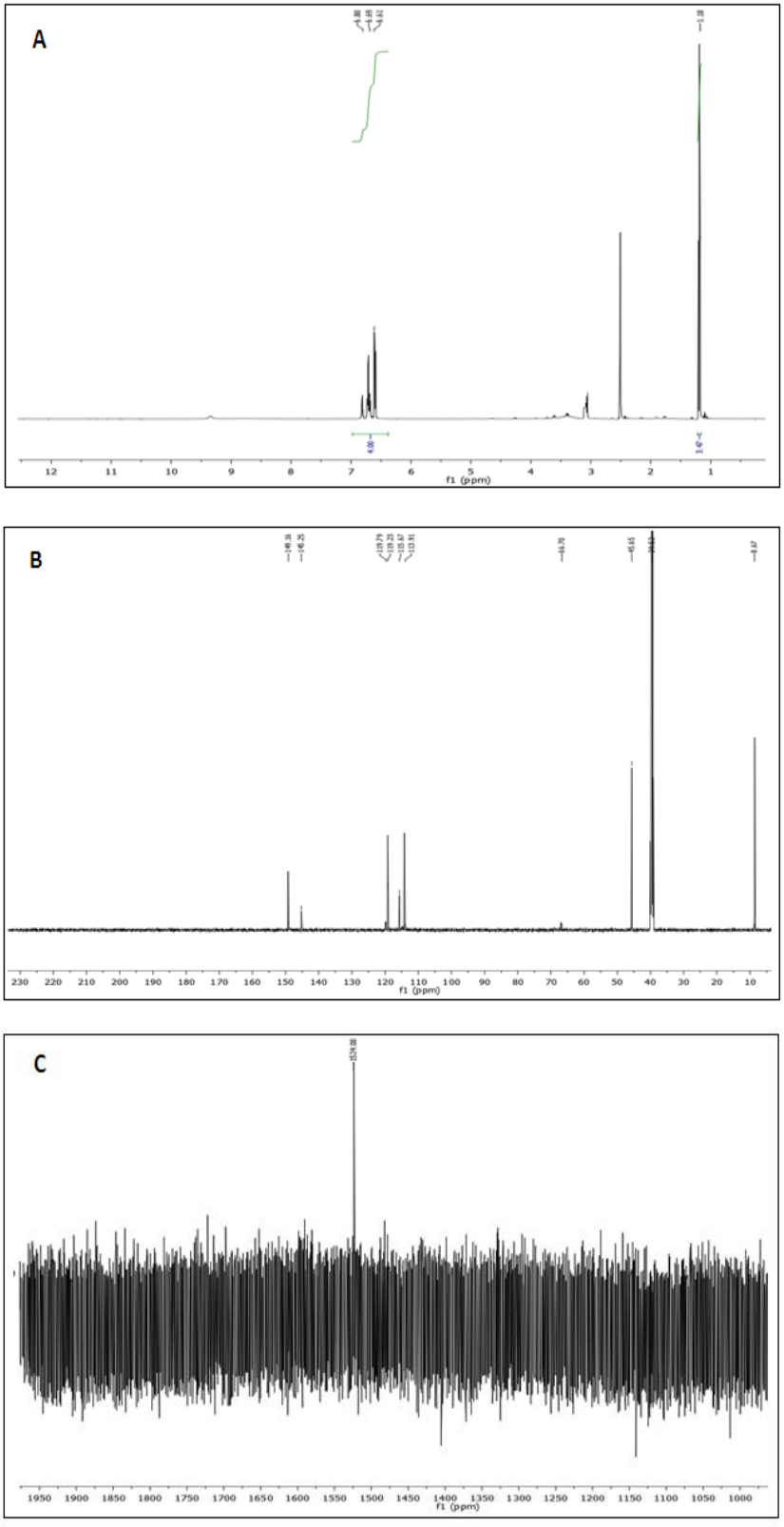

Figure 3.17. NMR spectra of compound **311**. (A) ^{1}H NMR, (B) ^{13}NMR and (C) ^{125}Te NMR

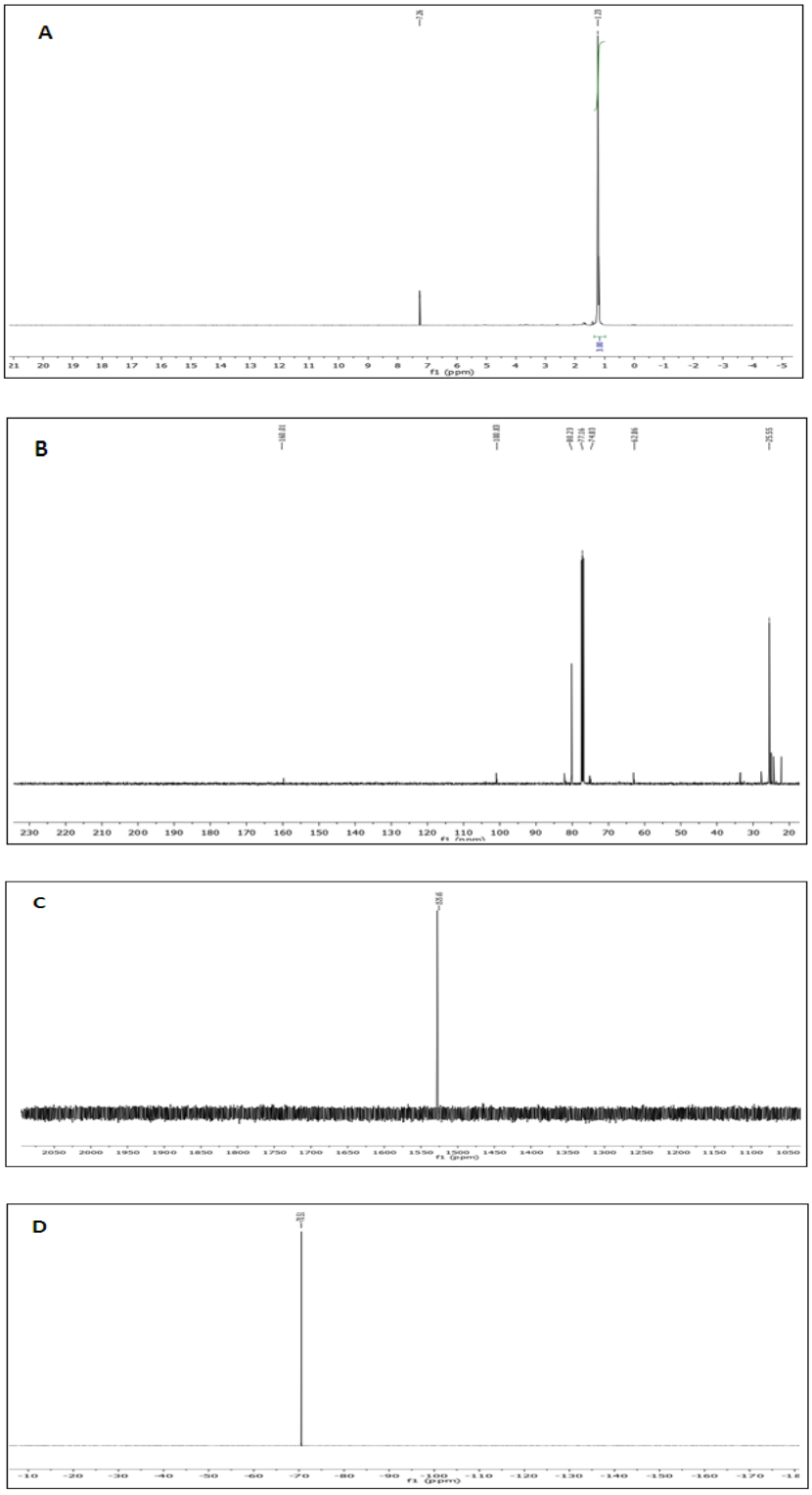

Figure 3.18. NMR spectra of compound **312.** (A) ^{1}H NMR, (B) ^{13}NMR, (C) ^{125}Te NMR and (D) ^{19}F NMR in DMSO-d_6

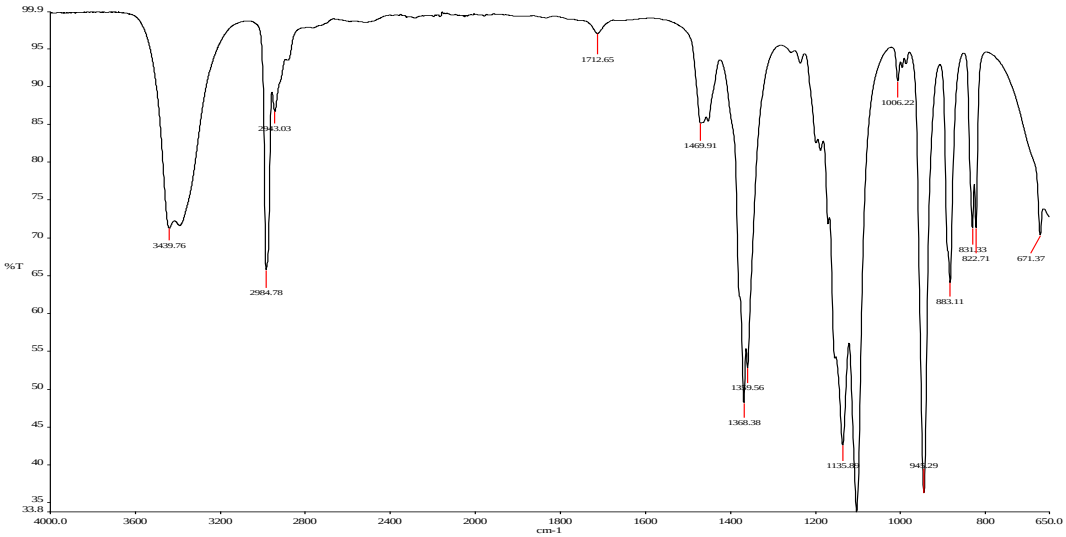

Figure 3.19. IR spectrum of free Pinacol

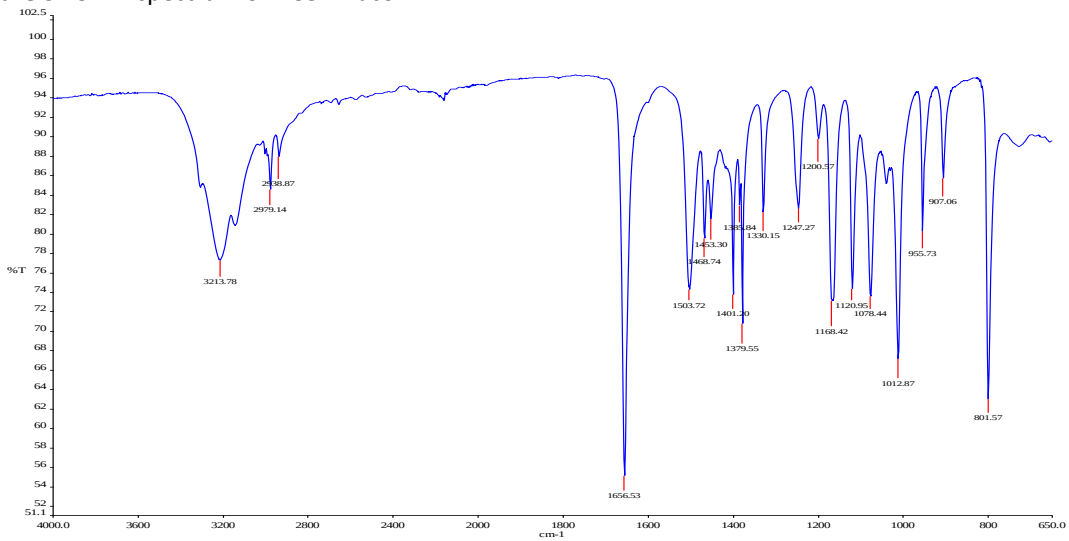

Figure 3.20. IR spectrum of compound **301**

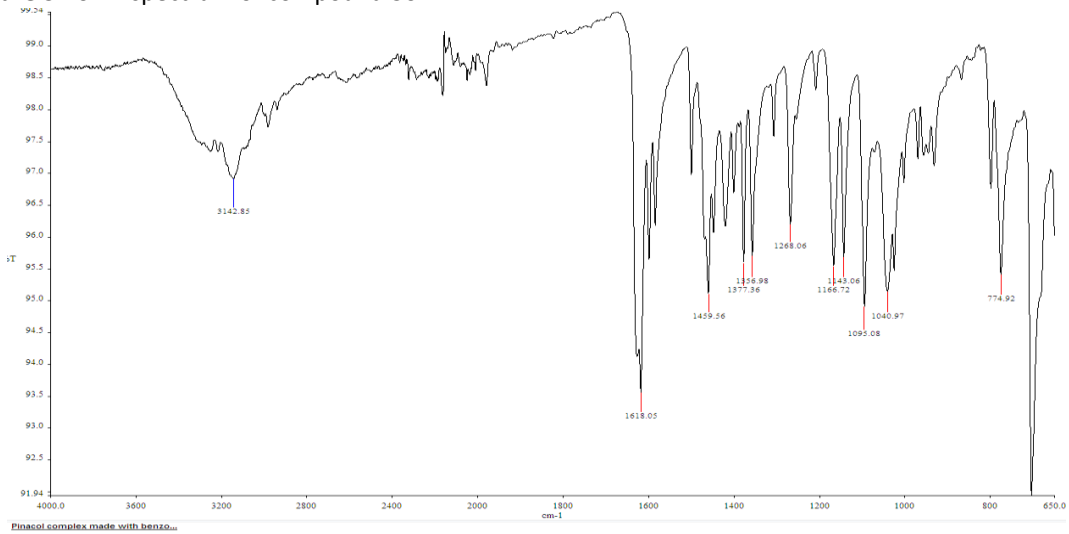

Figure 3.21. IR spectrum of compound **302**

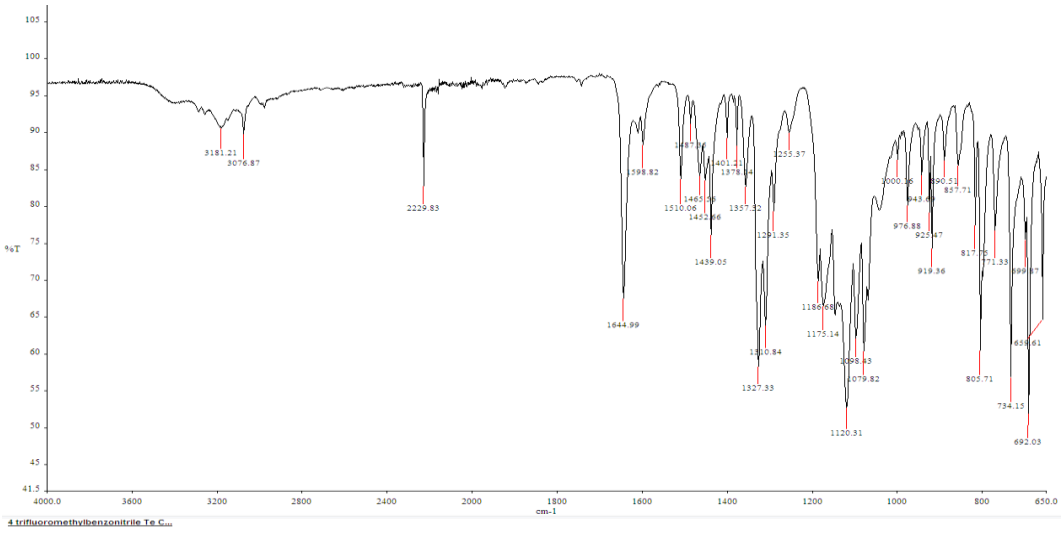

Figure 3.22. IR spectrum of compound **303**

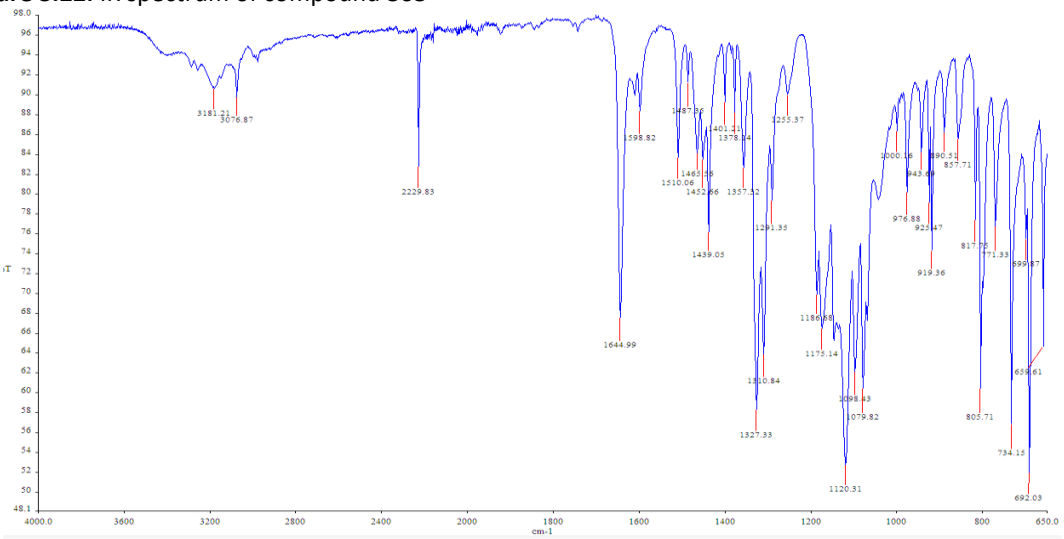

Figure 3.23. IR spectrum of compound **304**

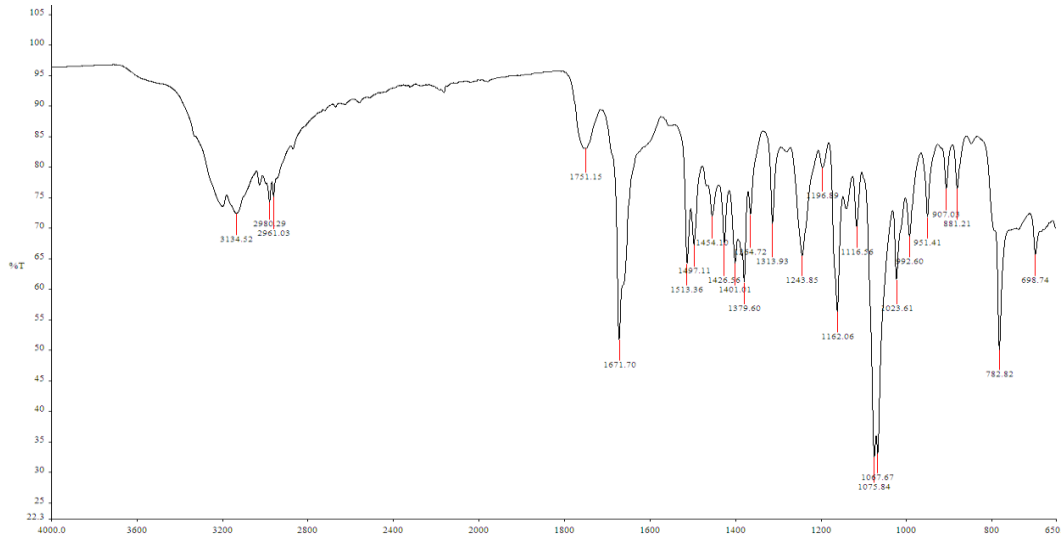

Figure 3.24. IR spectrum of compound **305**

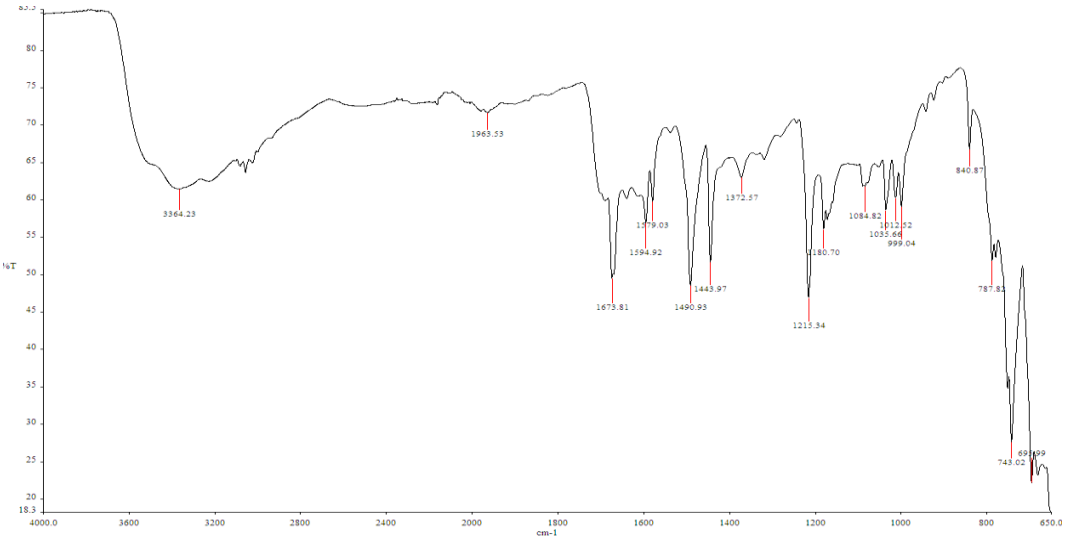

Figure 3.25. IR spectrum of compound **310**

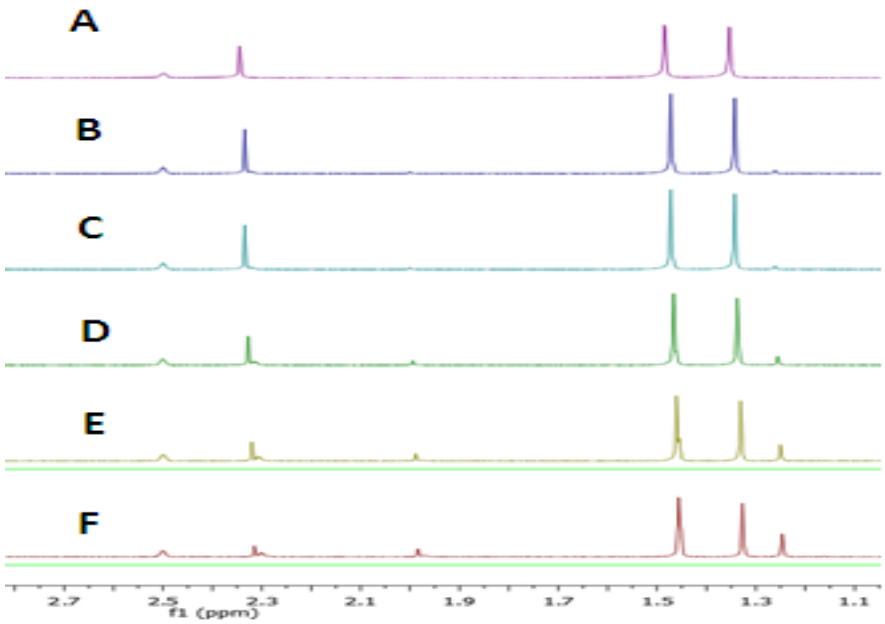

Figure 3.26. A: ^{1}H NMR of **301** (0.5 mM in DMSO-d_6), B: **301** + 10uL D_2O (10 equivalents), C: **301** + 20uL D_2O (20 equivalents), D: **301** + 30uL D_2O (30 equivalents), E: **301** + 40uL D_2O (40 equivalents) and F: **301** + 50uL D_2O (50 equivalents)

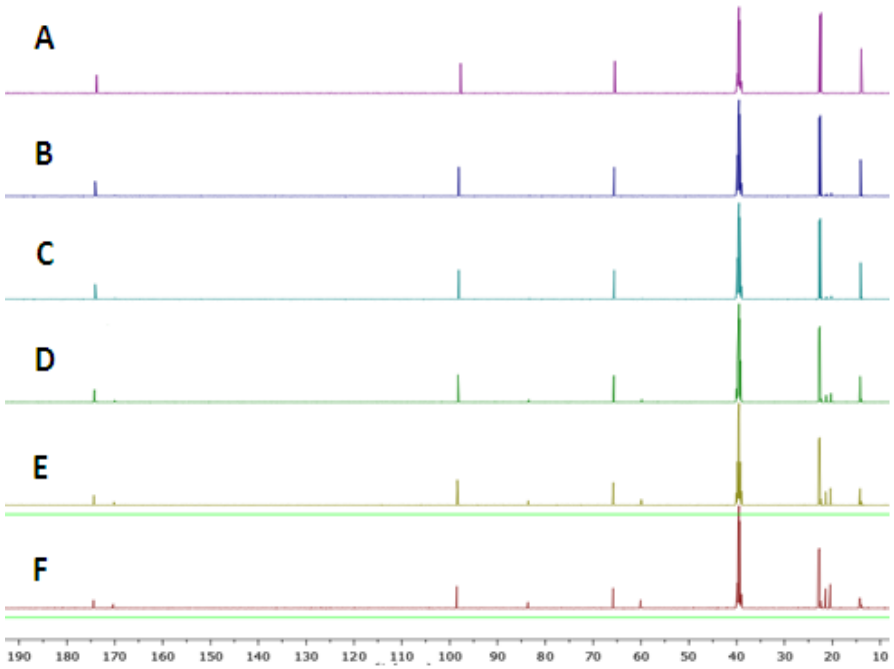

Figure 3.27. A: ^{13}C NMR of **301** (0.5 mM in DMSO-d_6), B: **301** + 10uL D_2O (10 equivalents), C: **301** + 20uL D_2O (20 equivalents), D: **301** + 30uL D_2O (30 equivalents), E: **301** + 40uL D_2O (40 equivalents) and F: **301** + 50uL D_2O (50 equivalents)

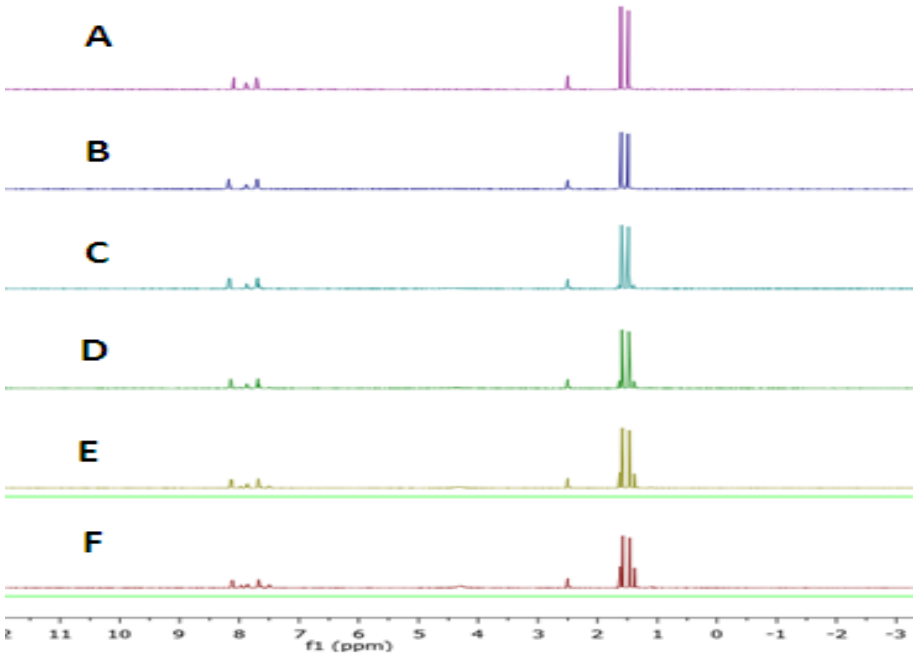

Figure 3.28. A: ^{1}H NMR of **302** (0.5 mM in DMSO-d_6), B: **302** + 10uL D_2O (10 equivalents), C: **302** + 20uL D_2O (20 equivalents), D: **302** + 30uL D_2O (30 equivalents), E: **302** + 40uL D_2O (40 equivalents) and F: **302** + 50uL D_2O (50 equivalents)

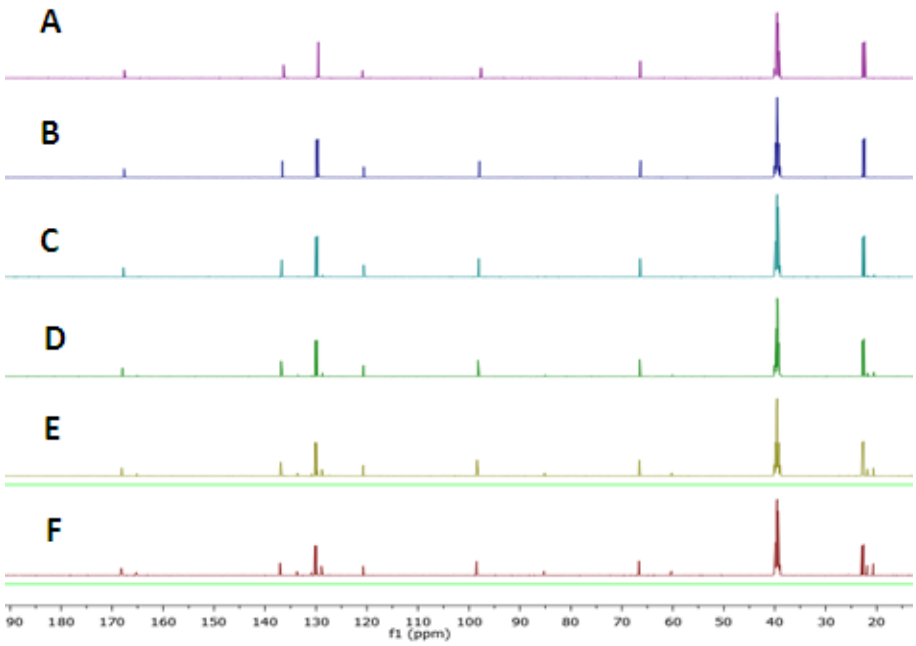

Figure 3.29. A ^{13}C NMR of **302** (0.5 mM in DMSO-d_6), B: **302** + 10uL D_2O (10 equivalents), C: **302** + 20uL D_2O (20 equivalents), D: **302** + 30uL D_2O (30 equivalents), E: **302** + 40uL D_2O (40 equivalents) and F: **302** + 50uL D_2O (50 equivalents)

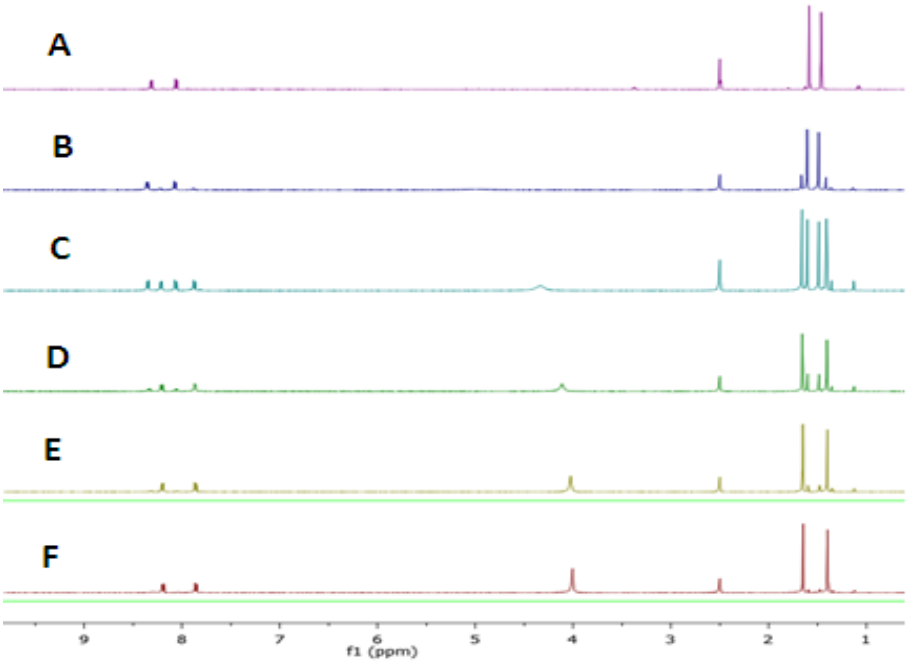

Figure 3.30. A: ^{1}H NMR of **303** (0.5 mM in DMSO-d_6), B: **303** + 10uL D_2O (10 equivalents), C: **303** + 20uL D_2O (20 equivalents), D: **303** + 30uL D_2O (30 equivalents), E: **303** + 40uL D_2O (40 equivalents) and F: **303** + 50uL D_2O (50 equivalents)

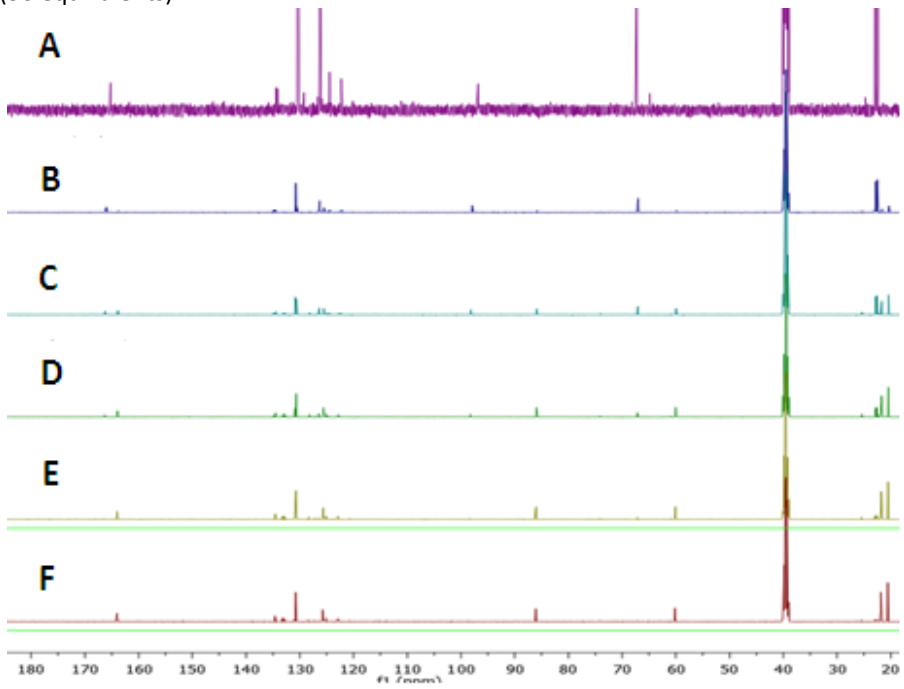

Figure 3.31. A: ^{13}C NMR of **303** (0.5 mM in DMSO-d_6), B: **303** + 10uL D_2O (10 equivalents), C: **303** + 20uL D_2O (20 equivalents), D: **303** + 30uL D_2O (30 equivalents), E: **303** + 40uL D_2O (40 equivalents) and F: **303** + 50uL D_2O (50 equivalents)

3.4 References

1. M. Beg and H. Clark, *Canadian Journal of Chemistry*, 2011, **40**, 393-398.
2. F. Palacios, J. Vicario and D. Aparicio, *European Journal of Organic Chemistry*, 2006, **2006**, 2843-2850.
3. A. V. Makarycheva-Mikhailova, V. Y. Kukushkin, A. A. Nazarov, D. A. Garnovskii, A. J. L. Pombeiro, M. Haukka, B. K. Keppler and M. Galanski, *Inorganic Chemistry*, 2003, **42**, 2805-2813.
4. R. H. Wiley and L. L. Bennett, *Chemical Reviews*, 1949, **44**, 447-476.
5. A. Decken, C. R. Eisnor, R. A. Gossage and S. M. Jackson, *Inorganica Chimica Acta*, 2006, **359**, 1743-1753.
6. B. T.M, d. R. I, G. R.A and J. S.M, *Canadian Journal of Chemistry*, 2003, **81**, 1482-1491.
7. V. V. Kuznetsov, Y. E. Brusilovskii and A. V. Mazepa, *Chemistry of Heterocyclic Compounds*, 2001, **37**, 920-923.
8. B.-J. Zhao, D. H. Evans, N. A. Macías-Ruvalcaba and H. J. Shine, *The Journal of Organic Chemistry*, 2006, **71**, 3737-3742.
9. J. Milne, *Canadian Journal of Chemistry*, 2011, **69**, 987-992.
10. M. Filella and P. M. May, *ENVIRONMENTAL CHEMISTRY*, 2019, **16**, 289-295.
11. A. Makino and S. Kobayashi, *Journal of Polymer Science Part A: Polymer Chemistry*, 2010, **48**, 1251-1270.

Chapter 4

Conclusions and future perspectives

A series of new Te(IV) complexes were synthesized with the aim to discover new stable Te(IV) species with high antimicrobial and anticancer activity. Despite the large success of metal-based complexes in medicinal chemistry for the cure of several diseases, in particular as antimicrobial and anticancer agents (i.e. platinum, ruthenium, gold…), very few examples of Tellurium-based drugs are reported. In particular, only two Tellurium compounds entered in clinical trials as antitumor compounds, named AS-101 and SAS. Both these species are based on a Te(IV)-scaffold with O-donor ligands that are displaced in physiological condition by hydrolysis. The novel compounds synthesized can be divided in two different families:

1) Compounds **201-208** (described in chapter 2) where the ligands used are substituted 1,2-diols with only one vicinal carbon functionalized;
2) Compounds **301-313** (described in chapter 3) where the ligands used are substituted 1,2-diols with both vicinal carbons functionalized.

The stability of the first series of compounds with regard hydrolysis, has been evaluated combining experiment data (*via* multinuclear ^{1}H, ^{13}C, ^{19}F, ^{125}Te-NMR) with theoretical calculations. A correlation between the alkyl chain length of the ligand and the aqueous stability was observed, with longer chains, that are more steric encumbered and more lipophilic, showing increased stability for the corresponding Te(IV) compounds. Theoretical investigation demonstrated that longer chains prevents the approach of water molecules in proximity of the Te(IV) centre with consequently decrease in the hydrolytic rate. This trend was confirmed using two different theoretical methods, the implicit solvation and the explicit solvation approach. The antimicrobial activity of some of these compounds was tested with promising high activity against Gran negative *E. Coli* (MIC_{50} values in the low micromolar concentration). Due to the biological conditions, the species responsible of the antimicrobial activity was identified as the hydrolysed product $[TeOCl_3]^-$, which is further reduced to elemental Tellurium (black precipitate observed at the bottom of the plates). The second series of compounds (chapter 3) were obtained using identical conditions as for the first series but modifying both the vicinal carbons in the 1,2-diol chain. With pinacol, also known as (1,1,2,2 tetramethyl-1,2 ethanediol), completely different products were obtained. These species were salts where the anion is $[TeCl_6]^{2-}$ and the cation is an oxazoline derivative. These oxazolines

ligands are formed by the reaction between one activated molecule of acetonitrile (used as solvent) and pinacol, in the presence of $TeCl_4$. Analogues species are isolated also using different nitriles, in particular benzonitrile and 4-trifluoromethyl-benzonitrile. $TeCl_4$ could act as a catalyst in the formation of these species and the reaction also works at r.t. This is a great advantage with respect the common procedures for the syntheses ox oxazolines, that usually require stronger conditions.

These new compounds have been characterized using several spectroscopic techniques (multinuclear NMR, IR, Mass, Elemental Analyses) and some of them were also characterized by X-ray structure. The stability in aqueous conditions was studied experimentally *via* accurate multinuclear NMR analyses. These species decompose upon addition of 10 or more equivalents of H_2O and the kinetics of decomposition depends on the electric properties of the starting nitrile molecule. 4-trifluoromethyl-benzonitrile derivative decomposed faster and this is probably due to the electro-withdrawing properties of the CF_3 group that enhance the nucleophilic attack on the oxazoline ring. Theoretical investigation will be an important tool to understand the mechanism of formation of this second series of compounds. Due to note that these species are not forming with other bis-susbstituted diols (i.e. 1,1,2,2 tetraphenyl 1,2-ethanediol, catechol, hexafluoro 2,3 bis(trifluoromethyl) 2,3 butanediol, 2,3-butandiol) or with other nitriles (i.e. trichloroacetonitrile, cyclohexene-nitrile, naphto-nitrile). A theoretical approach will be also used in order to understand why these class of compounds can be isolated only with pinacol derivatives while with other bis-substituted 1,2-diol ligands or with other nitriles, analogues species are not obtained. Once the mechanism of formation and the mechanism of hydrolytic cleavage will be elucidated, anticancer activity and proteomics studies will allow to clarify the still not clear mechanism of action of Te(IV) compounds.

In particular, the following aspects will be considered regarding the anticancer activity:

- Study of the drug uptake
- Cytotoxycity against a panel of human cancer cell lines and non-cancer cell lines;
- ROS productions;
- Drugs uptake and correlation with the lipophilicity;
- Mechanism of drug uptake (active or passive transport);
- Flow cytometry;

- Evaluation of the selectivity for cancer against non-cancer cells;
- Proteomics.

Antimicrobial activity will be studied using the second series of compounds and the results compared with those obtained for the first series. This is a pioneer study on the biological role of tellurium and, due to the unclear role and mechanism of action of Te(IV)-compounds, there are several opportunities and chances to open a completely new field in medicinal chemistry, by developing novel stable Te(IV)-based drugs.

Appendix

Journal of Inorganic Biochemistry 198 (2019) 110719

Contents lists available at ScienceDirect

Journal of Inorganic Biochemistry

journal homepage: www.elsevier.com/locate/jinorgbio

Stability of antibacterial Te(IV) compounds: A combined experimental and computational study

Kenneth D'Arcy[a], Adam Patrick Doyle[b], Kevin Kavanagh[b], Luca Ronconi[c], Barbara Fresch[d], Diego Montagner[a,*]

[a] Department of Chemistry, Maynooth University, Maynooth, Ireland
[b] Department of Biology, Maynooth University, Maynooth, Ireland
[c] School of Chemistry, National University of Ireland Galway, Galway, Ireland
[d] Department of Chemical Science, University of Padova, Italy

A B S T R A C T

Inorganic Te(IV) compounds are important cysteine protease inhibitors and antimicrobial agents; AS-101 [ammonium trichloro (dioxoethylene-O,O′)tellurate] is the first compound of a family with formula $NH_4[C_2H_4Cl_3O_2Te]$, where a Te(IV) centre is bound to a chelate ethylene glycol, and showed several protective therapeutic applications. This compound is lacking in stability performance and is subjected to hydrolysis reaction with displacement of the diol ligand. In this paper, we report the stability trend of a series of analogues complexes of AS-101 with generic formula $NH_4[(RC_2H_3O_2)Cl_3Te]$, where R is an alkyl group with different chain length and different electronic properties, in order to find a correlation between structure and stability in aqueous-physiological conditions. The stability was studied in solution *via* multinuclear NMR spectroscopy (^1H, ^{13}C, ^{125}Te) and computationally at the Density Functional Theory level with an explicit micro solvation model. The combined experimental and theoretical work highlights the essential role of the solvating environment and provides mechanistic insights into the complex decomposition reaction. Antimicrobial activity of the compounds was assessed against different bacterial strains.

1. Introduction

Tellurium is a metalloid element with several available oxidation states going from −2 to +6 [1]. Tellurides of formula M_2Te are compounds formed by Te(-II) and noble elements such as Au or Ag that are highly unstable and in the presence of oxygen's are oxidised to tellurite $[Te(IV)O_3]^{2-}$ [2]. The biological properties of tellurium are poorly characterized, but it is known that some bacteria and fungi are able to uptake Te as amino acids, replacing the Sulfur atom and forming Tellurium-cysteine and Tellurium methionine [3,4]. The oxidation state +4 is the most stable and interesting from biological application, with multiple complexes of organo-tellurium(IV), containing a direct Te—C bond, reported. These complexes are stable in aqueous solution and seem to have a promising and potential role in protease inhibition and integrin inactivation [5–14]. Besides these families of organo-tellurium complexes, Albeck and co-worker's ultimately developed two "inorganic" tellurate Te(IV) compounds, named AS-101 [ammonium trichloro (dioxoethylene-O,O′)tellurate] and SAS [octa-*O*-bis-(*R*,*R*)-tartarate ditellurane] whose structure is depicted in Fig. 1. These complexes are effective inhibitors of cysteine protease and showed several protective therapeutic applications and *in vivo*, preclinical and clinical studies have been conducted [15–26].

Te(IV) compounds can inhibit integrin functions such as adhesion, migration and metalloproteinase secretion mediation in B16F10 murine melanoma cells. AS-101 in particular, can stimulate the proliferation of normal lymphoid cells producing lymphokines that are regulators of lymphopoiesis and myelopoiesis [17]. AS-101 also showed strong antibacterial activity in particular on Gram-negative bacterium *Enterobacter cloacae* [27]. Recently, Albeck and Cunha, reported that AS-101 is not stable in physiological conditions and is subjected to hydrolysis where the diol ligand is displaced with the formation of $[Te(IV)OCl_3]^-$, which is likely the bioactive species in biological investigation [28,29]. Due to the promising activity of AS-101 in term of anticancer and immune-modulating properties, we sought to design, synthesise and characterize a series of AS-101 analogues with different ligands, in order to investigate their stability properties in aqueous environment and ultimately found a tellurate Te(IV) complex stable enough to perform biological studies in physiological conditions.

The ethylene glycol of AS-101 has been substituted with a series of diols with increasing alkyl chain length and electron withdrawing groups, producing eight novel Te(IV) complexes with formula $NH_4[(RC_2H_3O_2)Cl_3Te]$ (where R = H (**1**); CH_3 (**2**); CH_2CH_3 (**3**); $CH_2CH_2CH_3$ (**4**); $CH_2CH_2CH_2CH_3$ (**5**); $CH_2CH_2CH_2CH_2CH_2CH_3$ (**6**); CH_2Cl (**7**); Ph. (**8**)). The aqueous stability has been evaluated using ^1H, ^{13}C and ^{125}Te NMR and theoretical studies allowed an understanding of the molecular basis of the observed trend. The modelling of the reaction

* Corresponding author.
E-mail addresses: barbara.fresch@unipd.it (B. Fresch), diego.montagner@mu.ie (D. Montagner).

https://doi.org/10.1016/j.jinorgbio.2019.110719
Received 28 February 2019; Received in revised form 7 May 2019; Accepted 13 May 2019
Available online 28 May 2019

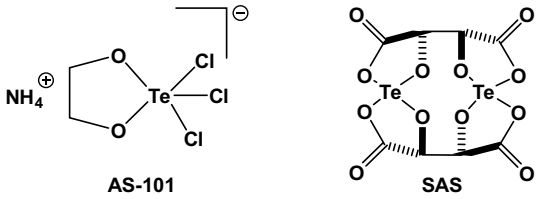

Fig. 1. Structure of the "inorganic" Te(IV) compounds AS-101 and SAS.

mechanism suggests that a longer alkyl chain substituent enhances the stability of the complex by interfering with the formation of water clusters necessary for mediating the proton transfer steps involved in the hydrolysis of the Te—O bonds. The antimicrobial activity was evaluated *in vitro* on *Escherichia coli* and other bacteria strains.

2. Experimental

2.1. Material and methods

$TeCl_4$ and all the diol ligands have been purchased from Sigma-Aldrich or TCI Europe. All solvents were used without further purification except for CH_3CN which was kept dry over molecular sieves under inert atmosphere. All NMR spectra were recorded on a Bruker Advance spectrometer with the probe at 293 K, operating at 500 MHz for the ^{1}H, at 125 MHz for the ^{13}C and at 158 MHz for the ^{125}Te nucleus, respectively. Spectra were recorded in DMSO-d_6 using Me_4Si as the internal standard for ^{1}H and ^{13}C while diphenyl ditelluride was used as external reference for ^{125}Te. All chemical shifts δ are reported in ppm. FT-IR spectra were recorded (compounds **1** and **3**) from either CsI disks (solid samples) or KRS-5 thallium bromoiodide cells (neat liquid samples) at room temperature on a Perkin Elmer Frontier FT-IR/FIR spectrophotometer in the range 4000–600 cm^{-1} (32 scans, resolution 4 cm^{-1}) and in the range 600–200 cm^{-1} (32 scans, resolution 2 cm^{-1}). Data processing was carried out using OMNIC version 5.1 (Nicolet Instrument Corporation). For all the other compounds Infrared (IR) spectra were recorded in the region 4000–400 cm^{-1} on a Perkin Elmer ATR (Attenuated Total Reflectance) precisely spectrum 100 FT/IR spectrometer. Elemental analysis (carbon, hydrogen and nitrogen) were performed with a PerkinElmer 2400 series II analyser. ESI (Electro Spray Ionisation) mass spectra were recorded in negative mode with a Waters LCT Premier XE Spectrometer. The stability of the complexes has been evaluated following the decomposition reaction by ^{1}H, ^{13}C and ^{125}Te NMR. Each compound was accurately weighted and dissolved in 400 μL of DMSO-d_6 to obtain 125 mM solution (0.05 mmoles). 10 μL of D_2O were added in three consecutive aliquots and the NMR spectra were recorded 1 h after each addition (each addition corresponds to 10 equivalents of water with respect the complex). The experiments were run in triplicate.

2.1.1. Effect of compounds on growth of E. coli

To each well of a 96-well plate (Sarstedt), 100 μL of fresh nutrient broth medium were added. A serial dilution of each compound was performed on the plate to give a concentration range of (150–0.59 μM). Cells suspension (100 μL) of *E. coli* (1 × 106 cells/mL) was added to each well and the plates were incubated at 37 °C for 24 h. The experiments were carried out in duplicate. The OD570nm of the cultures was determined using a microplate reader (Bio-Tek, Synergy HT) and all growth was expressed as a percentage of that in the control. The MIC_{50} and MIC_{80} (Minimum Inhibition Concentration) are defined as the lowest concentration to inhibit growth by 50% and 80%, respectively.

2.1.2. Computational method

Structures and energetics were modelled by Density Functional Theory (DFT) at the wB97XD/lanL2DZ level of theory, which performs well in prediction of reaction energies [30]. Implicit solvation was introduced with the *Solvation Model based on Density* (SMD) parametrization. The ground state geometry of each compound was optimized in implicit solvent by including the effect of the polarizable continuum in the self-consistent field procedure. The explicit microsolvation model was built by adding five water molecules to the reactant complex, the whole hydrated complex was then reoptimized in implicit DMSO. The initial positions of the water molecules were selected by maximizing the possibility of forming hydrogen bonds between water molecules and the compounds in order to find the most stable structures of reactants and products upon optimizations. The initial hypotheses were optimized, for the analysis we retained the three lower energy structures of the reactants (Fig. S19 in supplementary material) and the lowest energy structure of the hydrated products (Fig. S20). Frequency calculations allowed the characterization of the potential energy surface and the evaluation of the thermochemistry of the involved compounds. All computations were performed with Gaussian16 [31].

3. Results and discussion

The series of eight complexes with formula $NH_4[(RC_2H_3O_2)Cl_3Te]$ (where R = H (**1**); CH_3 (**2**); CH_2CH_3 (**3**); $CH_2CH_2CH_3$ (**4**); $CH_2CH_2CH_2CH_3$ (**5**); $CH_2CH_2CH_2CH_2CH_2CH_3$ (**6**); CH_2Cl (**7**); Ph. (**8**)), analogues of AS-101, have been synthesised as described in the Experimental part and in Scheme 1. Briefly, $TeCl_4$ and the correspondent diol were mixed in dry acetonitrile and the mixture was refluxed for several hours. The solids were collected by filtration after concentration of the CH_3CN solution or by addition of Et_2O. The complexes can be also synthesised by microwave as previously observed for AS-101 [32] and the reaction mechanism involves four steps as described by Sredni et al. [18]. The compounds were characterized by Elem. Analysis, IR spectroscopy, Mass spectrometry, ^{1}H, ^{13}C and ^{125}Te NMR (all the spectra are reported in the Supporting Information Figs. S1–8).

All the complexes show a unique ^{125}Te NMR peak in DMSO-d_6 around 1680 ppm, the typical region for these kind of species [33–34] and in the IR spectra is clearly visible the stretching of the ammonium counter cation at 3200 cm^{-1}. A detailed IR study in the range 4000–200 cm^{-1} was done for compounds **1** and **3**. Further insights into the coordination sphere of tellurium can be obtained by comparison with the IR spectra of the starting ethylene glycol, whose vibrations have been fully assigned previously [35,36]. For instance, in the mid-IR spectrum of compound **1** (Fig. S9) the bands associated with the –COH moieties of the diol (ν(OH) = 3400, δ_{ip}(COH) = 1424, δ_{oop}(COH) = 644 cm^{-1}) have disappeared, consistent with the coordination of the deprotonated glycol to the Te(IV) centre. The C—O stretching vibrations were detected at lower energy, in agreement with values reported for analogous derivatives [18]. New bands were recorded at 3234 ($\nu_a(NH_4^+)$) and 1408 ($\delta_a(NH_4^+)$) cm^{-1} accounting for the presence of the ammonium counterion [37]. In the far-IR region (Fig. S10), the spectrum of compound **1** appears dramatically different from that of ethylene glycol, the latter showing only one weak broad band at 520 cm^{-1} assigned to the δ(CCO) [35]. In line with the results reported by Albeck et al., [18] in the solid state the complex should present a distorted square-pyramidal geometry in which the two oxygen atoms of the deprotonated diol occupy the axial and one equatorial

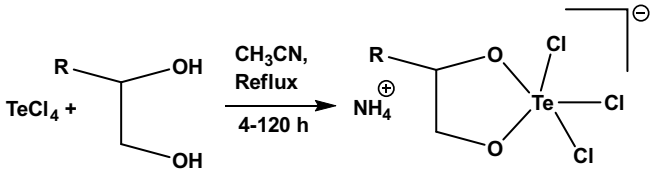

Scheme 1. Synthesis of the complexes $NH_4[(RC_2H_3O_2)Cl_3Te]$, where R = H (**1**); CH_3 (**2**); CH_2CH_3 (**3**); $CH_2CH_2CH_3$ (**4**); $CH_2CH_2CH_2CH_3$ (**5**); $CH_2CH_2CH_2CH_2CH_2CH_3$ (**6**); CH_2Cl (**7**); Ph. (**8**).

positions. Accordingly, two tellurium-oxygen stretching vibrations are foreseeable, ν(Te-O_{ax}) and ν(Te-O_{eq}), the former expected at higher frequency [38]. For **1**, Te-O vibrations were assigned to two new bands recorded at 607 and 528 cm^{-1}, respectively. Such assignments, together with the two intense bands observed at 467 and 406 cm^{-1} assigned to the overall deformation of the Te(O_2C_2)-ring, are fully consistent with those reported for analogous derivatives [39]. According to the very few relevant papers published to date, tellurium-chlorido derivatives exhibit Te—Cl stretching vibrations in the range 400–200 cm^{-1}, such as 378/312 ($TeCl_4$) [40], 220–250 ($[TeCl_6]^{2-}$) [41,42], 286/263 (Ph_2TeCl_2) [43] and 271/221 ([Te(dioxoethylene-*O,O'*)Cl_3], Raman) cm^{-1} [44]. In the present study, two new intense bands were recorded at 351 and 298 cm^{-1}, which can be reasonably assigned to the antisymmetric and symmetric stretching involving the -$TeCl_3$ moiety. The IR spectra of derivative **2** resemble closely those of **1**. The same pattern of bands was observed in the far-IR region, whereas in the 4000–600 cm^{-1} range the only minor differences would be attributed to the new vibrations involving the CH_3CH_2CH- pendant, such as those recorded at 3048 (ν(CH)), 2967/2872 ($\nu_{a,s}(CH_3)$), 1354 ($\delta_s(CH_3)$) and 776 ($\rho(CH_3)$) cm^{-1} [44]. The complexes are very stable in pure CH_3CN or DMSO solution, but they decompose upon addition of H_2O, as previously described by Albeck and co-worker's [26]. The hydrolysis reaction releases the free diol with the formation of trichloro-tellurium (IV) oxide $[TeOCl_3]^-$, as depicted in Scheme 2.

The displacement of the ligand is followed by ^1H, ^{13}C and ^{125}Te NMR (Fig. 2 for **3**): the signals of the coordinated and of the released diols appear shifted in the NMR spectra, and this effect is particularly remarked in the ^{13}C NMR for the two carbons bound to the two donor oxygen of the diols (Fig. 2 centre for compound **3** and Figs. S11–16). After addition of 10, 20 and 30 equivalents of water, as explained in the experimental part, the free diol is displaced with the formation of $NH_4[TeOCl_3]$, visible in the ^{125}Te NMR at δ 1560 ppm (Fig. 2 right). To confirm the nature of the decomposed product, 20 mg of compound **3** were dissolved in 1 mL of CH_3CN and 5 mL of H_2O and, after 2 h, the solution was dried under vacuum. The white solid obtained was washed with cold CH_3CN, H_2O and diethyl ether and further dried under high vacuum pressure. Mass spectrometry (Fig. S17, peak at (−) *m/z* 250.81 corresponding to $[Cl_3OTe]^-$) and Elem. Analysis confirm the nature of the product as $NH_4[Cl_3OTe]$ (Elem. Anal. %H (1.50), %N (5.23); found H (1.91), N (5.04)).

Analysing the integrals of the released ligand *vs* the integrals of the starting compound with respect the equivalents of water, it is possible to estimate on the stability of the complexes.

The data show that there was an evident direct proportion between the alkyl chain of the diol and the stability of the Te complexes; an increase of the chain length corresponds to an increase of the stability, with complex **6** more stable than **5**, **4**, **3**, **2** and **1** (Fig. 3). After addition of 30 eq. of water, compound **1** is almost completely decomposed while **6** is more resistant (55% not decomposed). Complex **7** with a Cl electro-withdrawing substituent is the least stable (it completely decomposes upon addition of 20 eq. of H_2O) while, unfortunately, it was not possible to evaluate the stability of complex **8**, since it was not obtained pure.

To gain a molecular understanding of the factors affecting the stability of the complexes we modelled at the quantum mechanical level complex **1** and complex **5**, representing the limiting case of short and long alkyl-chain substituent, respectively, and complex **7** with the chloro-methyl substituent. The optimized equilibrium geometries and the analysis of the electronic structures in terms of atomic charges [45,46] are reported in Fig. S18. Both atomic charges and structural parameters of the Te centre are not significantly affected by the change in the alkyl chain length nor by the chlorination of the substituent, therefore it can be concluded that the origin of the slightly different stability of the complexes does not stem from different strengths of the Te—O bonds. As it also emerges from the stability studies, the solvating environment plays a central role in establishing the equilibrium of the decomposition reaction of the complexes. Computationally, there are several approaches to treat solvation and we will use two of them in the following to elucidate the energetics of the complex decomposition. In the first approach (*implicit solvation*), the solvent is treated as a continuous, uniform dielectric medium characterized by its dielectric constant Ɛ. The solute molecules are placed inside an empty cavity within the dielectric medium and the interactions between solvent and solute consists primarily of electrostatic interactions, that is the mutual polarization of the solute and the solvent. We use the Solvation Model based on Density (SMD) which was found to perform well for predicting reaction energies in solution [47]. The reaction free energy, ΔG_r, obtained for the decomposition of the three complexes, **1**, **5** and **7**, by considering the free energy of reactants and products implicitly solvated in acetonitrile, DMSO and water are reported in Table 1, together with the free energy of the same reactions in gas-phase. Positive values of free energy of reactions reflect a stable complex which does not undergo significant decomposition. From the analysis of the values of the reaction free energy in implicit solvent we can draw two main conclusions:

i) We do see consistent trend in how the relative gas-phase stability of the three complexes is changed by solvation. Complex **5** is less prone to decomposition than complex **1** in all the considered solvents and complex **7** is the most destabilized by solvation. This can be understood by considering the solvation energies of the different species involved in the reactions (see Table S1 in the Supporting Information file) which show that the chloro-methyl substituted glycol is considerably more stabilized by solvation than the corresponding reactant complex. A word of caution must be given since the calculated difference in the reaction free energies between complex **1** and **5** ($\Delta\Delta G_r$ of about 1–1.3 kcal/mol) is small and falls within the error of the numerical method. On the other hand, such a small difference is consistent with the experimental results which report a decomposition of 0.8% for **1** and 0.4% for **5** in the case of 10 eq. of water (Fig. 3), corresponding to a difference in the reaction free energies of the two complexes of about 2 kcal/mol.

ii) Because of the active involvement of water molecules in the decomposition reaction, the implicit solvent calculations fail to predict the spontaneous decomposition of the reactants in water. Indeed, the use of a cavity model assumes that the solute electron density is not changed by specific interactions with individual solvent molecules and the reaction does not itself involve specific solvent molecules. The limitations resulting from these assumptions can be addressed by including explicit solvent molecules inside the cavity. We introduce an explicit micro-solvation environment by considering the complexes interacting with five water molecules (see the reactants in Fig. 4). The solute and its hydration shell are then considered solvated in DMSO with the implicit model to better reproduce the experimental condition of the NMR experiments. Multiple equilibrium geometries of reactants and products were

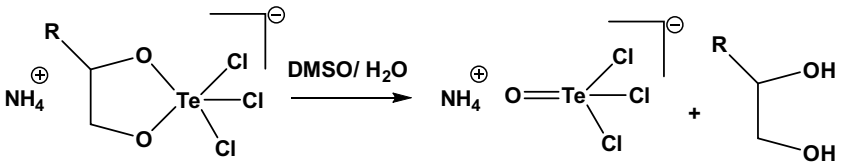

Scheme 2. Hydrolysis reaction of Te(IV) complexes

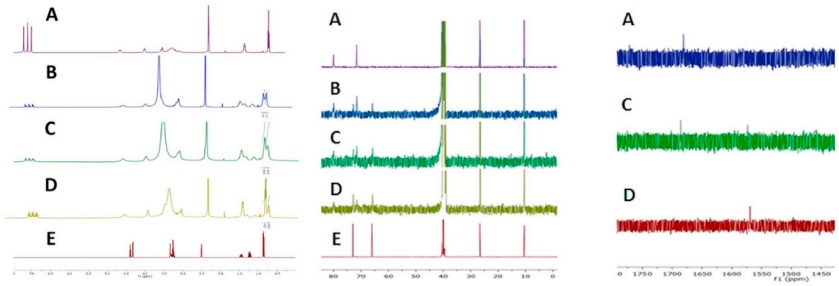

Fig. 2. ^{1}H (left), ^{13}C (centre) and ^{125}Te (right) NMR of: A) **3** (125 mM in 400 µL DMSO-d_6); B) **3** + 10 µL D_2O (10 eq.); C) **3** + 20 µL D_2O (20 eq.); D) **3** + 30 µL D_2O (20 eq.); E) free 1,2-butandiol ligand.

generated. We reported in Figs. S19 and S20 the structures of the three lower lying energy structures of the hydrated complex and the most stable structure of the products resulting from the decomposition of Compound **1**, **5** and **7**. The reaction free energies are reported in Table 1 for the different conformers of the reactants R1–R3 (Fig. S20). We recover the spontaneous decomposition of the complexes and an increased stability of the complex substituted with the longer alkyl chain in good agreement with the experimental findings. By defining the solvation contribution to the free energy of reaction as the difference between the ΔG_r calculated with the explicit micro-solvation shell model and its gas-phase value we find that these contributions are −27.3 kcal/mol, −18.2 kcal/mol and −12.6 kcal/mol for complex **7**, complex **1** and complex **5**, respectively. These results suggest that the trend in the stability of the complexes increasing with the length of the alkyl chain results from a less efficient hydration of the structure of the reactants relative to the decomposition products.

Indeed, the mechanism of the decomposition reaction involves multiple steps of proton transfer requiring the active involvement of clusters of water molecules. Mechanistic insights into the decomposition reaction are shown in Fig. 4 and they were obtained by investigating the reaction path starting from the most stable structure of the hydrated compound **1** (Reactant in Fig. 4). Structures with real frequencies corresponds to minima of the potential energy surface, that are equilibrium geometries of reactants, products and reaction intermediates. Geometries of transition states correspond to a saddle point of the Potential Energy Surface (PES) and are characterized by an imaginary frequency for the mode identifying the reaction coordinate. The mechanism of the decomposition reaction was assumed to consist of two subsequent hydrolysis steps. We identify a transition state (*TS1* in Fig. 4) corresponding to the rupture of the first Te—O bond at a free energy of +17.2 kcal/mol from the reactant complex. Breaking this bond requires both a nucleophilic attack of a water molecule to the Te centre together with a proton transfer from the water to the forming glycol molecule. Following the intrinsic reaction coordinate corresponding to the imaginary frequency of TS1 (see TS1.gif animation in the Supporting Information) we find a reaction intermediate where a -OH group is coordinated to the Te centre at an angle of about 120° from the plane of the -$TeCl_3$ moiety (*H1a* in Fig. 4). This structure can rearrange in other conformers (*H1b* and *H1c* in Fig. 4) where the most stable (+1.7 kcal/mol from the reactant) is characterized by the -OH group coordinated to Te in equatorial position. The hydrolysis of the second Te—O bond to form the free glycol molecules again requires the coordination of a second water molecule to the Te centre. This second nucleophilic attack to the Te centre comes most probably from the side opposite to the Te—O bond to break (see structure *preH2* in Fig. 4). This geometry implies that the water molecule attacking the Te centre transfers its protons to other acceptors and the protonation of the glycol is operated by a separate species (which might be a second water molecule or even a H_3O^+ ion). Most probably there are many possible paths for these multiple proton transfer steps and the mechanistic details depends on the relative position of the hydrating water molecules. The increasing of the decomposition ratio with the numbers of water equivalents observed experimentally is readily explained by considering that clusters formed by a higher number of water molecules are more efficient in mediating proton transfer steps trough the more extended H-bond network. From the intermediate structure where two -OH groups are coordinated to the Te centre (*H2* in Fig. 4) a further proton transfer step leads to the formation of the trichloro Tellurium (IV) oxide $[OCl_3Te]^-$ (*Products* in Fig. 4) where one of the vertexes of the square pyramid is occupied by a coordinated water molecule, at least in solution. In the mass spectrum of the decomposed product, as described before, the coordinated water molecule is not visible due to the ESI conditions.

Since AS-101 and Te(IV) species showed antimicrobial activity against *Enterobacter cloacae* and *Pseudomonas aeruginosa*, [27,48–51] some of the complexes synthesised, (**3**, **4** and **5**) together with the free ligands, were selected and screened for antimicrobial activity against a series of bacteria, including *Escherichia coli*, *Staphylococcus aureus*, methicillin resistant *Staphylococcus aureus* (MRSA), *Pseudomonas aeruginosa*, and the yeast *Candida albicans*.

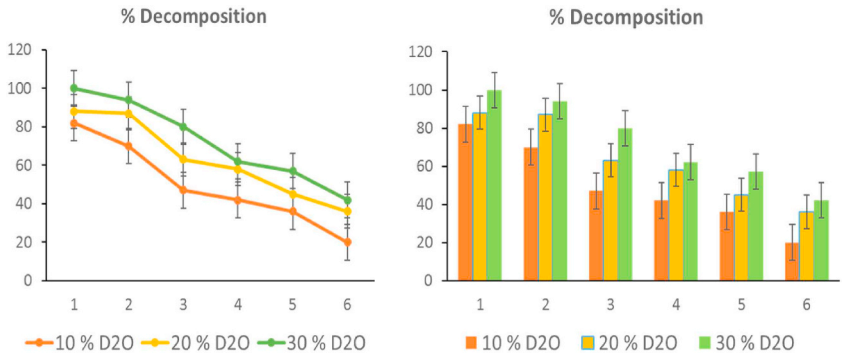

Fig. 3. Decomposition of complexes **1–6** with addition of water. Left, marked line representation; right, 2D column representation.

Table 1
Free energy of the decomposition reaction of compounds **1**, **5** and **7**. The table reports the gas-phase energy and the set of energies calculated with an implicit solvent model of acetonitrile, dimethyl sulfoxide (DMSO) and water. The reaction considered in gas-phase and in implicit solvent was $[(RC_2H_3O_2)Cl_3Te]^- + H_2O = [RC_2H_3(OH)_2] + [Cl_3OTe]^-$ where reactants and products were considered as non-interacting molecules each species was solvated separately. The second set of energies are calculated by explicit consideration of a hydration shell composed of five water molecules. The labels R1, R2 and R3 refers to three different conformers of the hydrated reactant differing by the positions of the water molecules, see Figs. S19 and S20 for the structures of reactants and products.

ΔG_r (kcal/mol)	Gas phase	Implicit solvation			Explicit microsolvation shell		
		Acetonitrile (ε = 35.688)	DMSO (ε = 46.826)	Water (ε = 78.3553)	R1	R2	R3
1	16.6	18.4	18.1	16.0	−1.6	−4.7	−5.4
5	17.5	19.4	19.4	17.2	4.9	−1.3	−2.8
7	23.3	18.2	17.9	15.9	−4.0	−11.5	−13.5

The compounds showed interesting activity against the Gram negative bacterium *E. coli* (MIC_{50} values between 15 and 20 μM as reported in Table 2) while they were less active or inactive against the other bacteria and *C. albicans*. The free diol ligands that are displaced in physiological conditions, have been analysed and they do not show any activity. We conclude that the similar activity of the complexes is probably due to the hydrolysed product $[Cl_3OTe]^-$. Interesting, a black metallic, granular layer was visible in the assay medium of *E. coli* treated plates and it is probably due to the reduction of the Te(IV) by the bacteria, as already observed by Yang and co-workers (Fig. 5) [48].

Table 2
MIC_{50} and MIC_{80} values of the compounds **3–5** in *E. coli*.

Compound	MIC_{50} (μM)	MIC_{80} (μM)
3	19.8 ± 0.5	40.5 ± 0.6
4	18.4 ± 0.4	37.8 ± 0.7
5	17.1 ± 0.6	35.7 ± 0.8

4. Conclusions

A series of Te(IV) compounds of formula $NH_4[(RC_2H_3O_2)Cl_3Te]$ where R is an alkyl chain with different length and electronic substituents, was synthesised and fully characterized and the stability in aqueous media was investigated. Experimental observations are matching with theoretical modelling using the explicit micro solvation method, showing that all the complexes release the diol ligand upon addition of water with hydrolytic cleavage of the Te—O bonds. The decomposition reaction consists in two subsequent hydrolysis steps and compounds with longer chains are more stable because the alkyl group causes a less efficient hydration of the products and hinders the necessary proton transfer steps in the reaction. Nevertheless, even if there is a correlation between alkyl chain length and stability, this latter is not enough to claim that the promising antimicrobial activity observed, in particular against Gram negative *E. coli* bacteria, is due to the starting compounds. We can conclude instead, that these compounds act as prodrugs by realising the hydrolysed product $NH_4[Cl_3OTe]$, which acts as the real bioactive species.

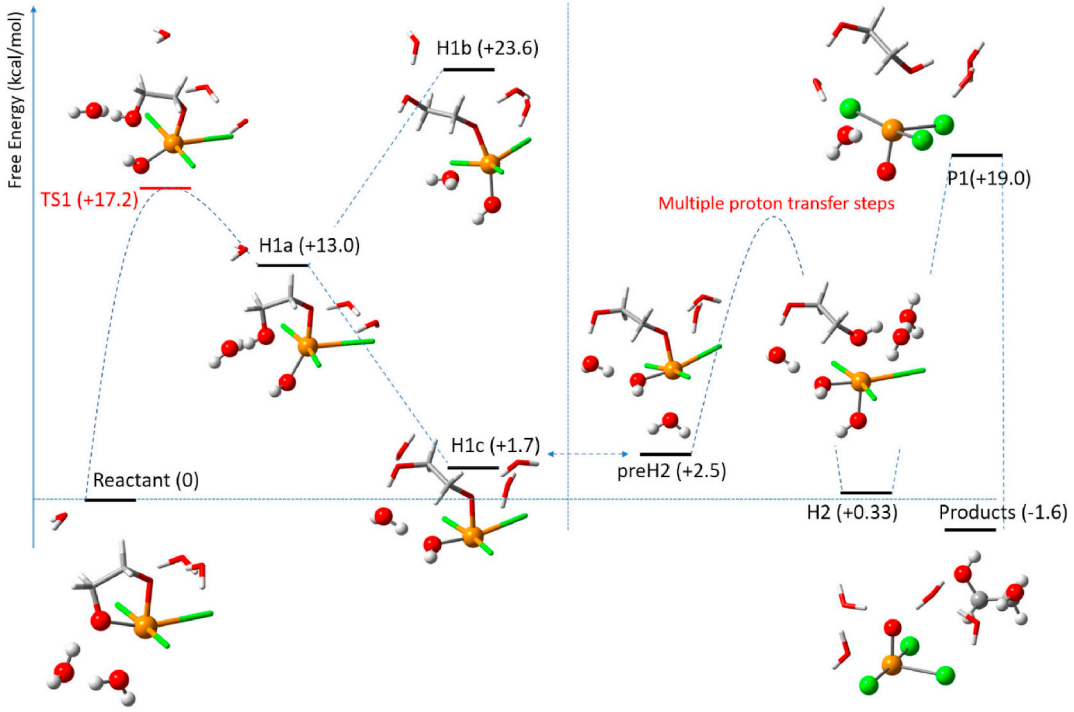

Fig. 4. Mechanistic insights into the decomposition reaction of **1** by considering an explicit micro-solvation shell formed by 5 molecules of water. The free energy of the structures relative to the reactant complex is reported in parenthesis (in unit of kcal/mol). Geometries corresponding to black lines are minima of the potential energy surface while TS1 is a transition state with an imaginary frequency of 131 cm^{-1} (see TS1.gif in SI). The vertical line in the middle of the picture divides the hydrolysis of the fist Te—O bond from the hydrolysis of the second Te—O bond which leads to the formation of the free glycol.

Fig. 5. Black precipitate observed at the bottom of the plate of *E. coli* treated with **3**.

Supplementary data to this article can be found online at https://doi.org/10.1016/j.jinorgbio.2019.110719.

Acknowledgments

KDA is grateful to INTEL for sponsoring the M.Sc. scholarship. BF acknowledges the support of the Italian Ministero dell'Istruzione, Università e Ricerca through the grant Rita Levi Montalcini (2013).

Declaration of competing interest

The authors declare no conflict of interest.

References

[1] I. Haiduc, R.B. King, M.G. Newton, Chem. Rev. 94 (1994) 301–326.
[2] M. Ruck, F. Locherer, Coord. Chem. Rev. 285 (2015) 1–10.
[3] S.E. Ramadan, A.A. Razak, A.M. Ragab, M. El-Meleigy, Biol. Trace Elem. Res. 20 (1988) 225–232.
[4] Y. Kalechman, I. Sotnik-Barkai, M. Albeck, B. Sredni, Cancer Res. 53 (1993) 5962–5969.
[5] A. Silberman, Y. Kalechman, S. Hirsch, Z. Erlich, B. Sredni, A. Albeck, ChemBioChem 17 (2016) 918–927.
[6] R.L.O.R. Cunha, M.E. Urano, J.R. Chagas, P.C. Almeida, C. Bincoletto, I.L.S. Tersariol, J.V. Comasseto, Bioorg. Med. Chem. Lett. 15 (2005) 755–760.
[7] H.L. Seng, E.R.T. Tiekink, Appl. Organomet. Chem. 26 (2012) 655–662.
[8] I.A.S. Pimentel, C. de Siqueira Paladi, S. Katz, W.A. de Souza Judice, R.L.O.R. Cunha, C.L. Barbieri, PLoS One 7 (2012) e48780.
[8] B. Sredni, Semin. Cancer Biol. 22 (2012) 60–69.
[9] G.M. Frei, M. Kremer, K.M. Hanschmann, S. Krause, M. Albeck, B. Sredni, B.S. Schnierle, Br. J. Derm. 158 (2008) 578–586.
[10] Y. Ogra, R. Kobayashi, K. Ishiwata, K.T. Suzuki, J. Inorg. Biochem. 102 (2008) 1507–1513.
[11] J. Ibers, Nat. Chem. 1 (2009) 508.
[12] M.S. Silva, L.H. Andrade, Org. Biomol. Chem. 13 (2015) 5924–5929.
[13] M. Brodsky, S. Yosef, R. Galit, M. Albeck, D.L. Longo, A. Albeck, B. Sredni, J. Iterf. Cytok. Res. 27 (2007) 453–462.
[14] M. Halperin-Sheinfeld, A. Gertler, E. Okun, B. Sredni, H.Y. Cohen, Aging 4 (2012) 436–447.
[15] B. Sredni, T. Tichler, A. Shani, R. Catane, B. Kaufman, G. Strassmann, M. Albeck, Y. Kalechman, J. Natl. Cancer. I 88 (1996) 1276–1284.
[16] S. Yosef, M. Brodsky, B. Sredni, A. Albeck, M. Albeck, ChemMedChem 2 (2007) 1601–1606.
[17] B. Sredni, R.R. Caspi, A. Klein, Y. Danziger, Y. Kalechman, M. BenYa'akov, T. Tamari, F. Shalit, M. Albeck, Nature 330 (1987) 173–176.
[18] M. Albeck, T. Tamari, B. Sredni, Synthesis (1989) 635–636.
[19] H. Rosenblatt-Bin, Y. Kalechman, A. Vonsover, R.H. Xu, J.P. Da, F. Shalit, M. Huberman, A. Klein, G. Strassmann, M. Albeck, B. Sredni, Cell. Immunol. (1998) 12–25.
[20] A. Albeck, H. Weitman, B. Sredni, M. Albeck, Inorg. Chem. (1998) 1704–1712.
[21] E. Okun, T.V. Arumugam, S.C. Tang, M. Gleichmann, M. Albeck, B. Sredni, M.P. Mattson, J. Neurochem. (2007) 1232–1241.
[22] E. Okun, Y. Dikshtein, A. Carmely, H. Saida, G. Frei, B.A. Sela, L. Varshavsky, A. Ofir, E. Levy, M. Albeck, B. Sredni, FEBS J. (2007) 3159–3170.
[23] P. Bhattacharyya, Annu. Rep. Prog. Chem. Sect. A Inorg. Chem. (2005) 117–127.
[24] Y. Kalechman, U. Gafter, T. Weinstein, A. Chagnac, I. Freidkin, A. Tobar, M. Albeck, B. Sredni, J. Biol. Chem. (2004) 24724–24732.
[25] H.-L. Seng, H.L. Seng, E.R.T. Tiekink, Appl. Organomet. Chem. (2012) 655–662.
[26] B. Sredni, R.-H. Xu, M. Albeck, U. Gafter, R. Gal, A. Shani, T. Tichler, J. Shapira, I. Bruderman, R. Catane, B. Kaufman, J.K. Whisnant, K.L. Mettinger, Y. Kalechman, Int. J. Cancer (1996) 97–103.
[27] M. Daniel-Hoffmann, B. Sredni, Y. Nitzan, J. Antimicrob. Chemother. 67 (2012) 2165–2172.
[28] A. Silberman, M. Albeck, B. Sredni, A. Albeck, Inorg. Chem. 55 (2016) 10847–10850.
[29] C.R. Princival, M.V.L.R. Archilha, A.A. Dos Santos, M.P. Franco, A.A.C. Braga, A.F. Rodrigues-Oliveira, T.C. Correra, R.L.O.R. Cunha, J.V. Comasseto, ACS Omega 2 (2017) 4431–4439.
[30] Y. Zhao, D.G. Truhlar, J. Chem. Theory Comput. 7 (2011) 669–676.
[31] M.J. Frisch, G.W. Trucks, H.B. Schlegel, G.E. Scuseria, M.A. Robb, J.R. Cheeseman, G. Scalmani, V. Barone, G.A. Petersson, H. Nakatsuji, M.C.X. Li, A.V. Marenich, J. Bloino, B.G. Janesko, R. Gomperts, B. Mennucci, H.P. Hratchian, J.V. Ortiz, A.F. Izmaylov, J.L. Sonnenberg, D. Williams-Young, F. Ding, F. Lipparini, F. Egidi, J. Goings, B. Peng, A. Petrone, T. Henderson, D. Ranasinghe, V.G. Zakrzewski, J. Gao, N. Rega, G. Zheng, W. Liang, M. Hada, M. Ehara, K. Toyota, R. Fukuda, J. Hasegawa, M. Ishida, T. Nakajima, Y. Honda, O. Kitao, H. Nakai, T. Vreven, K. Throssell, J.J.A. Montgomery, J.E. Peralta, F. Ogliaro, M.J. Bearpark, J.J. Heyd, E.N. Brothers, K.N. Kudin, V.N. Staroverov, T.A. Keith, R. Kobayashi, J. Normand, K. Raghavachari, A.P. Rendell, J.C. Burant, S.S. Iyengar, J. Tomasi, M. Cossi, J.M. Millam, M. Klene, C. Adamo, R. Cammi, J.W. Ochterski, R.L. Martin, K. Morokuma, O. Farkas, J.B. Foresman, D.J. Fox, Gaussian 16, Revision B.01, Gaussian, Inc., Wallingford CT, 2016.
[32] M.P. Vazquez-Tato, A. Mena-Menendez, X. Feas, J.A. Seijas, Int. J. Mol. Sci. 15 (2014) 3287–3298.
[33] D.B. Denney, D.Z. Denney, P.J. Hammond, Y.F. Hsu, J. Am. Chem. Soc. 103 (1981) 2340–2347.
[34] H.E. Gottlieb, S. Hoz, I. Elyyashiv, M. Albeck, Inorg. Chem. 33 (1994) 808–811.
[35] K. Krishnan, R.S. Krishnan, Proc. Indian Acad. Sci. Sect. A 64 (1966) 111–122.
[36] H. Frei, T.-K. Ha, R. Meyer, Hs.H. Günthard, Chem. Phys. 25 (1977) 271–281.
[37] K. Nakamoto, Infrared and Raman Spectra of Inorganic and Coordination Compounds 6th Ed. - Part A: Theory and Applications in Inorganic Chemistry, John Wiley & Sons Inc, Hoboken, 2009, pp. 192–204.
[38] K. Nakamoto, Infrared and Raman Spectra of Inorganic and Coordination Compounds 6th Ed. - Part A: Theory and Applications in Inorganic Chemistry, John Wiley & Sons Inc, Hoboken, 2009, pp. 217–220.
[39] K. Büscher, S. Heuer, Bernt Krebs, Z. Naturforsch. B 36 (1981) 307–312.
[40] A. Kovacs, K.-G. Martinson, R.J.M. Konings, J. Chem. Soc. Dalton Trans. (1997) 1037–1042.
[41] N.N. Greenwood, B.P. Straughan, J. Chem. Soc. A (1966) 962–964.
[42] D.M. Adams, D.M. Morris, J. Chem. Soc. A (1967) 2067–2069.
[43] N.S. Dance, W.R. McWhinnie, J. Chem. Soc. Dalton Trans. (1975) 43–45.
[44] D. Lin-Vien, N.B. Colthup, W.G. Fateley, J.G. Grasselli, The Handbook of Infrared and Raman Characteristic Frequencies of Organic Molecules, Academic Press Ltd., San Diego (CA), 1991, pp. 9–28.
[45] A.E. Reed, R.B. Weinstock, F. Weinhold, J. Chem. Phys. 83 (1985) 735–746.
[46] B. Fresch, H.G. Boyen, F. Remacle, Nanoscale 4 (2012) 4138–4147.
[47] A.V. Marenich, C.J. Cramer, D.G. Truhlar, J. Phys. Chem. B 113 (2009) 6378–6396.
[48] S.L. Chua, K. Sivakumar, M. Rybtke, M. Yuan, J.B. Andersen, T.E. Nielsen, M. Givskov, T. Tolker-Nielsen, B. Chao, S. Kjelleberg, L. Yang, Sci. Rep. 5 (2014) 10052.
[49] Z.H. Lin, C.H. Lee, H.Y. Yun, H.T. Chang, Chem. Asian J. 7 (2012) 930–934.
[50] E.H. Morales, C.A. Pinto, R. Lurasci, C.M. Munoz-Villagran, F.A. Cornejo, S.W. Simpkins, J. Nelson, F.A. Arenas, J.S. Piotrowski, C.L. Myers, H. Mori, C.C. Vasquez, Nat. Commun. 8 (2017) 15320.
[51] R.C. Molina-Quiroz, C.M. Munoz-Villagran, E. de la Torre, J.C. Tantalean, C.C. Vasquez, J.M. Perez-Donoso, PLoS One 7 (2012) e35452.